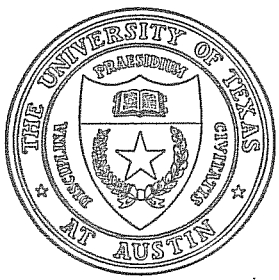

PMFSEL Report No.
August, 1989

REINFORCED CONCRETE FRAME CONNECTIONS CONSTRUCTED USING HIGH-STRENGTH MATERIALS

by

Gilson N. Guimaraes
Michael E. Kreger
James O. Jirsa

Partially Supported by
the Reinforced Concrete Research Council
Wire Reinforcement Institute
and National Science Foundation
Grant No. ECE-8320398

PHIL M. FERGUSON STRUCTURAL ENGINEERING LABORATO
Department of Civil Engineering / Bureau of Engineering Rese
The University of Texas at Austin

Any opinions, findings, conclusions, or recommendations expressed in this publication are those of the authors and do not necessarily reflect the views of the sponsors.

ABSTRACT

An experimental research project was developed at The University of Texas at Austin to investigate the behavior of interior slab-beam-column joints constructed with high-strength materials. Four full-scale specimens constructed using normal and high-strength materials were tested under cyclic bi-directional loading. High-strength concrete, high-strength steel reinforcement, and welded wire fabric reinforcing cages were used in three of the specimens. A fourth specimen was constructed using normal strength materials (f'_c = 4000 psi and Grade 60 bars). The specimens were designed according to current American Concrete Institute guidelines.

Test results indicate that the high-strength beam-column joints performed quite satisfactorily. The performance of the normal and high-strength steel reinforcement was comparable indicating that current recommendations can be extended to include the use of Grade 75 longitudinal reinforcement and welded wire fabric (f_y up to 80 ksi) as joint reinforcement. The effect of high-strength concrete on behavior was notable, especially with respect to stiffness, cracking, and energy dissipation. Current design recommendations for joint shear strength can be used for a safe estimate of unidirectional joint shear strength of interior joints constructed with high-strength materials.

ACKNOWLEDGEMENTS

The research was supported by the Reinforced Concrete Research Council, the Wire Reinforcement Institute, and the National Science Foundation under Grant No. ECE-8320398. Welded wire fabric reinforcement cages were donated by Ivy Steel and Wire Co. of Houston, Texas. Partial support for the first author was provided by the Brazilian government through the Conselho Nacional de Ensino e Pesquisa and by the Universidade Catolica de Goias. The support of these organizations is gratefully acknowledged.

TABLE OF CONTENTS

LIST OF TABLES

LIST OF FIGURES

CHAPTER 1 - INTRODUCTION

1.1 BACKGROUND

In seismic design, reinforced concrete structures must perform satisfactorily under severe load conditions. To withstand large lateral loads without severe damage, structures need strength and energy-absorption capacity. It is commonly accepted that it is uneconomical to design reinforced concrete structures for the greatest possible earthquake ground motion without damage. Therefore, the need for strength and ductility has to be weighed against economic constraints.

Moment-resisting reinforced concrete frames have gained wide acceptance as an economical structural system that allows energy dissipation without considerable structural damage. In moment- resisting frames, all the lateral force produced by earthquake forces is taken by the frame without the help of any shear wall or bracing system. In determining the design process, structural engineers generally agree on usage of the "strong column-weak beam" design philosophy for moment-resisting frames [10]. A beam sidesway failure mechanism (Figure 1.1) would occur when yielding begins at critical sections of the beams before the columns yield. This type of failure mechanism allows for a more rational, uniform energy dissipation by plastic beam hinging. Energy absorption can be provided by detailing the structure such that plastic beam hinges occur in the vicinity of the joints and the lower story column. Rotations in the plastic hinges provide the necessary energy dissipation mechanism without sacrificing the gravity load carrying capacity of the structure.

In the "strong column-weak beam" design philosophy, the column is expected to remain essentially elastic throughout the earthquake and beam plastic hinging is expected to form next to the column face. Therefore, the beam-column joint plays an important role in the satisfactory performance of the moment-resisting frame. Components of well detailed ductile moment-resisting frames, including the beam- column-joint connection, must exhibit good performance.

1.2 THE INTERIOR JOINT OF A MOMENT-RESISTING FRAME

The interior joint transfers forces between the floor system (beams and slab) and the columns. The beam-column-joint connection should be able to carry the large forces transmitted from the beams into the column during seismic excitation. A free-body diagram of the joint area (Figure 1.2) shows that if plastic hinges are to be formed next to the joint, large flexural forces in the beams result in very large shear and bond stresses through the joint.

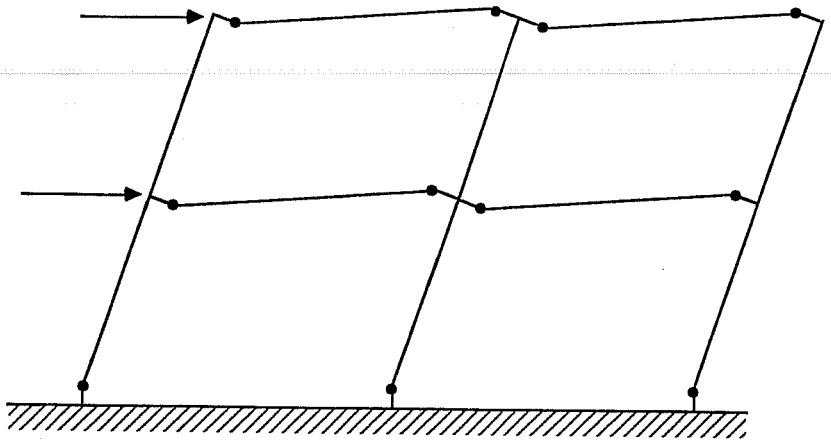

Figure 1.1 Beam sidesway mechanism

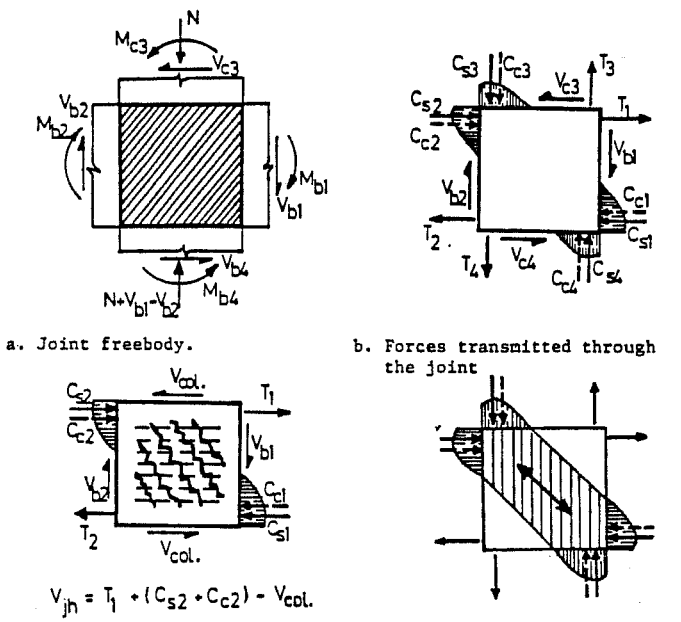

Figure 1.2 Interior joint force distribution

Figure 1.2 (a, b) shows resulting axial forces, shears and moments applied to an interior joint if a beam sidesway mechanism develops. The beam and column bars passing through the joint develop tension (T_1, T_2, T_3, and T_4) and compression (C_{s1}, C_{s2}, C_{s3} and, C_{s4}) forces. Resultants of the concrete compression stresses are represented by C_{c1}, C_{c2}, C_{c3}, and C_{c4}. In most cases, it is valid that $T_i = C_{si} + C_{ci}$ (i = 1, 2, 3, 4). If inflection points are assumed at midlength of column and beams (Figure 1.3), average column shear V_{col} can be calculated as:

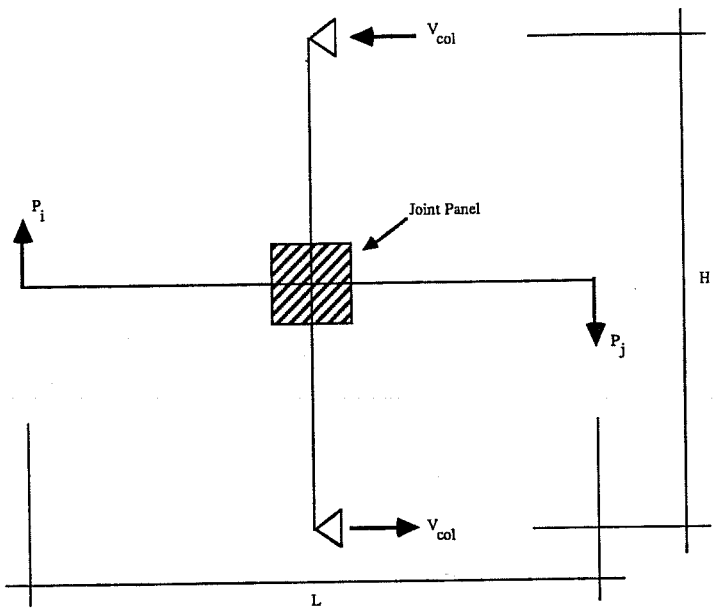

Figure 1.3 Column shear V_{col}

$$V_{col} = (P_i + P_j) * (\frac{L}{2H})$$

In addition, horizontal joint shear force V_{jh} and vertical joint shear force V_{jv} can be calculated.

$$V_{jh} = T_1 + T_2 - V_{col}$$

$$V_{jv} = T_4 + T_3 - V_{b2}$$

Two main joint mechanisms have been identified to resist the shear forces imposed across the joint: the panel truss mechanism and the concrete strut mechanism (Figure 1.2 c, d). In the concrete strut mechanism, a band of concrete carrying compression is formed between diagonally opposite corners of the joint. The formation of the strut depends on the presence of equilibrating compressive forces in the adjoining beams and column.

In the panel truss mechanism, shear is distributed along the boundaries of the joint concrete. It is assumed that when the joint concrete is severely cracked, shear is transferred through smaller inclined struts held in place by horizontal forces in joint ties and vertical forces provided by vertical reinforcement. Vertical as well as horizontal reinforcement is required to confine the joint concrete. It is possible that both the concrete strut and the panel truss mechanisms work together in transferring joint forces. However, efforts to isolate the contribution of each mechanism have proved unsuccessful. This is mainly due to the lack of a reliable technique to measure concrete and steel strains due to the different forces acting inside the joint.

A large amount of research on beam-column-joint behavior has been carried out especially in the United States, Canada, New Zealand, and Japan. This research has led to identification of several important variables affecting performance of interior joints [6,7,8,9,16]:

1) Material properties: the compressive (or tensile) strength of the concrete is of particular importance to joint shear strength. Typically, joint shear strength increases with compressive concrete strength.

2) Effect of lateral beams: tests show that the joint confinement provided by lateral beams is very effective in increasing the shear strength of the joint.

3) Amount of joint transverse reinforcement: transverse column ties are necessary to maintain the shear strength capacity of the joint by helping maintain the integrity of the joint concrete.

4) Bond deterioration: size of the longitudinal bars relative to joint dimensions influence stiffness of the structure and energy dissipating characteristics.

5) Column axial load: although column axial load was once thought to be important parameter affecting joint shear strength, it has been shown that its effect is not significant.

6) Presence of slab: although few tests have been conducted on specimens constructed with a floor slab, its effect on joint confinement and bending moment capacities is evident.

Research on beam-column-joint connections has led to design recommendations which have been incorporated into building codes. In the United States, the most important guidelines for designing beam- column joints are the American Concrete Institute 352 Committee Report [2] and Appendix A of the American Concrete Institute Building Code Requirements [1]. These recommendations include provisions for joint shear strength, transverse joint steel reinforcement, concrete confinement, bar anchorage and joint detailing.

1.3 TESTS ON INTERIOR JOINTS CONSTRUCTED USING HIGH STRENGTH MATERIALS

Production of high strength concrete having uniaxial compressive strengths in excess of 12,000 psi is technically and economically feasible. The increasing usage of high strength concrete indicates substantial economic savings can be obtained in medium and high-rise construction. In addition, use of high strength steel and welded wire fabric increases productivity and reduces labor costs.

However, research on beam-column joint behavior has been limited primarily to the study on joints constructed using conventional strength steel reinforcement (Grade 40 or 60) and concrete with compressive strengths below 6,000 psi. Since, current beam-column joint design guidelines were based on tests conducted on specimens constructed with normal strength materials, their use in the design of high strength beam-column joints may be inappropriate. Building code officials and structural engineers in general have expressed concern over the use of current design recommendations for joints constructed using high strength concrete and high strength steel reinforcement (Grade 75). Some of the controversial issues raised include the possible loss of ductility with use of Grade 75 steel reinforcement, inadequate joint shear strength for joints constructed using high strength concrete, unknown confinement properties of the welded wire fabric when used as joint transverse reinforcement, and bond behavior along high strength longitudinal reinforcement.

A research project was developed at the University of Texas at Austin to investigate the behavior of interior beam-column joints constructed with high strength materials. Four full-scale specimens constructed using normal and high strength materials were tested under cyclic bidirectional loading. High strength concrete (f'_c = 12,000 psi) , high strength steel reinforcement, and welded wire fabric reinforcing cages were used in three of the specimens. A fourth specimen was constructed using normal strength materials and was also part of the U.S.-New Zealand-Japan-China Cooperative Research Project (see Appendix A for summary) [5,17,18]. The specimens were designed to demonstrate the influence of material variations on beam-column joint performance.

1.4 OBJECTIVES

The objectives of this study are the following:

a) Analyze the influence of material variations in beam- column joint performance, especially bond and shear considerations.

b) Discuss applicability of current design recommendations to design of high strength beam-column joints constructed with high strength materials.

c) Study the use of welded wire fabric as transverse joint reinforcement.

d) Analyze the influence of the slab in beam positive and negative moment capacity.

e) Evaluate the effects of bidirectional loading on stiffness degradation, bond deterioration, and joint shear strength.

f) Examine energy dissipation characteristics of specimens constructed using high strength materials.

CHAPTER 2 - EXPERIMENTAL PROGRAM

2.1 INTRODUCTION

Four reinforced concrete beam-column-slab connections were tested under cyclic bidirectional loading. The specimens were constructed using normal and high strength materials. The table below shows the concrete cylinder compressive strength and the reinforcing steel grade used in designing the specimens.

Specimen	Concrete Strength, psi	Steel Grade, ksi
J2	4,000	60
J4	4,000	75
J5	12,000	60
J6	12,000	75

Fabrication of all column ties and beam shear reinforcement in the high strength steel specimens was done with welded wire fabric.

All specimens were large scale interior connections with beams aligned in the primary directions as shown in Figure 2.1. To evaluate the shear strength of the joint, beam and column cross sections and reinforcement were chosen so that shear stresses in the joint would reach strength design limits according to ACI Building Code recommendations [1]. The specimen proportions were similar to those of typical elements in multistory reinforced concrete buildings. Points of inflection (loading points) were assumed at column midheight and at beam midspan.

2.2 SPECIMEN DETAILS

All specimens had beams 17 ft long and a column 13.90 ft high. The beams were 16 in. wide and 20 in. deep and the column had a 20 in. square cross section. A 5 in. thick slab was cast with the corners removed to permit transport through the laboratory. Specimen geometry is shown in Figure 2.1.

Tables 2.1 and 2.2 show the 28-day concrete cylinder compressive strengths and the strengths of the reinforcing steel. Table 2.3 shows the reinforcement used as well as reinforcement percentages for each specimen calculated with respect to gross cross sectional areas.

Beam reinforcement was chosen to provide high shear forces in the joint. Bottom beam reinforcement was approximately half of the top reinforcement. In some specimens,

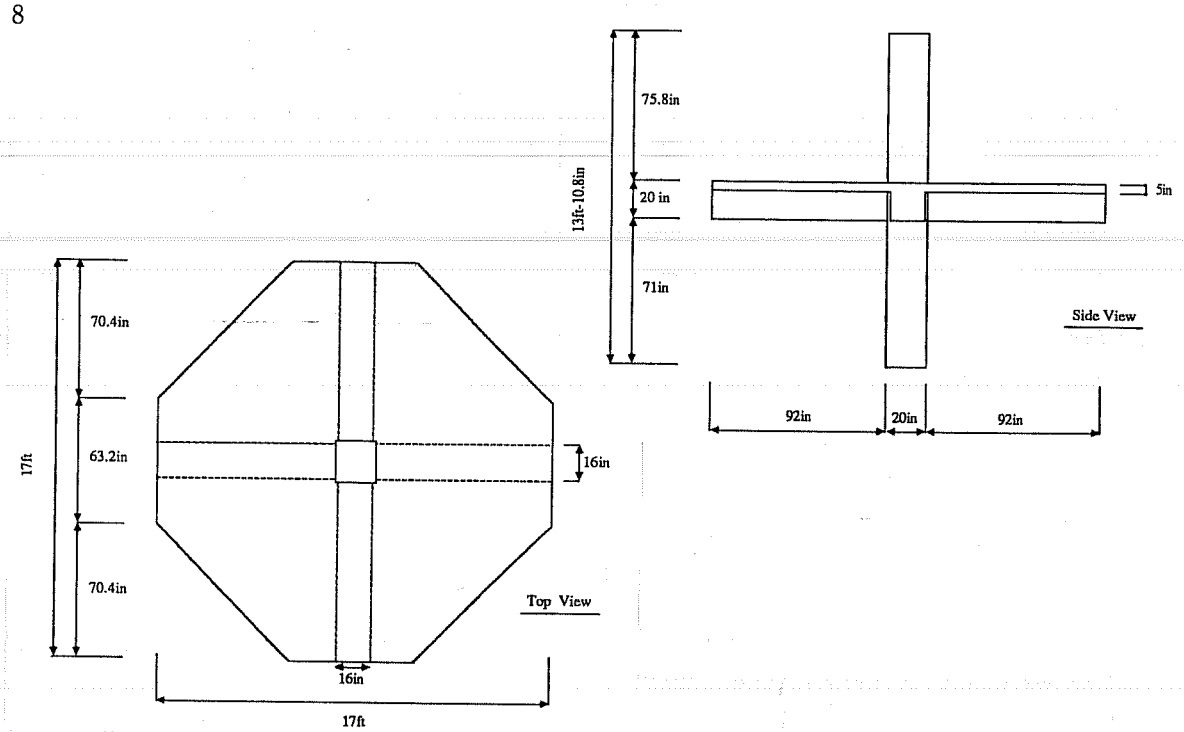

Figure 2.1 Specimen dimensions

beam top or bottom reinforcement consisted of six reinforcing bars placed in two layers. For example, in specimen J2 top reinforcement consisted of 6-#8 bars placed in two layers with four bars in the top layer and two bars in the lower layer. Six #6 bars were used as bottom reinforcement in specimen J2, with four bars placed in the bottom layer and two placed in the upper layer.

Column longitudinal reinforcement was chosen to provide the column with bending moment capacity at least 20% greater than the beam moment capacities under bidirectional loading. High reinforcement ratios in the column were needed to obtain the necessary flexural capacity without affecting the joint dimensions. Increasing the column flexural capacity by increasing the cross sectional area would also increase the joint shear strength, and consequently, the joint would not fail in shear. It should be noted this mode of failure is undesirable in an earthquake resistant high-rise building where a different failure criterion is preferable.

Details of the transverse reinforcement in the column and joint were chosen to satisfy the requirements of Appendix A of the ACI Code [1]. Five sets of perimeter hoops and cross ties were placed within the joint area. Six sets were used in specimen J4. One set was always placed above the uppermost top reinforcing bar and another was placed below the lowest bottom bar. Therefore, three layers were placed within the top and bottom beam bars

Table 2.1 - 28-Day Concrete Compressive Strength (psi)

Specimen	J2	J4	J5	J6
Slab, Beams, Joint, Lower Column	3,700 (4,010)	4,800 (4,590)	10,310 (11,300)	11,860 (13,360)
Upper Column	3,780	4,420 (4,220)	12,720 (13,800)	10,040 (10,200)

( ) Compressive strength at the time of testing (psi)

Table 2.2 - Reinforcing Steel Strength

Grade	Bar	Yield Strength (ksi)	Ultimate Strength (ksi)
60	#3	80.8	118
	#4	79.7	111
	#6	74.2	108
	#7	65.6	101
	#8	67.2	106
	#9	66.6	106
	#10	78.8	108
75	#3WWF*	84.8	90
	#4WWF*	82.6	99
	#7	79.5	120
	#8	80.0	108
	#9	75.8	119
	#10	81.4	121

* Welded Wire Fabric Cage Reinforcement

Specimen	Design Strength		Beam Reinforcement			Column Reinforcement		Slab Reinforcement	
	f'c (psi)	fy (ksi)	Longitudinal		Transverse	Longitudinal	Transverse	Top	Bottom
			Top	Bottom					
J2	4,000	60	6#8 (1.5%)	6#6 (0.8%)	2- #4 @4"	16 #9 (4.0%)	3- #4 @4"	#3 @ 12" (0.2%)	#3 @ 24" (0.1%)
J4	4,000	75	4 #8 (1.0%)	4#7 (0.8%)	3- #3 @4"	16 #9 (4.0%)	3- #3 @3"	#3 @ 12" (0.2%)	#3 @ 24" (0.1%)
J5	12,000	60	6#10 (2.3%)	2#10 4#8 (1.8%)	3- #4 @3.5"	20 #10 (6.2%)	4- #4 @2"	#3 @ 12" (0.2%)	#3 @ 24" (0.1%)
J6	12,000	75	6#9 (1.9%)	4 #9 (1.3%)	3- #4 @4"	20 #10 (6.2%)	4- #4 @2.5"	#3 @ 12" (0.2%)	#3 @ 24" (0.1%)

Notes:
1. Beam longitudinal reinforcement consisting of six bars was placed in two layers.
2. Steel reinforcement ratio (shown in parentheses) is based on gross cross sectional area.
3. Slab reinforcement is Grade 60 steel for all specimens.
4. Joint transverse reinforcement is the same as column transverse reinforcement.

Table 2.3 - Specimen Details

(four layers in specimen J4). Welded wire fabric was used for all transverse reinforcement in the high strength steel specimens (including the joint region).

All closed stirrups terminated in standard 135° hooks. Grade 60 steel cross ties had a 135° hook at one end and a 90° at the opposite end. During cage fabrication, the 90° and 135° hooks were alternated from one layer to the next. Welded wire fabric cross ties had 135° hooks at both ends. All hooks terminated in a six-bar-diameter extension. Specimens J2 and J4 had one cross tie in each layer, and specimens J5 and J6 had two cross ties in each layer.

Figures 2.2 and 2.3 show the reinforcement details used in specimen J2. Figures 2.4 and 2.5 show the details of the reinforcement used in specimen J6 where welded wire fabric was used for transverse reinforcement.

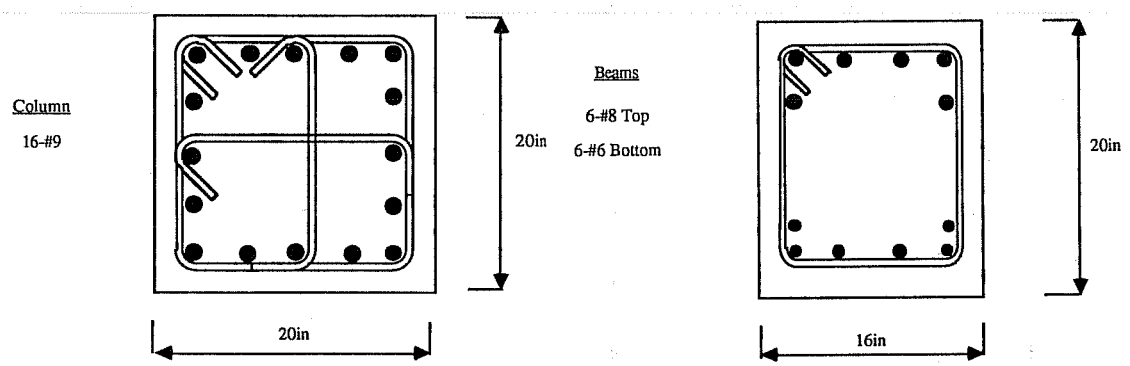

Figure 2.2 Specimen J2 reinforcement details

The 5-in. thick slab was reinforced with #3 Grade 60 steel placed in top and bottom layers with bars placed parallel to both beams. The area of bottom reinforcement was half that of the top reinforcement. All slab bars were continuous over the beams as shown in Figure 2.6.

Concrete cover was 1.5 in. for beam and column reinforcement and 0.75 in. for slab bars.

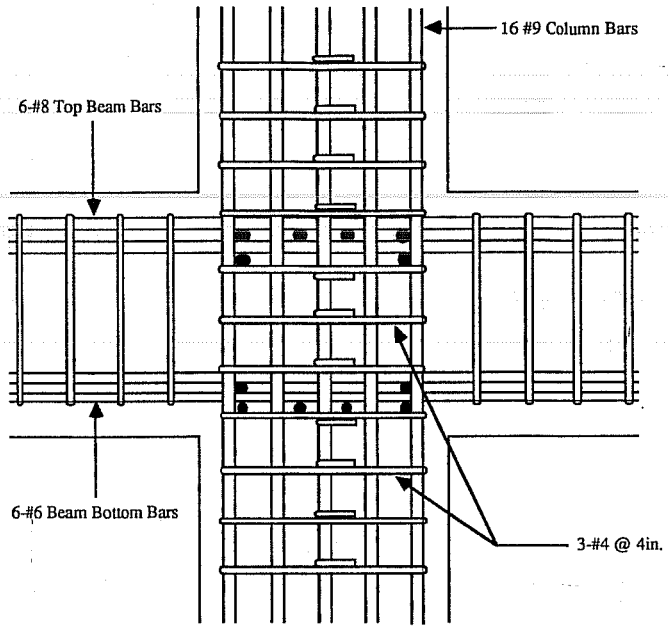

Figure 2.3 Side view of joint details for Specimen J2

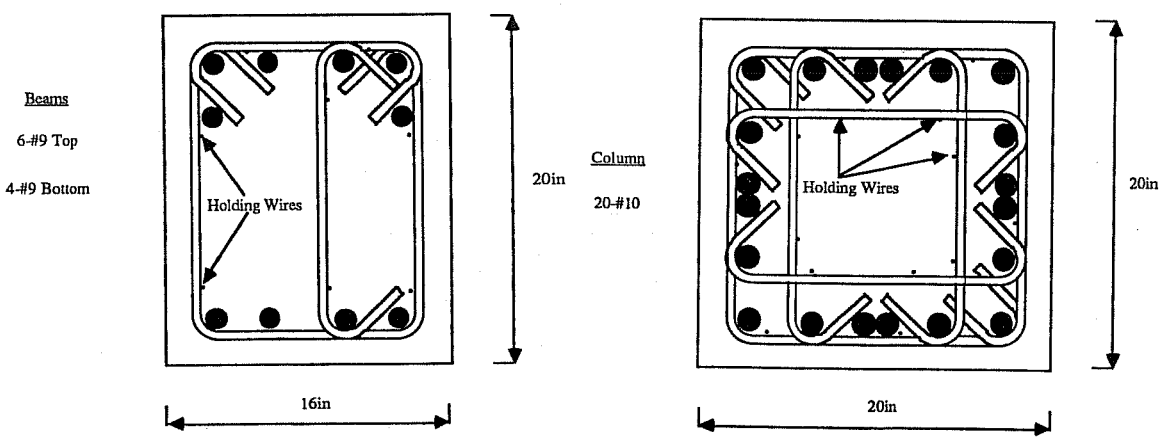

Figure 2.4 Specimen J6 reinforcement details

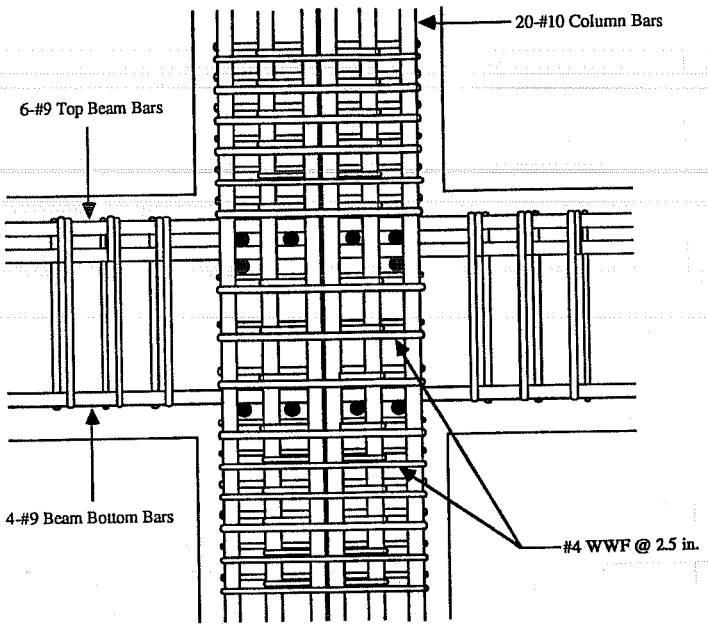

Figure 2.5 Side view of joint details for Specimen J6

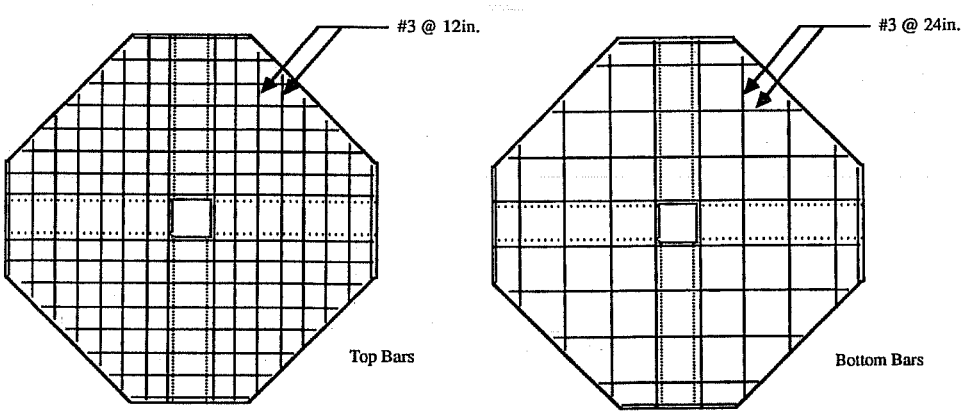

Figure 2.6 Slab reinforcement

2.3 SPECIMEN FABRICATION

The specimens were fabricated on a shored wooden platform. The forms were coated with lacquer and tape was used to close any gaps that would have allowed concrete to bleed through during the casting operation. All strain gages were attached to reinforcement before cage fabrication. The column cages were fabricated outside the platform and placed in the forms in a position that allowed fabrication of the beam cages. East-west beam reinforcement was placed above reinforcement in the north-south beams. Afterwards, beam and column cages were simultaneously lowered into final position in the formwork. Figure 2.7 shows the steel cage for specimen J6 before being lowered into the forms. Bottom and top slab bars were then placed and held in position using slab bolsters. Finally, all inserts for instrumentation and loading were placed in the joint, beams, and column, and securely tightened to the forms.

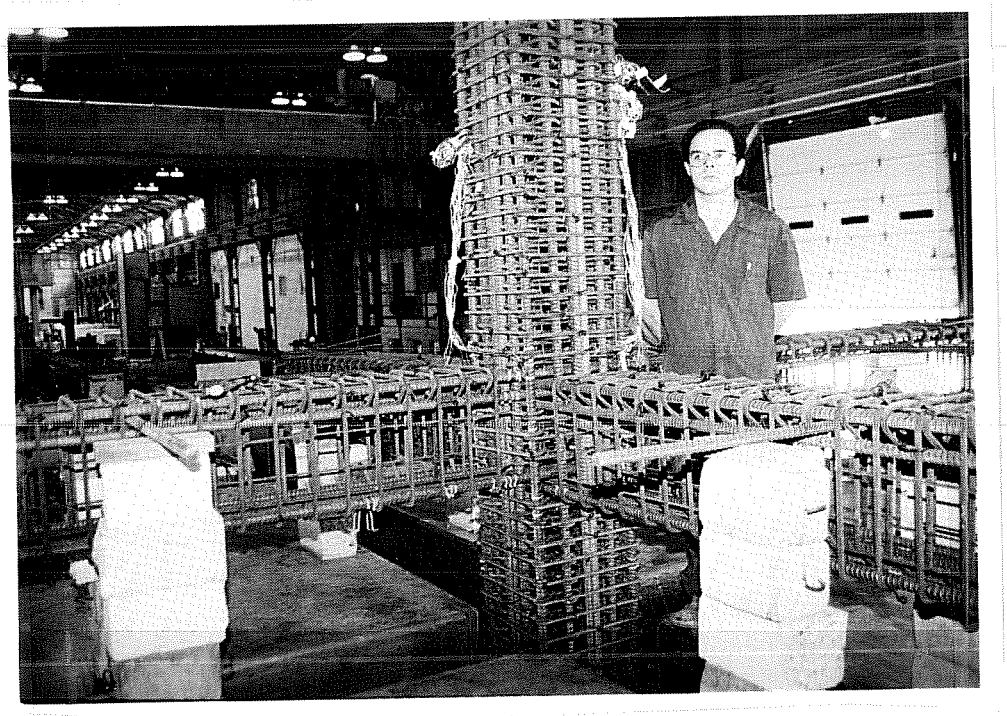

Figure 2.7 WWF steel cages for Specimen J6

Ready mixed concrete was used in the casting operation. The specimen was cast in two stages. First, the bottom portion of the column, beams, and the slab were cast in one operation. After a few days, the specimen was moved directly to the test position on the laboratory floor and the top portion of the column was cast. All concrete was placed with a bucket and consolidated with mechanical vibrators.

High strength concrete was used in specimens J5 and J6. Due to a very low water-cement ratio required to achieve high concrete strengths, a high-range water-reducer (superplasticizer) was added to the concrete at the batching plant. After adding superplasticizer, the concrete slump typically increased from less than one inch to more than 9 inches making placement quite easy. The small aggregate (3/8 in. maximum size) and high cement content increased the plasticity of the mix; segregation did not occur.

2.3.1. Fabrication of Welded Wire Fabric Reinforcing Cages. High strength welded wire fabric was used for all transverse reinforcement in specimens J4 and J6. Quality of construction and productivity was increased significantly. To illustrate quality control, one can observe in Figure 2.8 the fabrication quality of steel crossties as obtained from the fabricators. Five 17-in. crossties with standard ACI bends are shown. The first cross-tie on the left is from a WWF cage and the others are Grade 60 reinforcing steel. Differences in the quality of fabrication are evident, since all five crossties were supposed to be identical. Such deviations from desired dimensions later influenced the quality of construction (poor tolerance) and productivity in the assembly of reinforcing cages.

Figures 2.9 and 2.10 show the assembly sequence for the column and beam welded wire fabric cages. The column cage was fabricated horizontally. Steel bars were placed on vertical stands to support the column longitudinal reinforcement at the column ends. The column cage assembly started with the interior cross ties being placed on two longitudinal column bars as shown in Figures 2.9(a) and (b). Cross-tie cages were secured temporarily for later adjustment. More longitudinal bars were placed before the outer tie cages as shown in Figures 2.9(c) and (d). Outer tie cages were temporarily secured to crossties. The remaining longitudinal reinforcement was positioned and the cages were secured into proper position as shown in Figures 2.9(e) and (f). Finally, the column cage was erected and placed into the forms. Assembly sequence for the beam cage is shown in Figure 2.10.

Holding wires (see Figure 2.4) in the welded wire fabric are provided only for fabrication of the wire fabric. They are not considered as part of the longitudinal reinforcement for beams and columns. However, the position of holding wires in the welded wire fabric cages is very important in the assembly of the reinforcing cages. Holding wires are shown in Figure 2.4. Poor positioning of the holding wires can make cage assembly extremely difficult or even impossible. The holding wires may determine final positions of the cross ties and

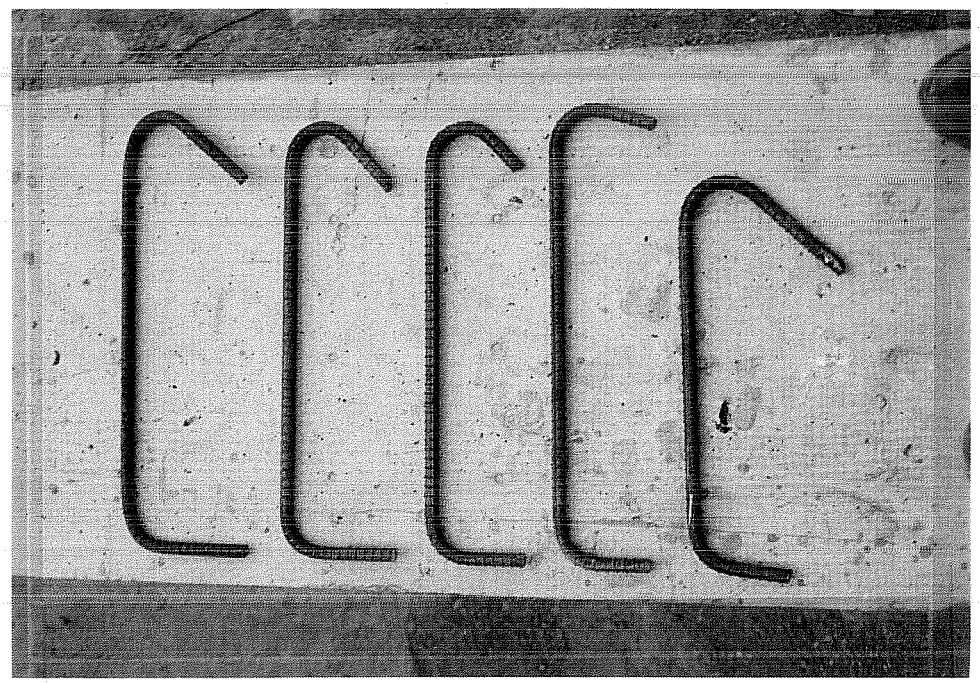

Figure 2.8 Column crossties

consequently the longitudinal reinforcement. If the column longitudinal reinforcement is not placed properly, problems may occur when placing beam longitudinal reinforcement through the column cage, especially in heavily reinforced members. Holding wires significantly reduce the manual labor involved in the assembly because not all ties need to be secured to the longitudinal reinforcement. Careful planning of the fabrication operation is important for welded wire fabric cages.

2.4 TEST SETUP

Figures 2.11 and 2.12 show the connection of the specimens to the reaction wall and the strong floor. The lower end of the column was grouted to a steel box which rested on a spherical angular contact bearing. The bearing was connected to the floor through perpendicular steel C-shaped sections. The spherical bearing allowed rotation of the steel box about any axis and restricted all horizontal movement. The upper end of the column was grouted to another steel box which was connected to the reaction wall through square

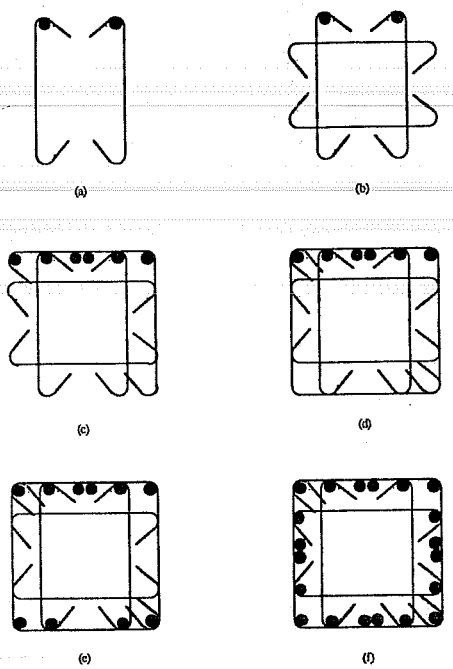

Figure 2.9 Assembly of WWF column cage for Specimen J6

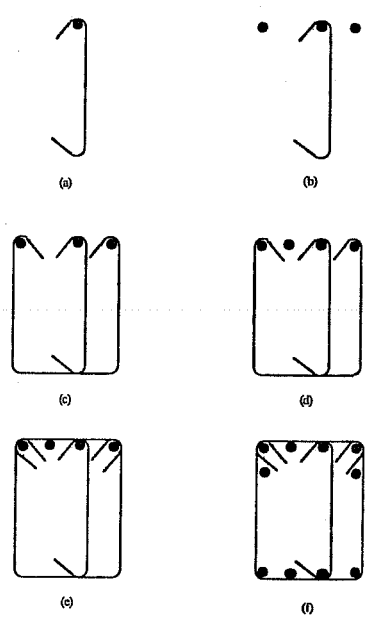

Figure 2.10 Assembly of WWF beam cage for Specimen J6

steel tubes and Dywidag bars. Two steel tubes restricted displacement of the upper end of the column perpendicular to the wall. Four high strength Dywidag bars were used to transfer forces to the wall when loading parallel to the wall. However, the bars did not provide enough stiffness to prevent all of the lateral displacement in the north-south direction (parallel to the wall). Therefore, measurements were corrected for rigid body motion of the specimen in the north-south direction. The upper connection was flexible enough to allow rotation of the column end about any axis contained in a horizontal plane.

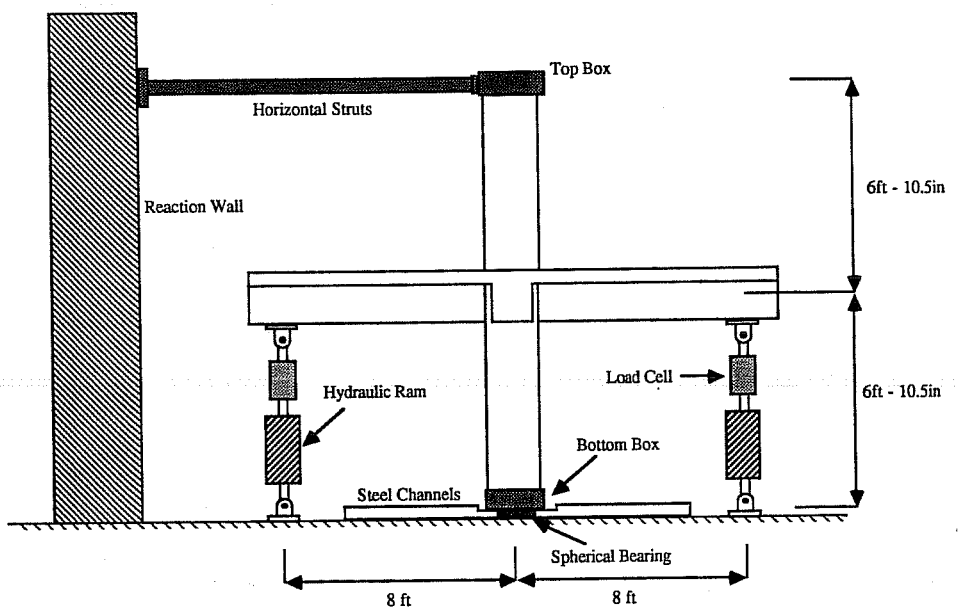

Figure 2.11 North view of loading setup

The specimens were loaded by manually controlled double-action hydraulic rams connected at the beam ends to the reaction floor. The rams were capable of resisting compression and tension forces which permitted upward and downward displacements to be applied to beam tips. The use of manual hydraulic pumps permitted careful control of beam tip deflections to produce the required loading history. Figure 2.13 shows the test setup.

2.5 LOADING PROGRAM

The idealized deflected shape of a beam-column-joint subassembly in a frame structure under lateral load is shown in Figure 2.14(a). The same deflected shape can be achieved by pinning the column ends and displacing the beam ends vertically in opposite directions

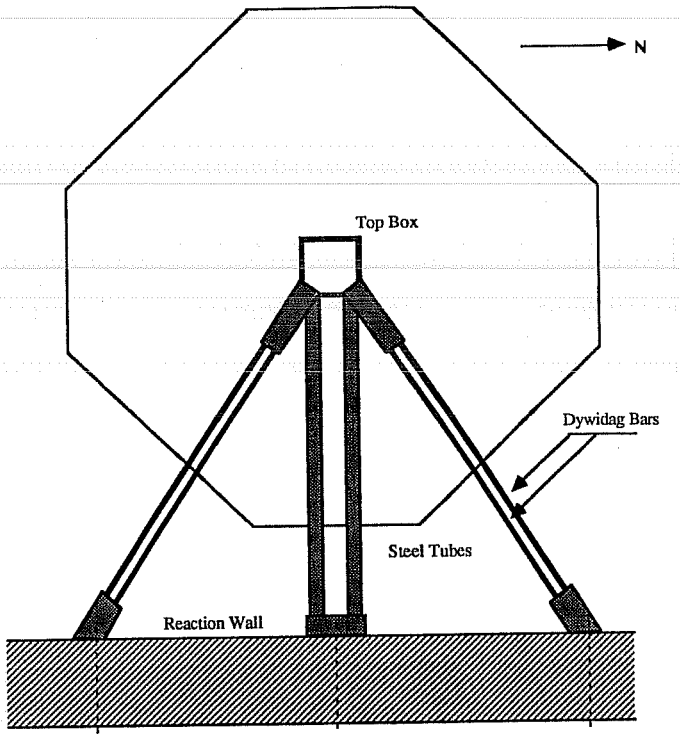

Figure 2.12 Top view of loading setup

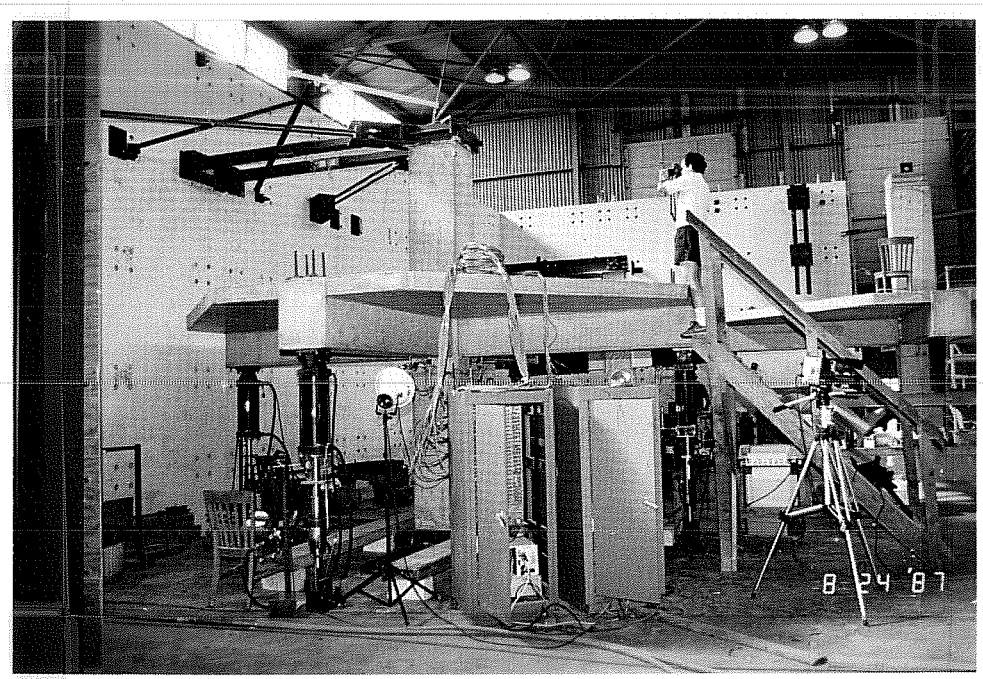

Figure 2.13 Specimen in test setup

(Figure 2.14(b)). The latter approach is used in the laboratory for economical and practical reasons. In these tests, the beam tips were always displaced in equal amounts. The interstory drift angle R is then defined as the sum of the beam tip displacements divided by the beam span:

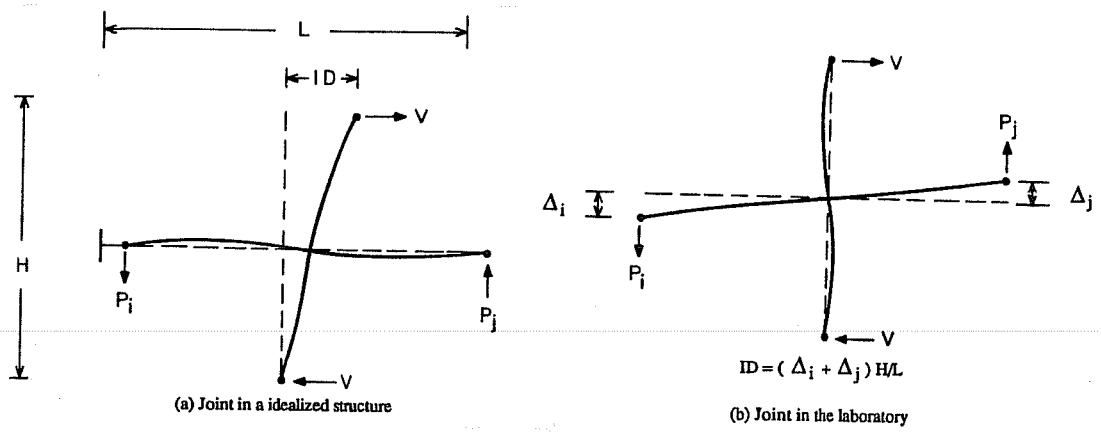

Figure 2.14 Idealized vs. laboratory model

$$R = \frac{(\Delta_i + \Delta_j)}{L}$$

Interstory displacement (ID) shown in Figure 2.14(a) is obtained by multiplying the interstory drift angle R by the column height H.

The loading history is shown in Figure 2.15. The loading history was displacement controlled by interstory drift angle during each cycle. Specimens were loaded in the east-west and north-south directions. East-west was the primary loading direction (perpendicular to the reaction wall). This loading program was used in the series of specimens tested as part of the U.S.-Japan-New Zealand Cooperative Research Project described in detail in References

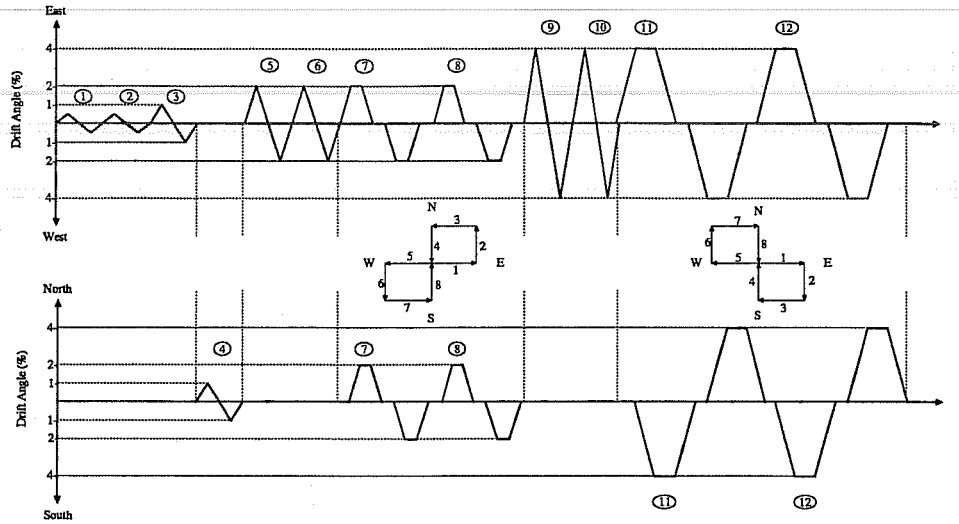

Figure 2.15 Loading history

5 and 18. Since control specimen J2 was part of that series, the same loading pattern was used for the specimens constructed with high strength materials.

During cycles 1, 2, 3, 5, 6, 9 and 10, the specimen was loaded in the E-W direction only. During cycle 4, unidirectional loading occurred in the N-S direction. Bidirectional cycles occurred at the 2% drift level (cycles 7 and 8) and at the 4% drift level (cycles 11 and 12). Bidirectional loading described diagonally opposed quadrants, since the loading direction was alternated at every quarter cycle. The bidirectional loading pattern used for 2% interstory drift was antisymmetrical to the pattern used for the 4% drift level.

The specimen was loaded by moving the beam tips in opposite directions until reaching the specified drift in each cycle. For example, under loading in the E-W direction, the east beam end was displaced upward (loading ram in compression) and the west beam end was displaced downward (ram in tension) by the same amount. Since the top beam reinforcement was always greater than the bottom beam reinforcement, the downward load was always higher than the upward load. Therefore, no special precautions were taken to prevent lifting of the specimen from its bottom connection. During bidirectional load cycles the specimen was first displaced to the prescribed drift level in the E-W direction, then while maintaining the E-W displacement, the specimen was displaced to the required drift in the N-S direction. After reaching the maximum drift, displacements were first reduced to zero

in the E-W direction then in the N-S direction. The bidirectional loading in the opposite quadrant was performed in the same manner.

Unidirectional loading is considered positive when the east or north beam ends are displaced upward (consequently the west or south beam ends will be displacing downward). Conversely, loading is negative when the west or south beam ends are displaced upward. For example, positive loading in cycle 3 is denoted by "Cycle 3/pos" and occurs when the east beam end is displaced upward; negative loading in cycle 10 is denoted by "Cycle 10/neg" and occurs when the west beam end is displaced upward. During bidirectional loading, positive is whenever the north beam end is displaced upward (independent of how the E-W beams are displaced). For example, positive loading in cycle 7 is denoted by "Cycle 7/pos" and occurs when both north and east beam ends are displaced upward. Conversely, negative loading occurs whenever the south beam end is displaced upward: negative loading in cycle 12 is denoted by "Cycle 12/neg" and occurs when both south and east beam ends are displaced upward. This sign convention is used throughout.

2.6 INSTRUMENTATION

The specimens were instrumented to obtain as much information as possible regarding the overall deformation pattern shown in Figure 2.16. This deformation pattern will be discussed in detail later.

Basically, three types of measuring devices were used: load cells, potentiometers, and strain gages. The forces applied by the hydraulic rams to the beam tips were measured by load cells attached to the rams. Beam tip deflections were monitored by 12-in. deformation potentiometers. These measurements allowed interstory drift and interstory shear to be calculated. Story shear V is given by (see Figure 2.14):

$$V = (P_i + P_j) * (\frac{L}{2H})$$

Two-inch deformation potentiometers were placed at the upper end of the column to permit correction of the interstory drift due to rigid body motion of the entire specimen. Although the rigid body motion measured in the E-W direction was negligible, up to 20% of the interstory drift in the N-S direction was due to rigid body motion of the specimen.

The elements contributing to the interstory drift are the beams, column, and joint. Isolating the contribution of each of these elements is important to understand the behavior and failure mode of the specimen. Therefore, potentiometers were placed to measure the beam, column, and joint component of the interstory drift angle. Both elastic and inelastic

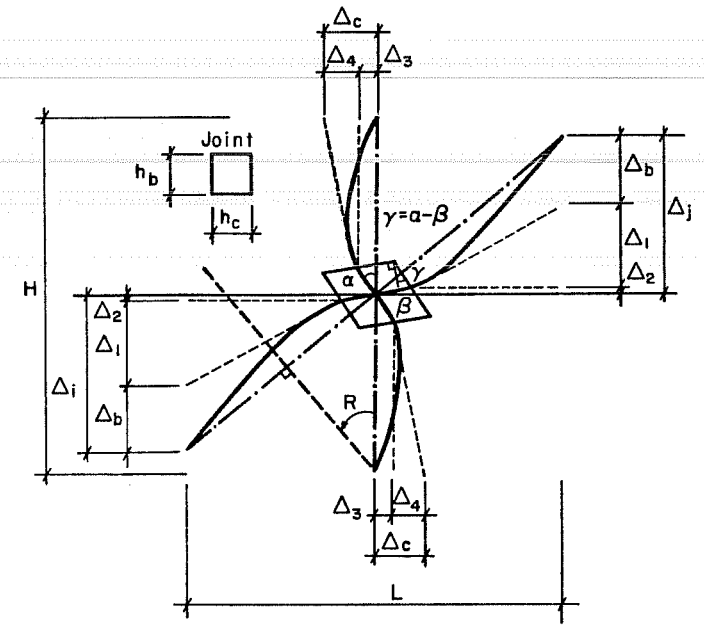

Figure 2.16 Assumed deformation pattern for specimens

deformations were included in these measurements. Column and beam deformations were assumed to be dominated primarily by flexure, and joint deformations were assumed governed by joint shear.

Instrumentation for measuring joint shear distortion is shown in Figure 2.17. These measurements permitted calculation of angles α and β shown in Figure 2.16. Angle α was measured by the two horizontal potentiometers and angle β by the two vertical potentiometers. Joint shear distortion γ is given by $\gamma = \alpha$ - β. Since the potentiometers used for these measurements were mounted on a steel frame fixed relative to the reaction floor, it was also possible to calculate column tip deflection Δ_c and beam tip deflection Δ_b given by

$$\Delta_c = \Delta_3 + \Delta_4$$

$$\Delta_b = \Delta_i - \Delta_1 - \Delta_2$$

Where:

$$\Delta_1 = \frac{\alpha(L - h_c)}{2}$$

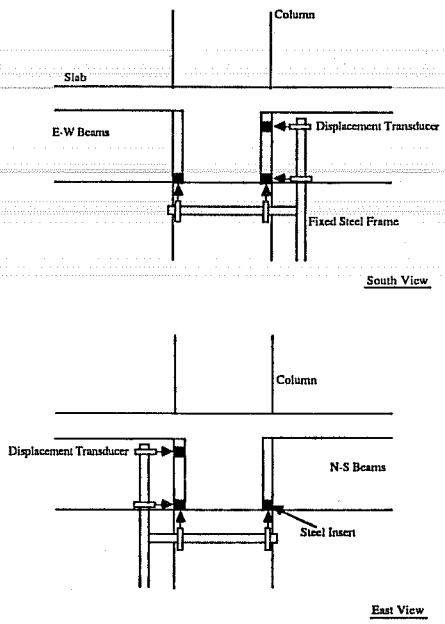

Figure 2.17 Instrumentation for joint shear distortion measurements

$$\Delta_2 = \frac{\beta h_c}{2}$$

$$\Delta_3 = \frac{\alpha h_b}{2}$$

$$\Delta_4 = \frac{\beta(H - h_b)}{2}$$

Column tip deflection angle is defined as $\theta_c = \Delta_c/(H/2)$ and beam tip deflection angle $\theta_b = \Delta_b/(L/2)$. Using the equations above, θ_c and θ_b can be given by the following:

$$\theta_c = (\alpha - \beta)(h_b/H) + \beta$$

$$\theta_b = (\alpha - \beta)(h_c/L) - \alpha + R$$

Therefore, the apparent contribution of beam, column, and joint deformations to the interstory drift angle can be determined using the measurements obtained by the instrumentation in Figure 2.17, the interstory drift, and the specimen dimensions.

Instrumentation used for measuring beam and column end rotations is shown in Figures 2.18 and 2.19. Average curvatures can be obtained by dividing the rotations by the length of the member over which they occurred. A second procedure was used to obtain curvatures along the beam length by measuring the inclination of several vertical sections along the beams with respect to their original position. These readings were taken manually using a pocket-size digital inclinometer (Figure 2.20). Steel angles were mounted on threaded rods imbedded in beams with epoxy. The inclinometer measures the angle between the steel section and vertical. Relative rotations and curvatures can be calculated from these measurements. Part of the instrumentation placed near the joint region is shown in Figure 2.21.

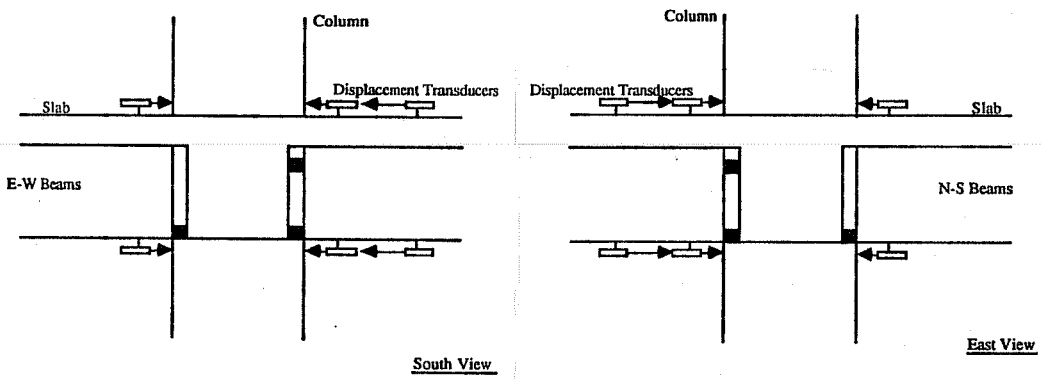

Figure 2.18 Instrumentation for beam end rotations

Strain gages were placed on reinforcement in the slab, column, beams, and joint reinforcement. Figures 2.22 and 2.23 show strain gage positions on beam bars of specimens J2 and J6 respectively. Figures 2.24 and 2.25 show strain gage positions on column bars and joint reinforcement of specimens J2 and J6 respectively. One quadrant of the slab was monitored with strain gages placed on the slab bars as shown in Figure 2.26.

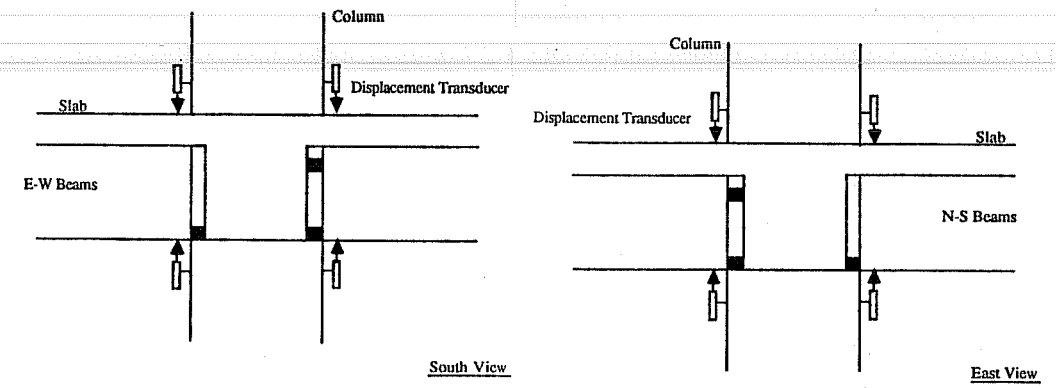

Figure 2.19 Instrumentation for column end rotations

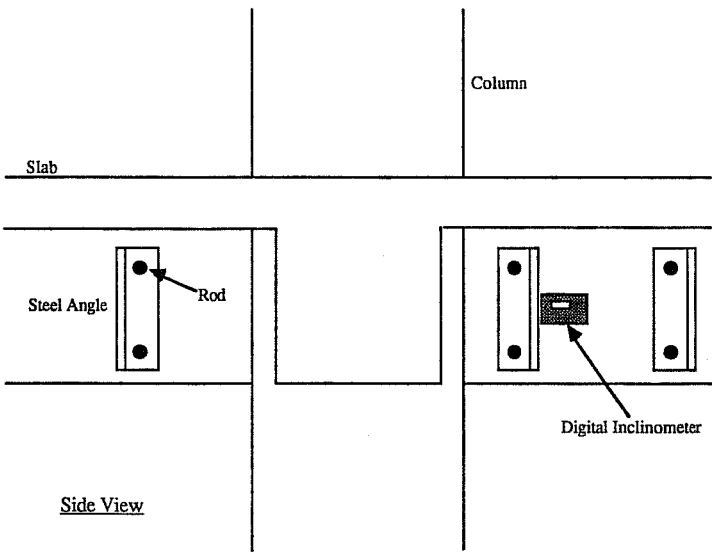

Figure 2.20 Instrumentation for curvature measurements with digital inclinometer

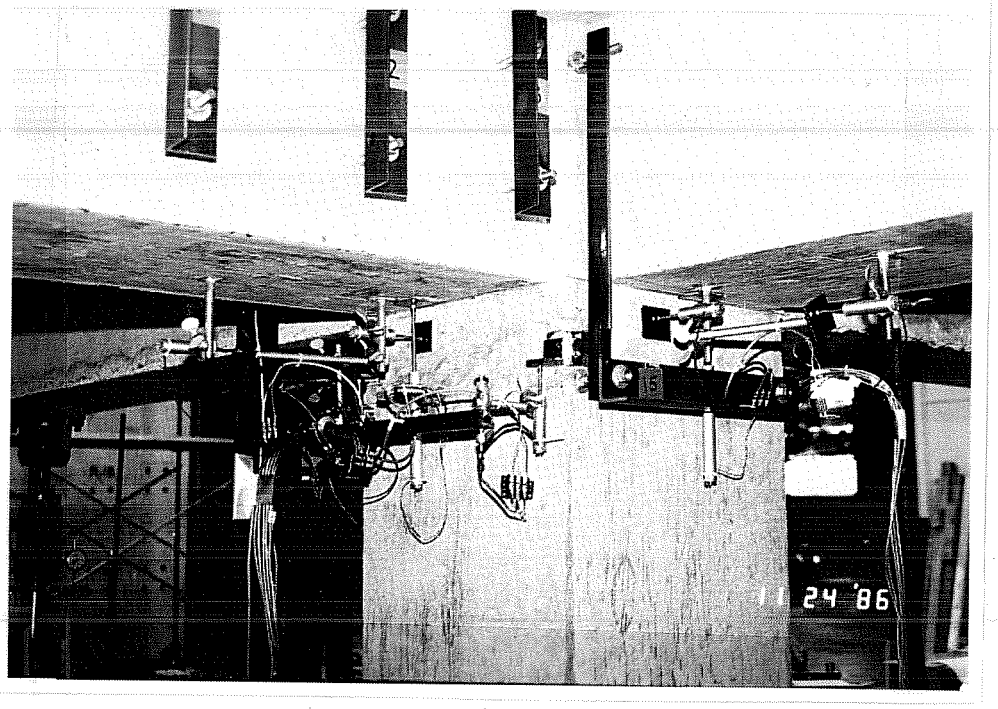

Figure 2.21 Beam-column joint instrumentation

2.7 DATA ACQUISITION

All instrumentation, except the digital inclinometer, was connected to a scanner which was controlled by a microcomputer. Approximately 320 load stages were monitored during each test. Data was recorded on floppy disks, and commercially available computer software was used to reduce and analyze the results. A hard copy of the readings collected at each load stage was printed during the test.

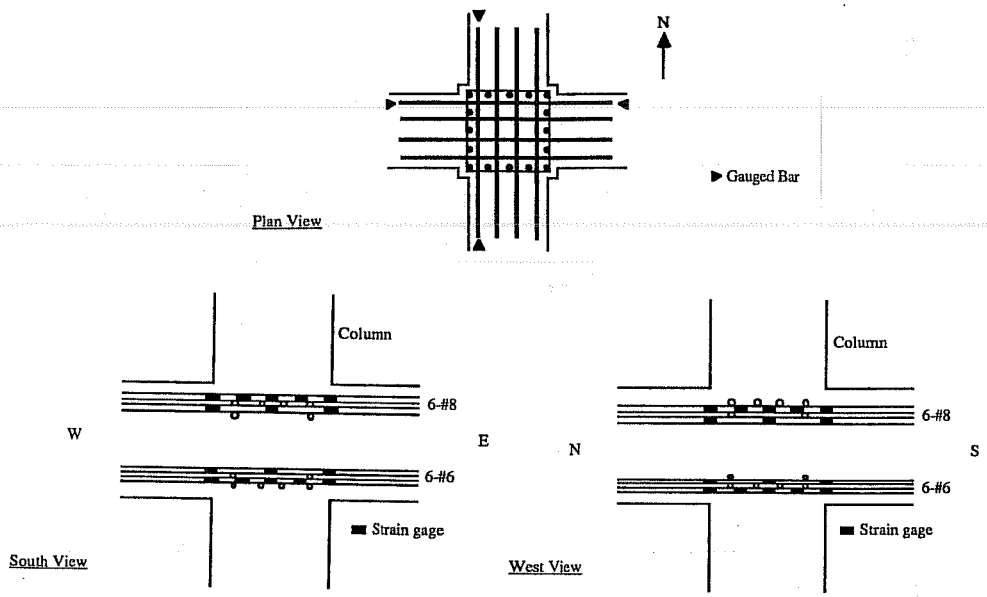

Figure 2.22 Strain gage position on beam bars for Specimen J2

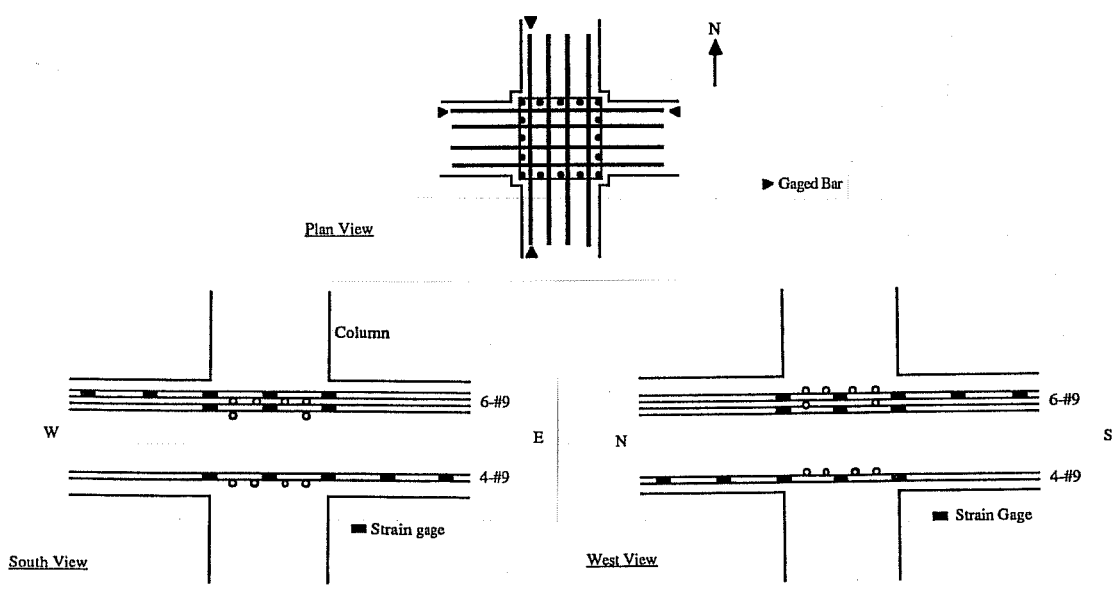

Figure 2.23 Strain gage positions on beam bars for Specimen J6

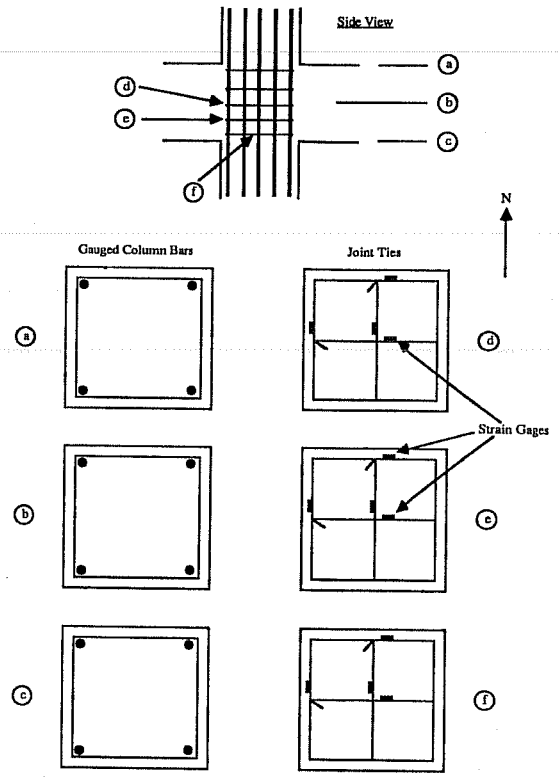

Figure 2.24 Strain gage positions on column bars and joint ties (Specimen J2)

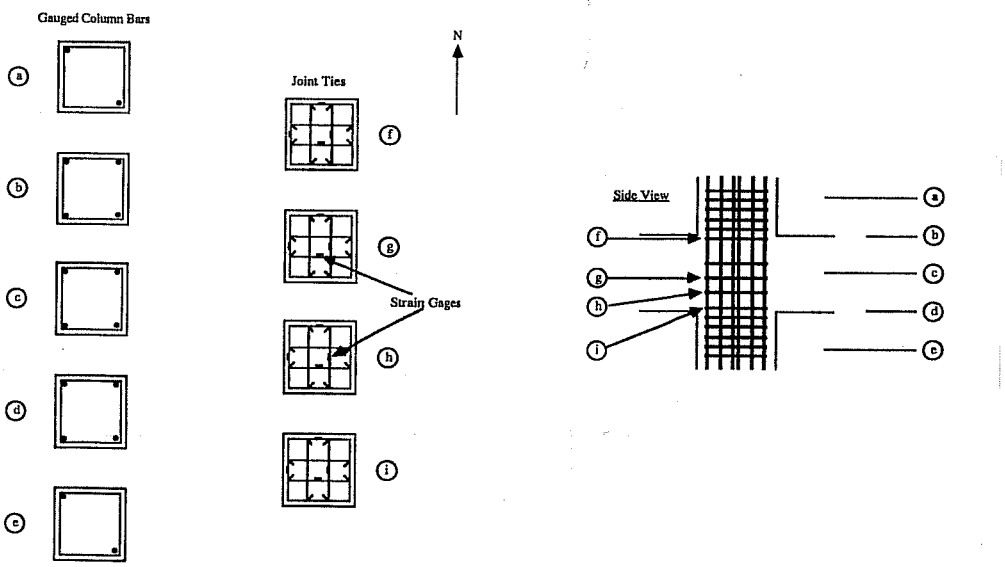

Figure 2.25 Strain gage positions on column bars and joint ties (Specimen J6)

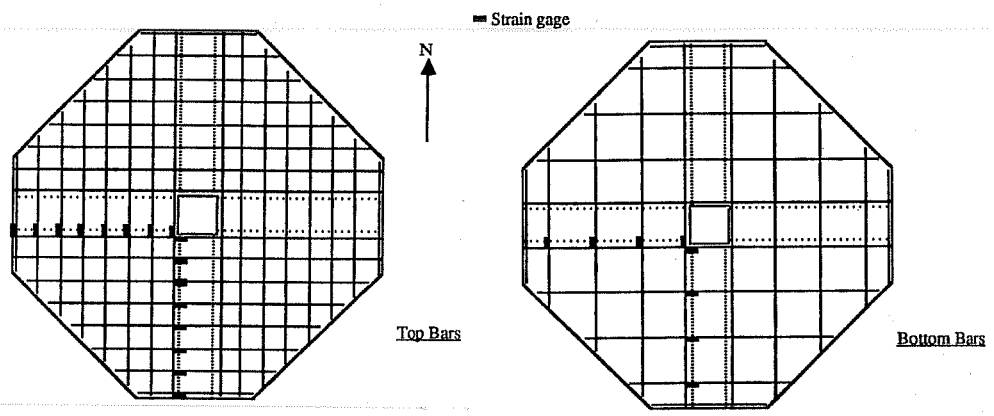

Figure 2.26 Strain gage positions for slab bars

CHAPTER 3 - EXPERIMENTAL RESULTS

3.1 INTRODUCTION

The behavior will be described using story shear and drift angle relations, and cracking patterns. The contribution to interstory drift will be analyzed through story shear relationships with joint shear distortion, column tip deflection angle, and beam tip deflection angle. Member end rotations and curvatures will also be discussed. Finally, selected results from joint, slab, beam, and column bar strains will be shown.

The test results indicated that the behavior of specimens with high strength steel was almost identical to those with normal strength steel. Since the behavior of specimens J2 and J5 was similar to specimens J4 and J6, respectively, differences in behavior between normal and high strength concrete specimens will be emphasized.

Many of the figures and tables show primarily data obtained from instrumentation placed in the E-W direction since that was the main loading direction. Except for cycle 4, N-S loading occurred during bidirectional cycles only. However, where differences between E-W and N-S behavior are important, the results are described.

3.2 GENERAL SPECIMEN BEHAVIOR

3.2.1. Story Shear - Drift Angle Relationships. Overall behavior of the specimen can be shown graphically through story shear-drift angle relationships. Figures 3.1 through 3.4 show the E-W component of story shear vs drift angle for specimens J2, J4, J5 and J6. Figures 3.5 and 3.6 show the N-S component of story shear vs drift angle for specimens J2 and J5. Overall behavior of specimens J2 and J5 in both directions is very similar to that of specimens J4 and J6 respectively. Loops corresponding to cycles 3 (1% story drift), 5 (2% story drift), and 9 (4% story drift) are indicated in Figures 3.1 - 3.4 (E-W). In addition, loops corresponding to cycles 4 (1% story drift), 7 (2% story drift), and 11 (4% story drift) are indicated in Figures 3.5 and 3.6 (N-S).

The vertical segments shown at 2% and 4% bidirectional drift cycles are due to loading interaction. Loading or unloading in one direction decreased the load in the other direction. In these cycles, vertical segments due to bidirectional interaction are also evident at zero drift levels since loading and unloading occurred there also. A large drop in the story shear was observed in the last bidirectional cycle indicating failure of the specimen.

Pinching of the hysteresis loops occurred for all specimens. Significantly pinched loops occurred for the 4% bidirectional cycles. Stiffness deterioration is quite apparent, especially during 4% drift cycles as loads approached failure.

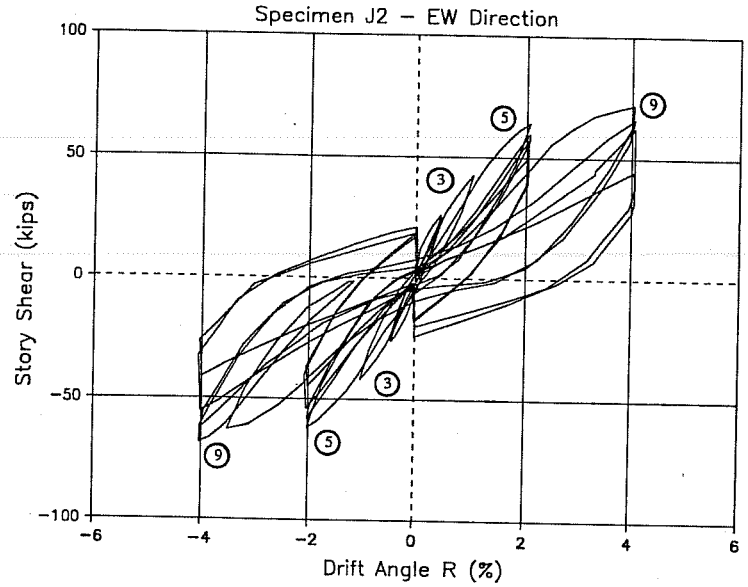

Figure 3.1 Story shear vs drift angle for Specimen J2 (EW Direction

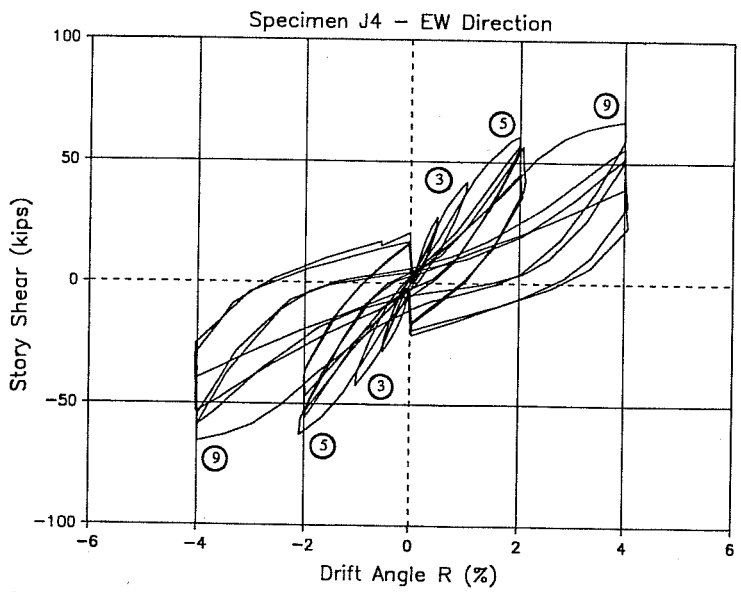

Figure 3.2 Story shear vs drift angle for Specimen J4 (EW Direction

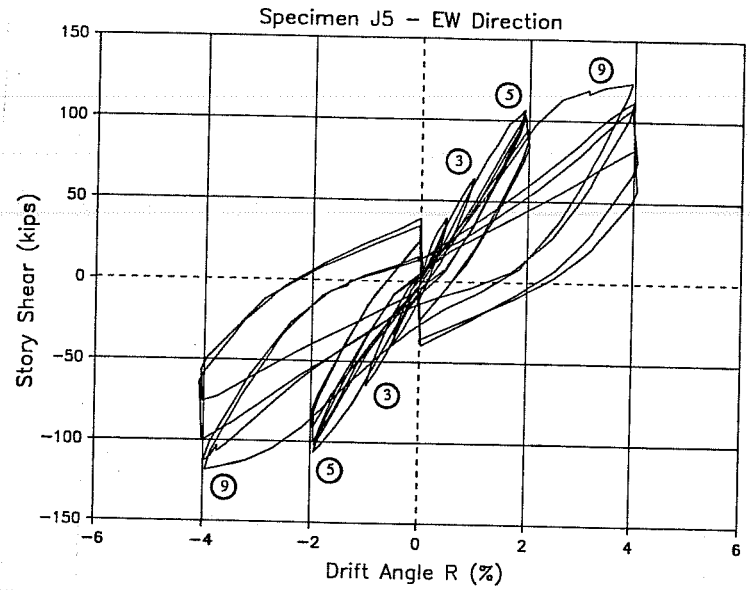

Figure 3.3 Story Shear vs Drift Angle for Specimen J5 (EW Direction)

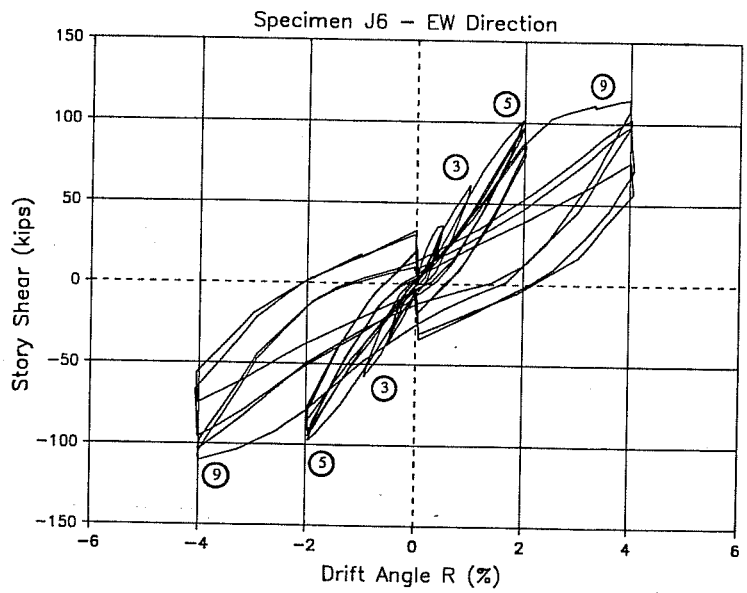

Figure 3.4 Story Shear vs Drift Angle for Specimen J6 (EW Direction)

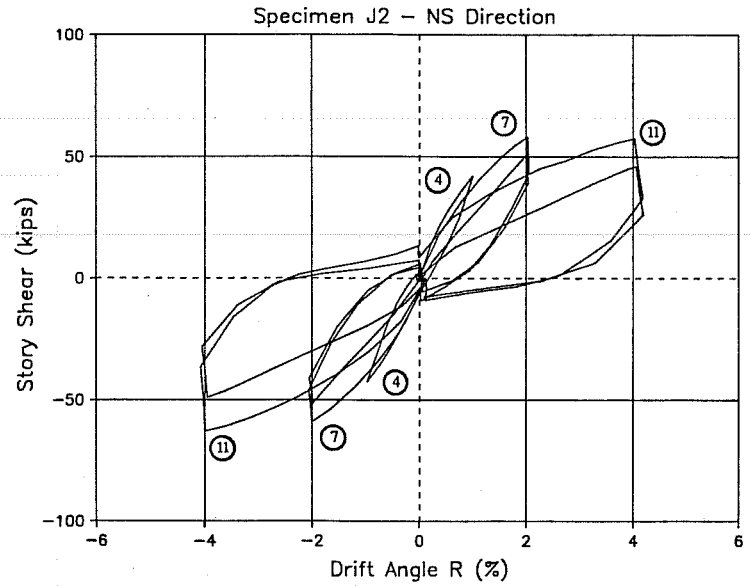

Figure 3.5 Story Shear vs Drift Angle for Specimen J2 (NS Direction)

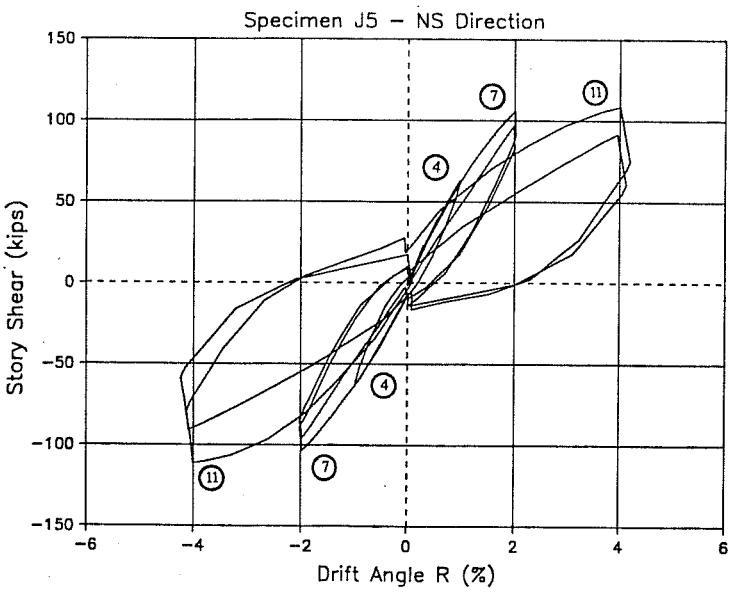

Figure 3.6 Story Shear vs Drift Angle for Specimen J5 (NS Direction)

Table 3.1 shows the maximum measured values of story shear in unidirectional (E-W) and bidirectional loading. Also shown are calculated ultimate story shears assuming beam hinges form next to the joint. The measured value exceeded the calculated value for all specimens. For E-W unidirectional loading, maximum story shear always occurred at cycle 9 (4% drift) in positive loading. The biaxial resultant shown in the same table is defined as the maximum value of the square root of sum of the squares of E-W and N-S story shears obtained during bidirectional cycles. These values were maximum at the positive peak of cycle 7 (2% story drift) for specimens J4 and J5, and at the positive peak of cycle 11 (4% story drift) for specimens J2 and J6. Although most of the maxima occurred during the 4% story drift cycles, the values obtained at 2% story drift do not differ from the values measured at 4% story drift by more than 5% for bidirectional loading nor by more than 15% for unidirectional loading.

3.2.2. Drift Angle and Story Shear Orbits. Figures 3.7 and 3.8 show story drift angle orbits for specimens J2 and J5. Orbits for specimens J4 and J6 are similar. Loading history was displacement controlled. When displacements were varied in one direction, the drift angle was kept constant in the other direction.

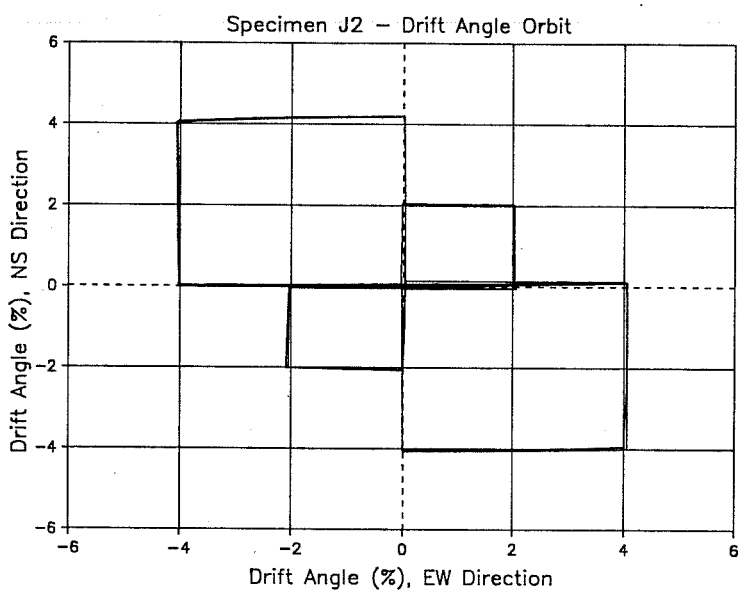

Figure 3.7 Drift Angle Orbit (Specimen J2)

Specimen	Unidirectional Loading (EW)			Bidirectional Loading					
	Calculated Story Shear (kips)	Measured Maximum Story Shear (kips)	Cycle no.	Calculated Story Shear		Measured Maximum Story Shear		Measured Biaxial Resultant (kips)	Cycle no.
				EW	NS	EW	NS		
J2	48.7	72.0	9/pos	48.7	48.7	37.6	63.0	73.4	11/pos
J4	54.6	67.0	9/pos	54.6	54.6	42.6	55.0	69.6	7/pos
J5	80.2	123.9	9/pos	80.2	79.3	86.9	105.8	136.9	7/pos
J6	88.1	114.7	9/pos	88.1	88.6	72.4	107.6	129.7	11/pos

Table 3.1 - Story Shear in Unidirectional and Bidirectional Loadings

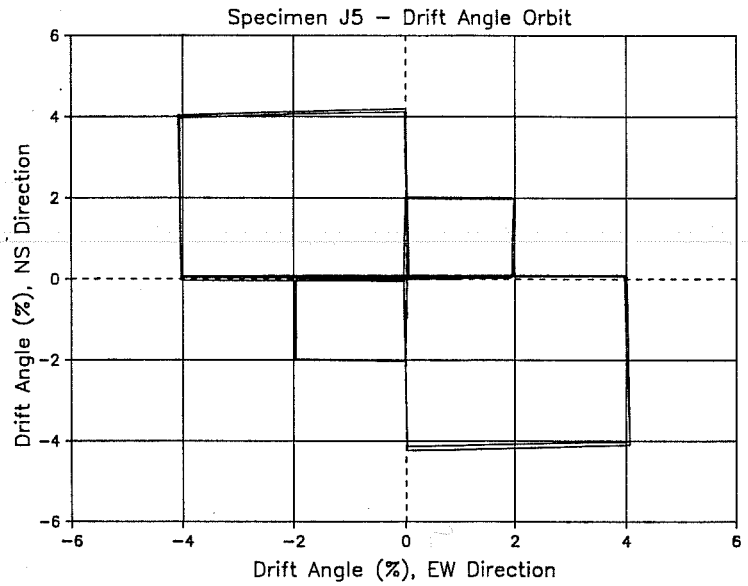

Figure 3.8 Drift Angle Orbit (Specimen J5)

Figures 3.9 and 3.10 show story shear orbits for specimens J2 and J5. When deformations changed in one direction, story shear in the other direction changed even though the drift angle remained constant at the peaks of bidirectional cycles (2% and 4% drift) and at zero story drift. The orbits are nearly symmetrical along the diagonal. A small decrease in the story shear occurred during the second loading cycle at a given drift level. The loss was higher for 4% bidirectional drift cycles (quadrants 2 and 4).

3.2.3. Crack Patterns. Crack patterns are important to assess visually the damage during a given loading cycle. Figures 3.11 through 3.14 show crack patterns at the end of the test for specimens J2, J4, J5 and J6. The east view shows the north and south beams and the east side of the column. The south view shows east and west beams and the south side of the column. Also, cracking at the top surface of the slab is shown.

In general, the most severe concrete cracking and spalling occurred in or around the joint region. This was expected since the specimens were designed to fail in joint shear, and beam plastic hinges were anticipated to form next to the column face.

3.2.3.1. Specimens J2 and J4. Cracking of specimen J2 was very similar to that of specimen J4 (Figures 3.11 and 3.12). During the first loading cycle, flexural cracks developed in the E-W beams, column and slab. During cycle 3 (1% drift) joint shear cracks appeared in the southeast corner of the joint, flexural slab cracks extended from top to bottom of

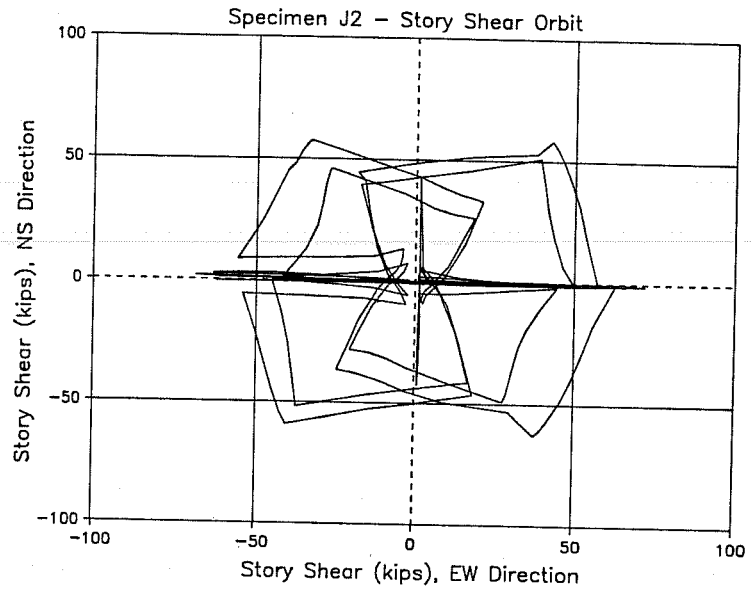

Figure 3.9 Story Shear Orbit (Specimen J2)

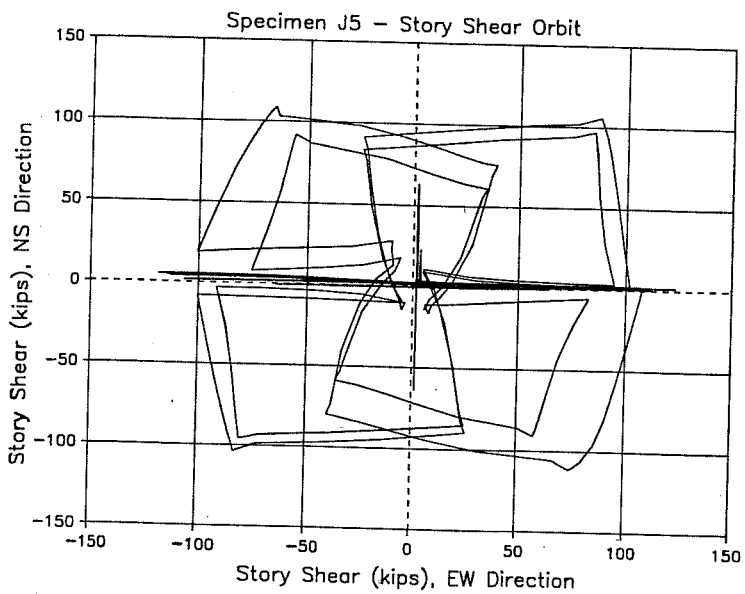

Figure 3.10 Story Shear Orbit (Specimen J5)

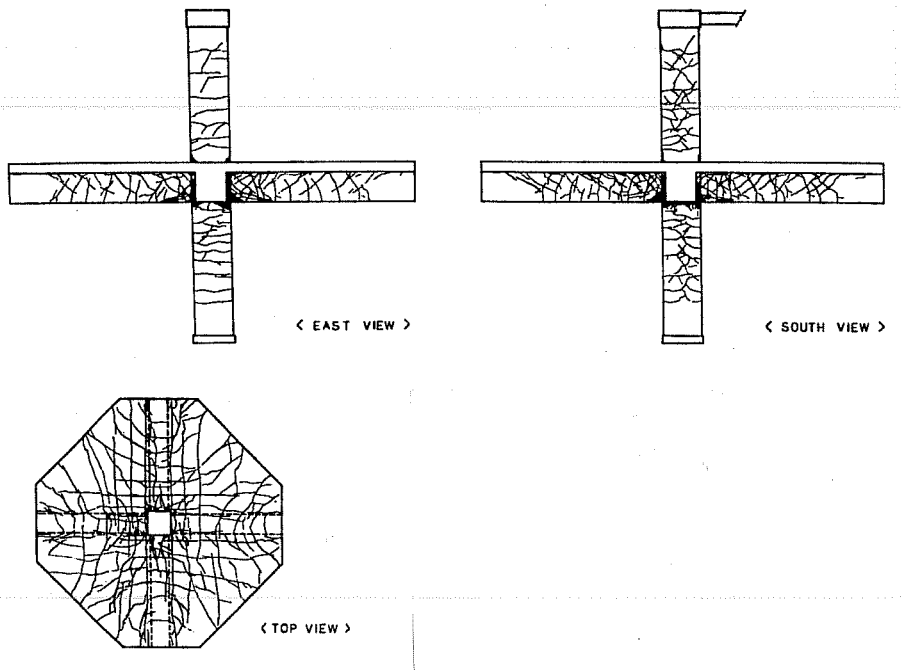

Figure 3.11 Crack Patterns for Specimen J2

the slab, and torsional cracks formed in north and south beam ends. Inclined flexure-shear cracks developed in E-W beams, some extending from flexural slab cracks on the bottom of the slab. In regions of higher bending moment in the slab, cracks extended across the entire width of the slab, and propagated through the entire slab depth.

In the N-S direction (cycle 4, 1% story drift), flexural cracks developed in N-S beams, east and west column faces, and in the E-W direction of the slab. Inclined flexure-shear cracks appeared in N-S beams. Torsional cracks appeared in E-W beams in specimen J4. For specimen J2, torsional cracks appeared in E-W beams in bidirectional cycle 7 (2% drift).

During cycle 5 (2% story drift), inclined shear cracks appeared in the upper column. Small vertical cracks formed in the lower column near the joint region in specimen J2. In specimen J4, these vertical cracks formed during cycle 7 (2% drift).

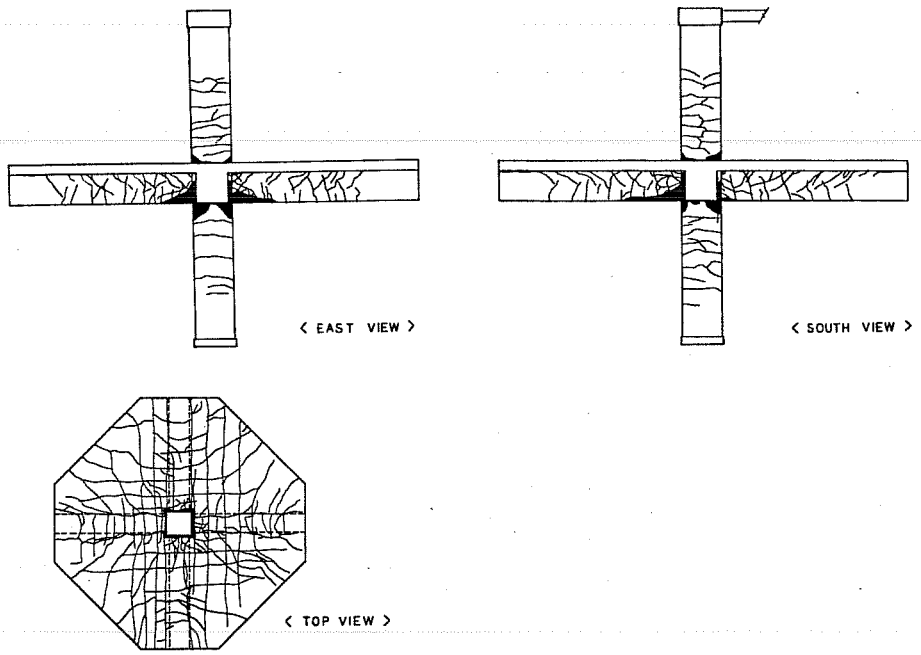

Figure 3.12 Crack Patterns for Specimen J4

During cycle 7, inclined shear cracks formed in the lower column. First crushing and spalling of concrete occurred at upper and lower column ends near the northeast and southwest corners of the joint and, for specimen J2, at the bottom of the east beam. During cycle 9 (4% story drift), crushing of joint concrete continued to the southeast corner of the joint and, for specimen J4, concrete spalling occurred in the east and west beam bottom faces. During bidirectional loading (cycle 11, 4% drift) more concrete crushing occurred in the top of the slab near column corners. The slab had a confining effect on the top part of the joint, since cracking in the joint region below the slab did not propagate to the column above the slab.

Most concrete crushing and spalling occurred in final stages of loading and was concentrated in corners of the joint and in beam bottom faces. Some bottom beam bars and column bars in the joint region were exposed at the end of the test.

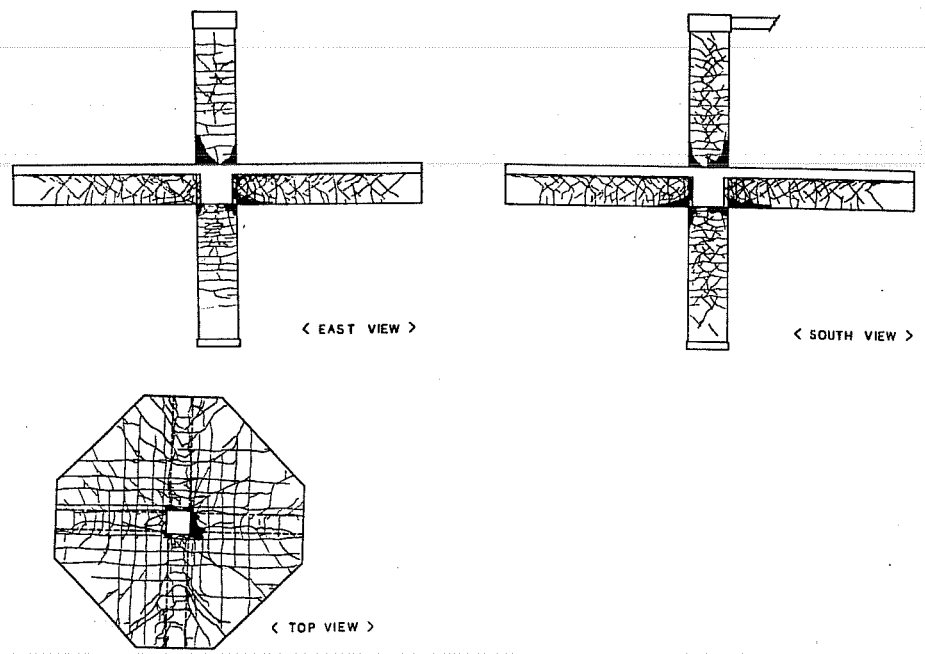

Figure 3.13 Crack Patterns for Specimen J5

3.2.3.2. Specimens J5 and J6. Crack patterns for specimen J5 are quite like those of specimen J6 (Figures 3.13 and 3.14). Furthermore, crack patterns for the high strength concrete specimens are similar to crack patterns for the normal strength concrete specimens. The most important differences are described below.

An important distinction observed in crack patterns for the normal and high strength concrete specimens is the presence of splitting cracks in the members of specimens J5 and J6. During cycle 5 (1% drift), horizontal splitting cracks formed on the side faces of east and west beams at the level of the bottom reinforcement. During cycle 7 (2% drift), vertical splitting cracks formed in the middle of the east and west sides of the upper and lower columns. In addition, the number of horizontal splitting cracks in the beams increased. Similar splitting cracks did not form in normal strength concrete specimens.

Cracking and spalling of concrete in the joint region was not as pronounced as in specimens J2 and J4. In specimens J5 and J6 only minor concrete crushing and spalling

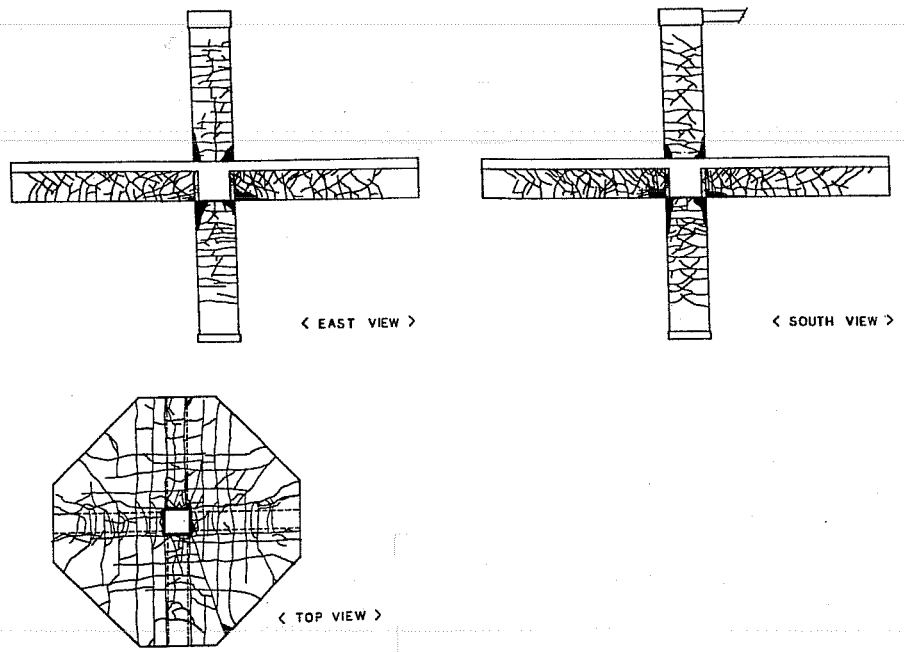

Figure 3.14 Crack Patterns for Specimen J6

occurred before 4% drift cycles. Crushing of the concrete in joint corners did not occur until the last two cycles of the loading history. However, crushing and spalling at corners of the column and in the top of the slab near the column was more pronounced in specimens J5 and J6. Cracking of high strength concrete released larger tensile forces than normal strength concrete and resulted in sudden, rather "violent" cracks which produced loud noises.

3.3 COMPONENTS OF INTERSTORY DRIFT ANGLE

As mentioned in Chapter 2, the elements contributing to interstory drift are beams, columns, and joint. Given the deformation pattern in Figure 2.16 and using the equations provided in Section 2.6, the contribution of each of these elements can be related to story drift angle R by the following equation.

$$R = \left(1 - \frac{h_b}{H} - \frac{h_c}{L}\right) * \gamma + \theta_b + \theta_c$$

Where:

R = interstory drift angle

γ = joint shear distortion

$(1 - \frac{h_b}{H} - \frac{h_c}{L}) * \gamma$ =joint contribution to the drift angle

θ_b = beam tip deflection angle; beam contribution

θ_c = column tip deflection angle; column contribution

Given the deflection level, the instrumentation necessary to implement the above equation is shown in Figure 2.17. The beam tip deflection angle, θ_b, is sensitive to measurements obtained from the horizontal displacement transducers placed against the vertical side of the joint (vertical angle α). The column tip deflection angle, θ_c, depends mostly on measurements obtained from the vertical displacement transducers placed against the horizontal side of the joint (horizontal angle β).

3.3.1. Story Shear vs Joint Shear Distortion. According to the deformation pattern in Figure 2.16, joint shear distortion γ is given by $\gamma = \alpha$ - β. In these tests, angle α was usually much larger than angle β; sometimes by an order of magnitude. In turn, joint shear distortion was sensitive to variations in measurements obtained on the vertical side of the joint.

Figures 3.15 through 3.18 show story shear versus joint shear distortion in the E-W direction for specimens J2, J4, J5 and J6. These figures show larger joint distortion in negative loading when the beam on the same side of the horizontal transducers measuring angle α was displaced upwards. The larger shear distortion in negative loading in the E-W direction and, in positive loading in the N-S direction was due to locating the instrumentation in the southeast corner of the joint. This property of the measuring system also occurred during tests of specimens in the U.S.-Japan-New Zealand Research Project [5].

Joint degradation in shear is greater for normal strength concrete specimens through 2% story drift levels. In addition, high strength concrete specimens showed very narrow loops especially up to 2% story drift levels. All specimens showed significant increase in joint distortion at 4% story drift levels, especially in bidirectional loading. Bidirectional interaction is clear since values of joint distortion increased in one direction when loading in the other direction was applied.

In general, joint shear distortion was larger in normal strength concrete specimens. This occurred throughout the entire loading history. Distortions close to 3% were measured in specimens J2 and J4, while the high strength concrete specimens J5 and J6 rarely had

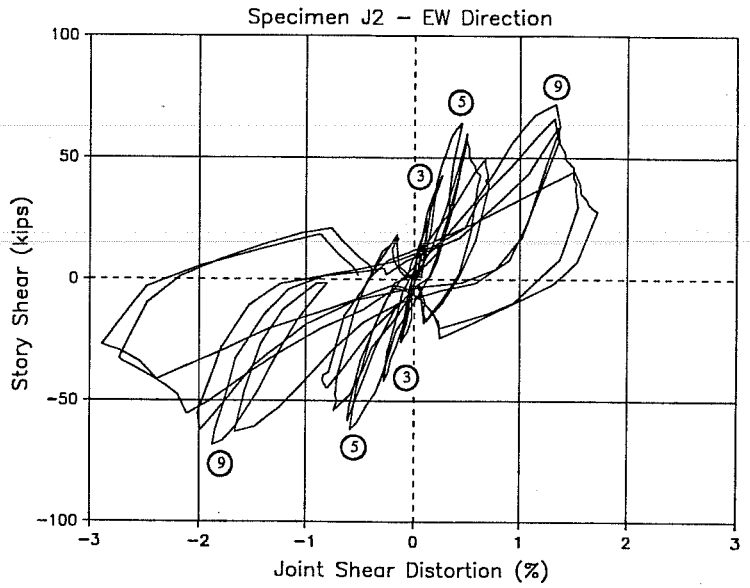

Figure 3.15 Story Shear vs Joint Distortion for Specimen J2 (EW Direction)

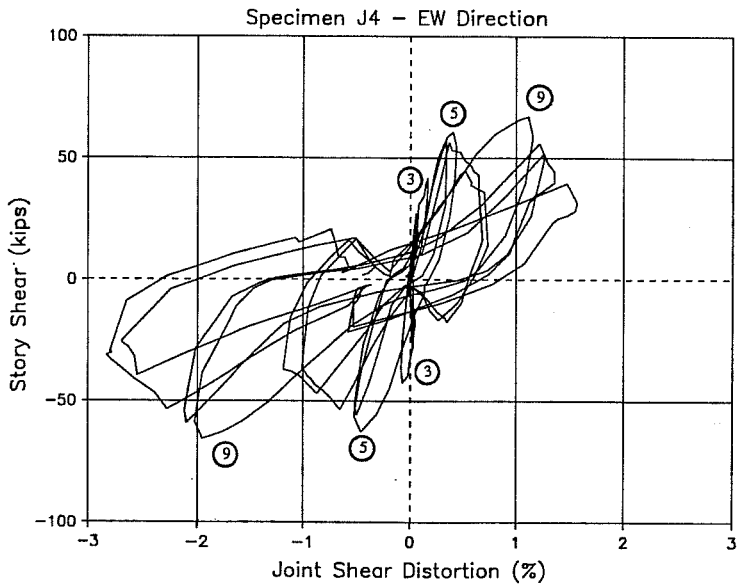

Figure 3.16 Story Shear vs Joint Distortion for Specimen J4 (EW Direction)

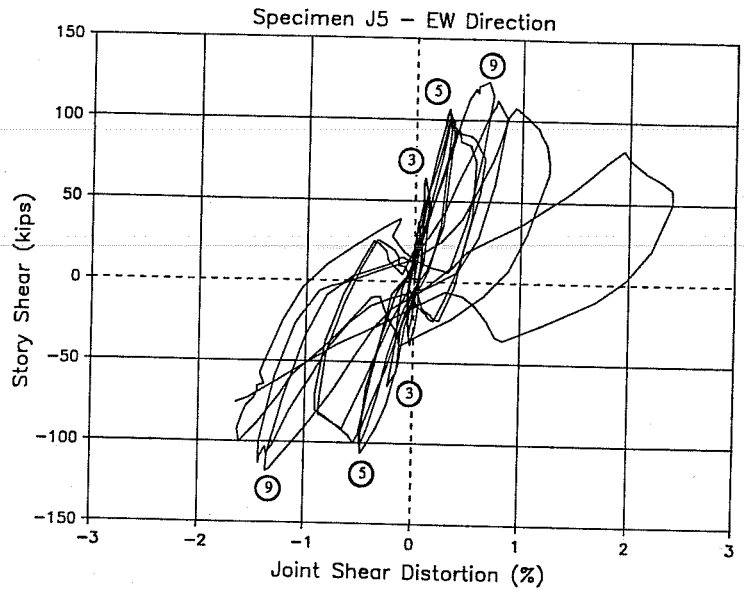

Figure 3.17 Story Shear vs Joint Distortion for Specimen J5 (EW Direction)

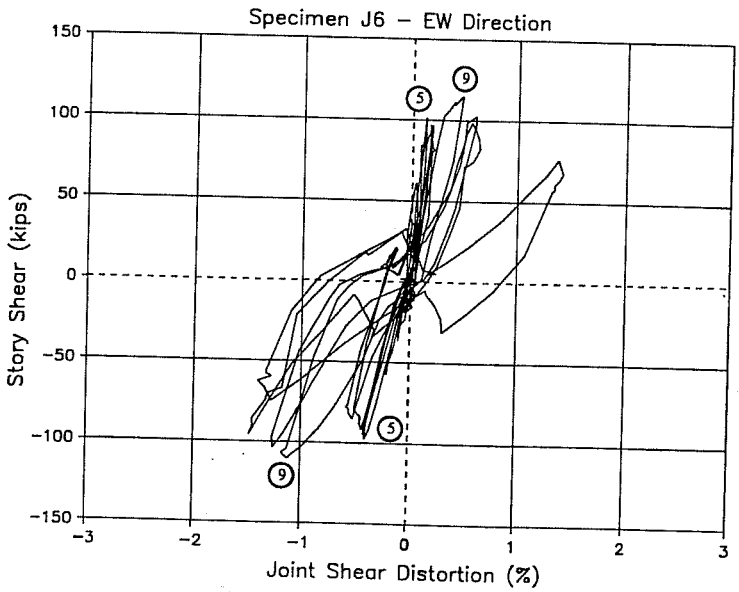

Figure 3.18 Story Shear vs Joint Distortion for Specimen J6 (EW Direction)

joint distortions in excess of 2%. Although joint distortions in specimens J2 and J4 are almost identical, specimen J6 shows slightly smaller values compared with specimen J5.

3.3.2 Story Shear vs Column Tip Deflection Angle. Figures 3.19 and 3.20 show story shear versus column tip deflection angle θ_c for specimens J2 and J5 (E-W direction). Curves for the high strength steel specimens J4 and J6 are very similar.

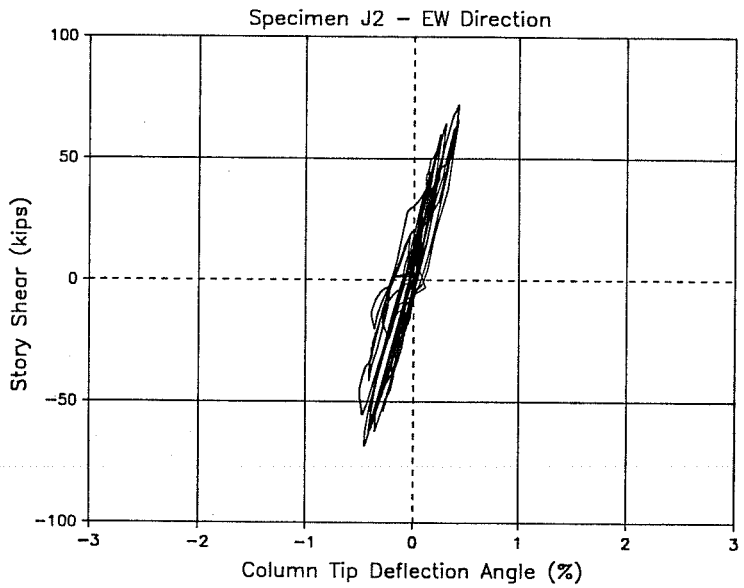

Figure 3.19 Story Shear vs Column Tip Deflection Angle for Specimen J2 (EW Direction)

In general, column tip deflection angle was the smallest of all three components of story drift angle. This comes from the strong column- weak beam design philosophy where the column should be the strongest element of the subassembly. Hysteresis loops are extremely narrow indicating generally elastic behavior. Overall, values of θ_c were usually lower than 1%. High strength concrete specimens reached the larger values of θ_c.

3.3.3. Story Shear vs Beam Tip Deflection Angle. Figures 3.21 and 3.22 show story shear versus beam tip deflection angle θ_b for specimens J2 and J5 (E-W direction). Curves for high strength steel specimens J4 and J6 are very similar.

Overall, beam deformations contributed the most to interstory drift angle. Maximum beam tip deflection angles ranged from approximately 3% in positive bending to just over 2% in negative bending. The beam tip deflection angle is more sensitive to values of

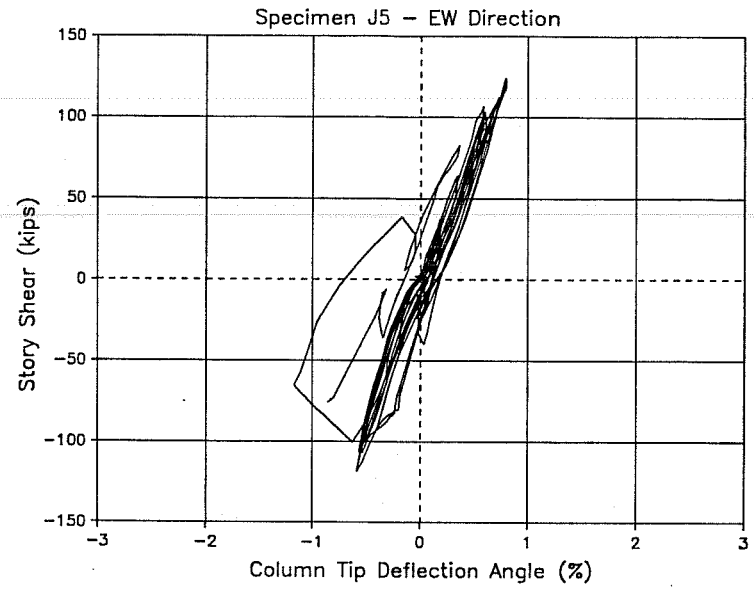

Figure 3.20 Story Shear vs Column Tip Deflection Angle for Specimen J5 (EW Direction)

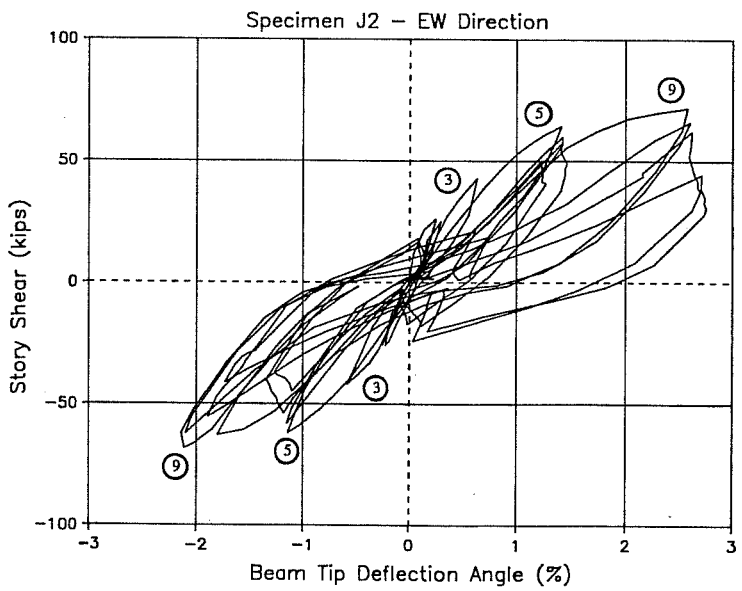

Figure 3.21 Story Shear vs Beam Tip Deflection Angle for Specimen J2 (EW Direction)

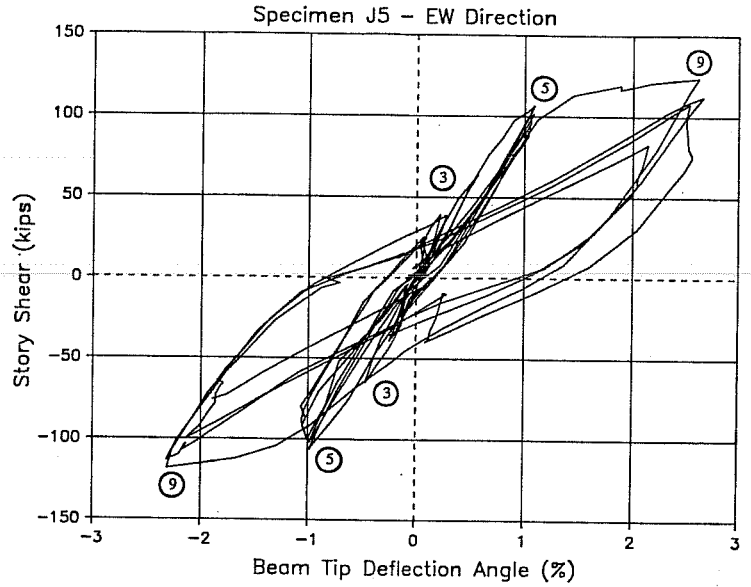

Figure 3.22 **Story Shear vs Beam Tip Deflection Angle for Specimen J5 (EW Direction)**

angle α. This difference is due to placement of horizontal transducers in the southeast corner of the joint, as previously discussed.

The curves show pinched hysteresis loops, especially at higher drift levels. Very narrow loops occurred in curves for high strength concrete specimens up to 2% bidirectional drift. A significant increase in the beam component occurred when loading to the 4% drift level (cycle 9). The maximum value of θ_b in cycle 8 was 1.25%, increasing to 2.6% in cycle 9 for specimen J2. More significantly, for specimen J5 the maximum value of θ_b in cycle 8 was 1.0% and increased to 2.63% in cycle 9. This significant increase is probably due to formation of plastic beam hinges at the column face.

3.3.4. Member End Deformations. Column and beam end rotations were measured for all specimens. Instrumentation for beam end rotations is shown in Figure 2.18, and for column end rotations is shown in Figure 2.19. Member end deformations include flexural deformations, bar slip through the joint, and crack opening. Shear deformations are neglected.

Beam end rotations were measured over two regions of the beam (Figure 3.23). Region 1 is the portion of the beam between the column face and approximately 4 inches away from the column face. Region 2 is the next 12 inches of the beam. Measurements within region 1 were taken for all four beams, and measurements within region 2 were taken for

east and north beams only. Average curvatures within these regions are obtained by dividing rotations by the length of the region (typically, 4 inches for region 1 and 12 inches for region 2). Displacement transducers for beam end rotations in region 1 were placed against the column approximately 2 inches above and below the surface of beams. Therefore, measurements include any column deformations within these 4 inches.

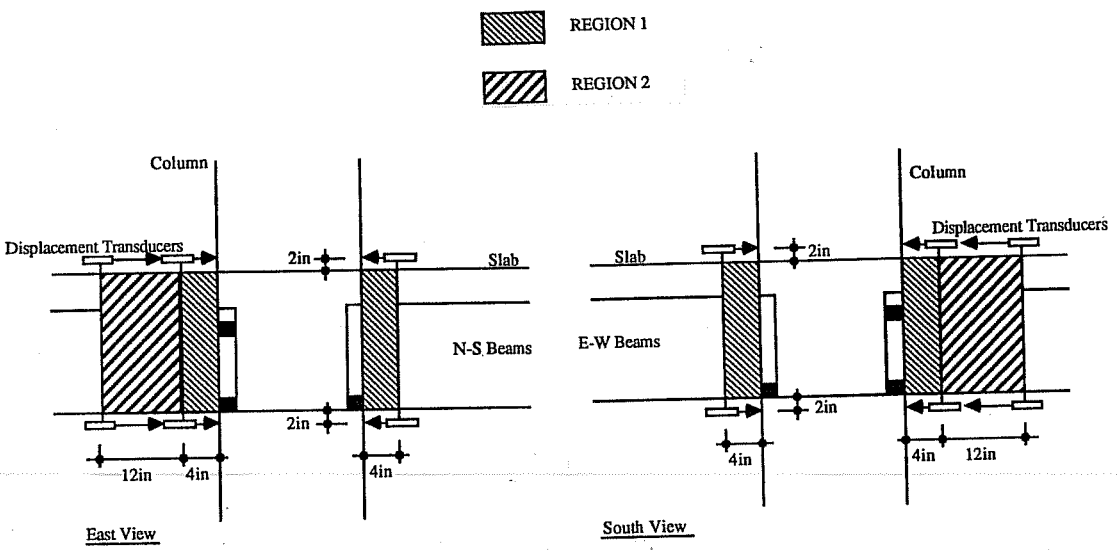

Figure 3.23 Beam Regions for Curvature Calculations

Figures 3.24 through 3.27 show beam shear versus beam end curvature for region 1 of the west beam of specimens J2, J4, J5 and J6. Curves for region 1 of the other 3 beams are very similar to curves shown in these figures (fewer cycles for the N-S beams). In general, normal strength concrete specimens showed larger curvatures. High strength concrete specimens showed very narrow loops through 2% story drift. In the first cycle at 4% story drift (cycle 9), specimens J5 and J6 show a well defined yield plateau in negative shear. Although this plateau exists in curves for specimens J2 and J4, it is not as clear. Large inelastic deformations and pinching of the hysteresis loops is significant at 4% story drift cycles. Most peak curvature values were under 4 miliradians/inch.

Figure 3.28 shows beam shear versus beam end curvature for region 2 of the east beam of specimens J2. Curves for region 2 for other beams and for beams of other specimens are very similar. Curvature values are very small, usually below 0.5 miliradians/inch (slightly

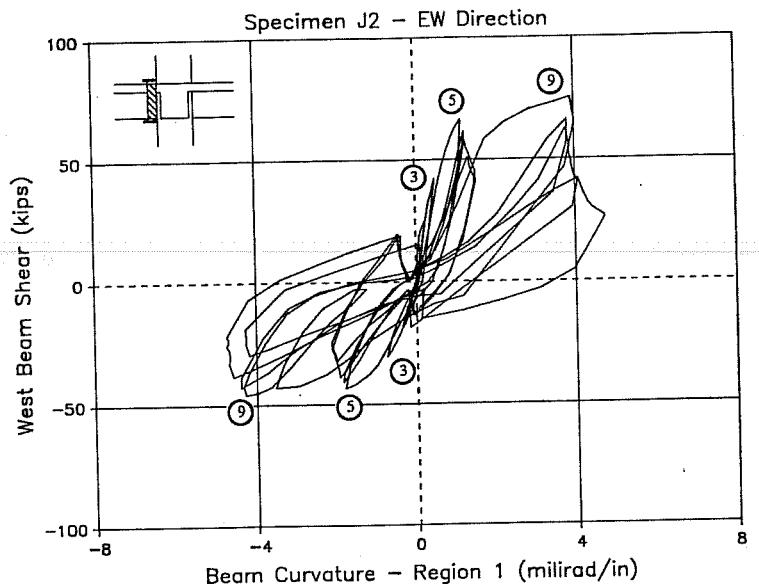

Figure 3.24 West Beam Shear vs Beam Curvature for Specimen J2

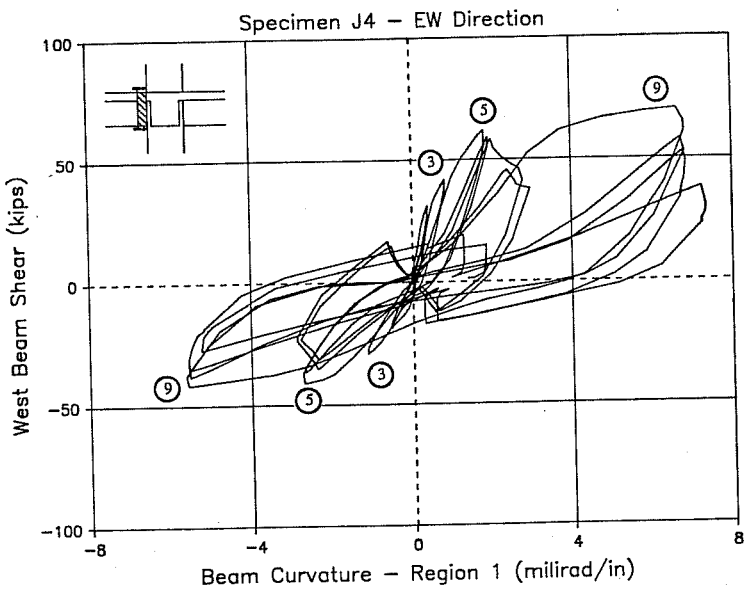

Figure 3.25 West Beam Shear vs Beam Curvature for Specimen J4

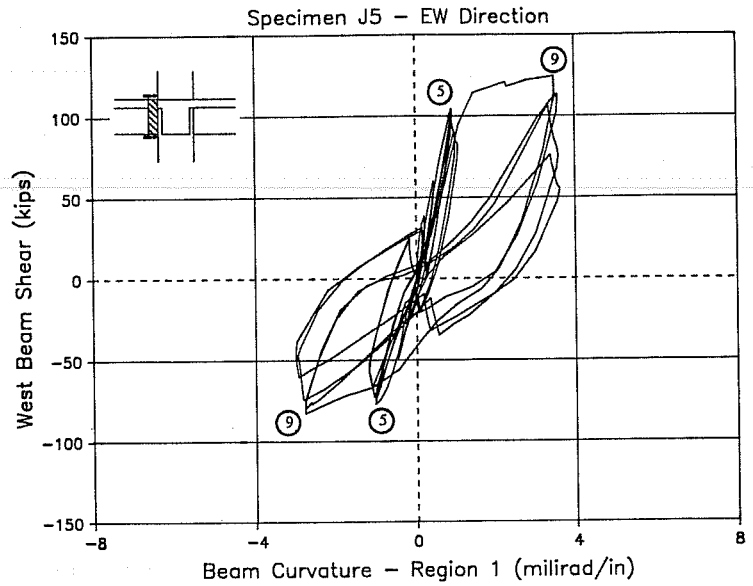

Figure 3.26 West Beam Shear vs Beam Curvature for Specimen J5

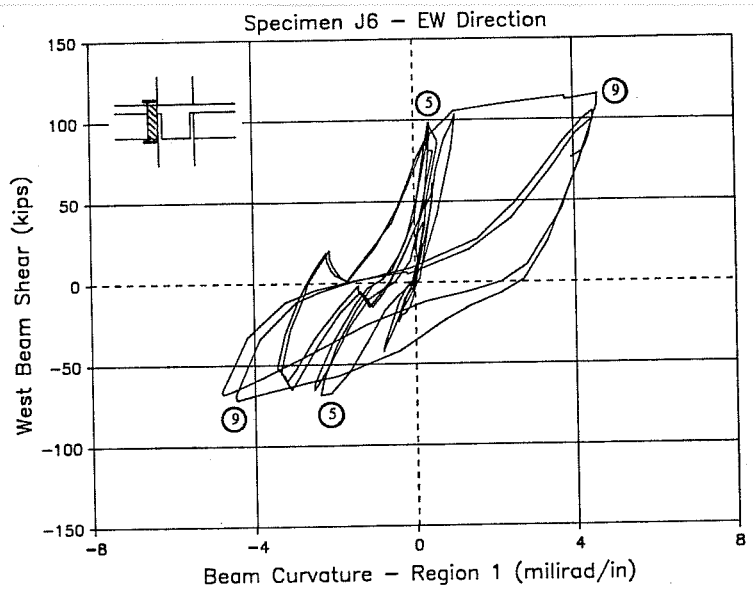

Figure 3.27 West Beam Shear vs Beam Curvature for Specimen J6

higher in the high strength concrete specimens). A linear behavior can be observed especially up to 4% story drift. Some growth of the plastic hinge seemed to occur into region 2 in the later cycles of the loading history, but the section remained largely elastic.

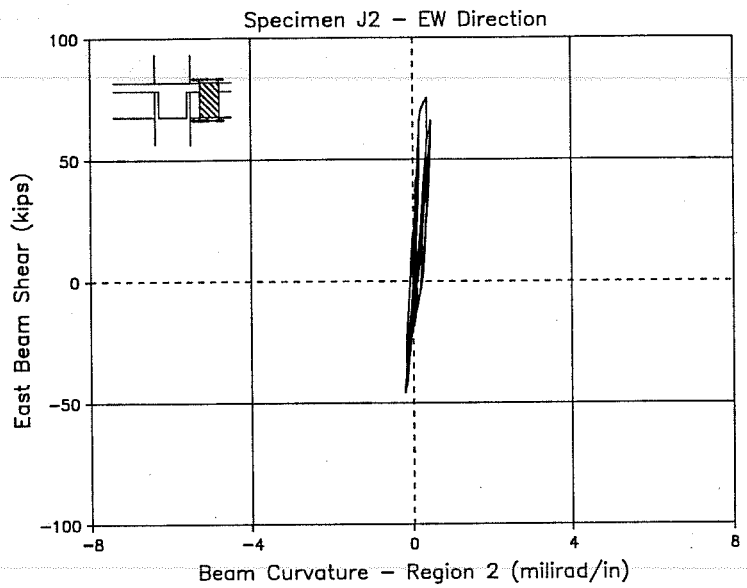

Figure 3.28 East Beam Shear vs Beam Curvature for Specimen J2

Column end rotations were measured using the instrumentation shown in Figure 2.19. Displacement transducers were placed approximately 4 inches from the beam surface. Therefore, beam deformations in the direction of the transducers are included in these measurements. Measurements taken in later cycles of the test tend to be questionable due to spalling and crushing of the concrete at the top of the slab and at the bottom of beams near the joint, where the transducers bear against the concrete.

Figures 3.29 and 3.30 show story shear in the E-W direction versus upper column curvature for specimens J2 and J5. Similar curves are available for specimens J4 and J6. These figures show behavior of the column end is more elastic compared to beam curvatures, especially through 2% drift cycles. Smaller values of curvature were measured. The curves show narrower loops up to 2% story drift. Inelastic deformations occurred at the 4% drift cycles, particularly in positive loading and are probably due to the significant amount of spalling of the concrete that generally occurred in the positive part of the first cycle at 4%

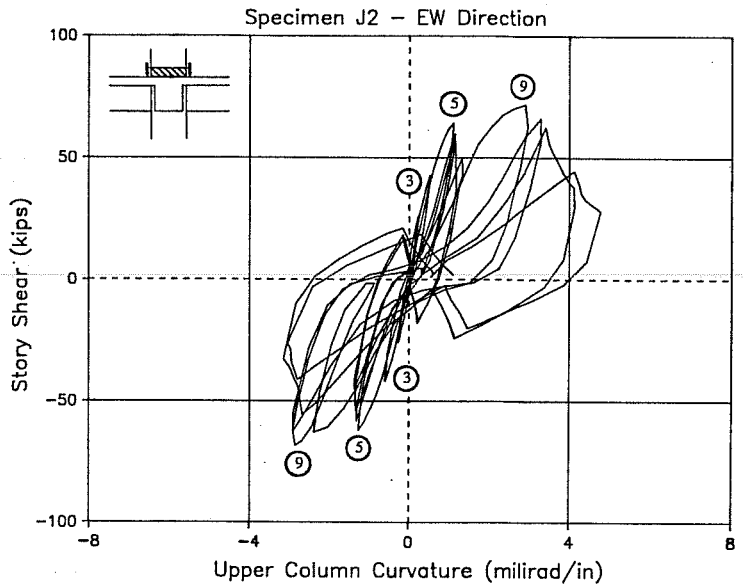

Figure 3.29 **Story Shear vs Column Curvature for Specimen J2 (EW Direction)**

story drift (cycle 9/pos). The transducers bear against spalled and crushed slab and/or beam concrete which contributes to bias in the measurements.

According to the assumed deformation pattern shown in Figure 2.16, the beam tip deflection angle should be larger than beam end rotation, and column tip deflection angle should also be larger than the column end rotation. This was generally true for beam measurements, but not so for column measurements. Frequently, column end rotation was larger than column tip deflection angle. This is probably due to errors in the measuring system (mentioned previously) and spalling of the concrete cover which affected column measurements more than beam measurements. The reliability of the measurements used to obtain column tip deflections is believed to be greater than those used for column end rotations.

3.4 REINFORCING BAR STRESSES AND STRAINS

Strain gages were placed on slab, beam, column, and joint reinforcing steel. About ninety 5mm strain gages were attached to the bars in each specimen.

Large deformations occurred during 4% drift cycles. Therefore, large strains were expected in the longitudinal reinforcement. A significant number of gages malfunctioned at

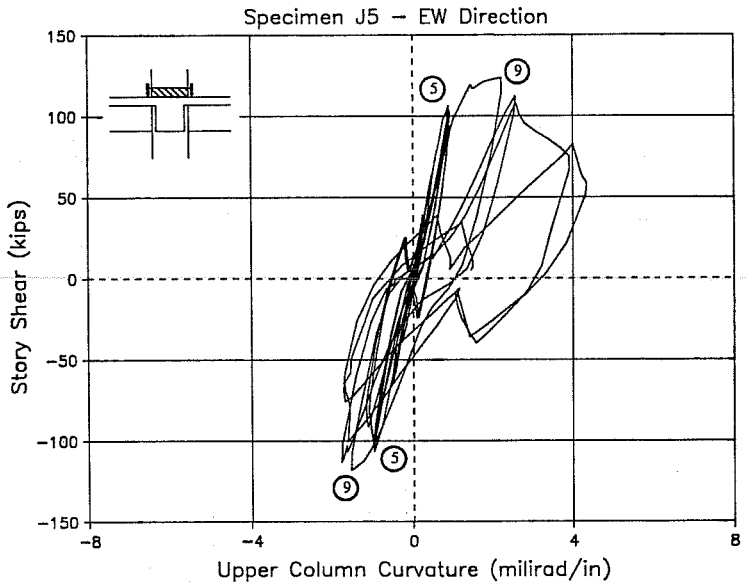

Figure 3.30 Story Shear vs Column Curvature for Specimen J5 (EW Direction)

this stage. Stress analysis became especially difficult for cycles at 4% drift because strains were well above yield strain and reflect changes due to complex previous loading history.

Conversion of strain to stress was done using a FORTRAN computer program run on a personal computer. The stress-strain model used for the conversion takes into account the loading history and the Bauschinger effect on the steel during cyclic loading.

Due to the large number of strain gages used, it is not possible to show graphs indicating stresses and strains measured in all gages. Therefore, figures in this section will show typical strains or stresses at strain gage positions which are considered to best illustrate the conclusions obtained.

3.4.1. Joint Ties. Strain in joint ties was measured by gages placed as shown in Figures 2.24 for specimen J2 and in Figure 2.25 for specimens J4, J5 and J6. Gages were placed on both inner and outer ties. High strength welded wire fabric was used for joint transverse reinforcement in specimens J4 and J6. Grade 60 steel was used in specimens J2 and J5.

Figures 3.31 and 3.32 show story shear versus strain measured from gages CS17 and CS24 for specimen J4. Location of gages CS17 and CS24 is shown in Figure 3.33. Gage CS17 was placed on a joint tie located above beam longitudinal top bars and gage CS24 was

located between beam top and bottom longitudinal bars. In general, strain increased with story drift angle. Mostly tension (positive) strains were measured during the test. Highest strains were measured in ties placed between beam longitudinal bars. Strains measured in ties placed above the beam top bars (level "f") or below beam bottom bars (level "i") were generally lower.

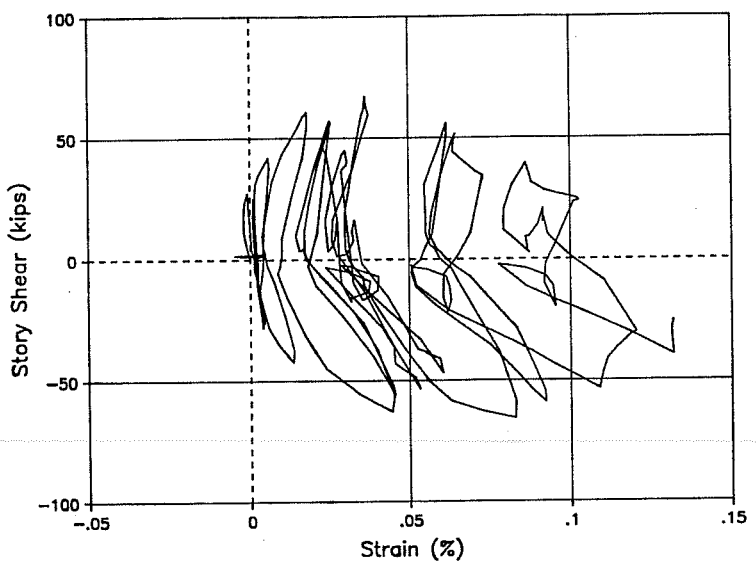

Figure 3.31 Story Shear vs Strain in Gage CS17 (Specimen J4)

None of the gages placed at level "f" showed yielding during the tests. Very few gages placed at level "i" indicated yielding. Most of the joint ties at levels "g" and "h" yielded during cycle 5 or cycle 7. Highest strains during the test occurred at 4% bidirectional drift, and bulging of the joint core at the end of the test was evident. No perceptible difference can be observed between strains measured in ties of high strength steel and strains measured in ties of normal strength steel.

Figure 3.34 shows strains measured at strain gage position X1 for specimen J5. Position X1 is located at the north face of the column as shown in Figure 3.33. The upper plot of Figure 3.34 shows strains measured at positive peaks of unidirectional loading cycles 1, 3, 5 and 9. Strain increase with drift angle is illustrated here, as well as higher strains at ties placed at levels "g" and "h".

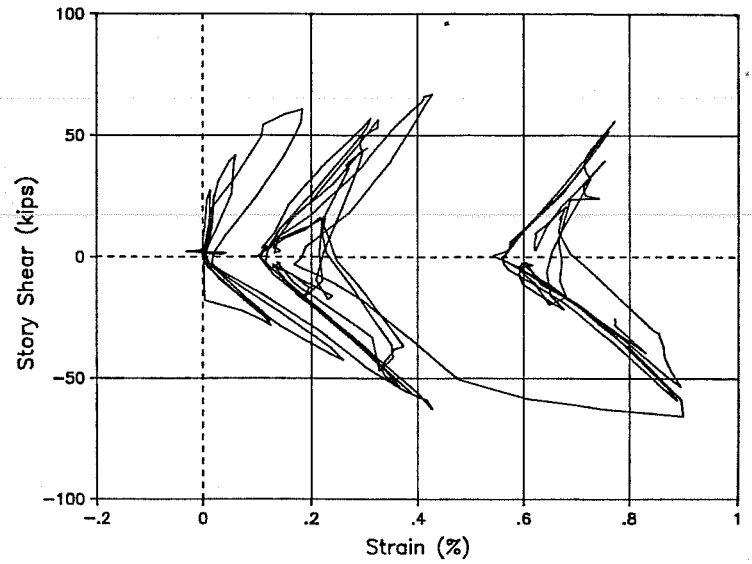

Figure 3.32 Story Shear vs Strain in Gage CS24 (Specimen J4)

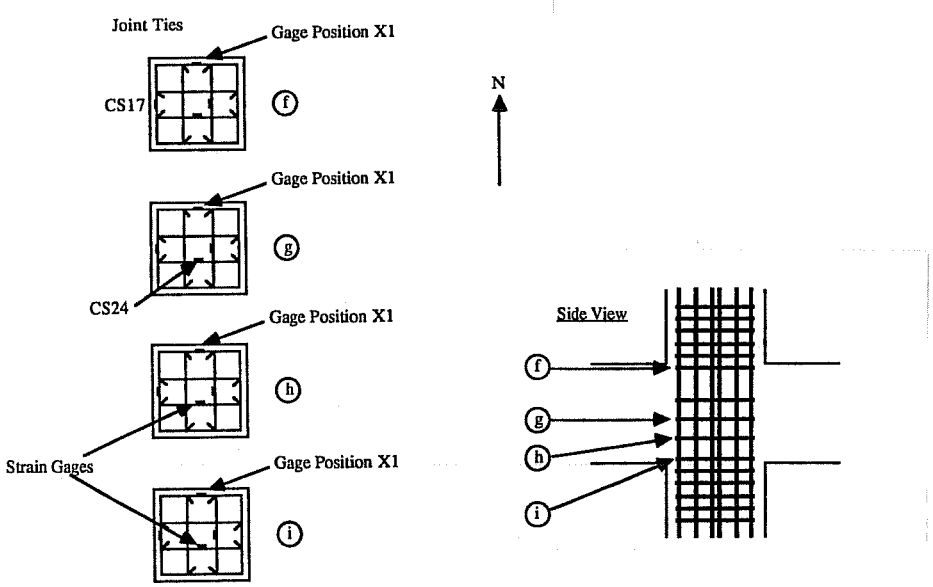

Figure 3.33 Strain Gage Positions on Joint Ties

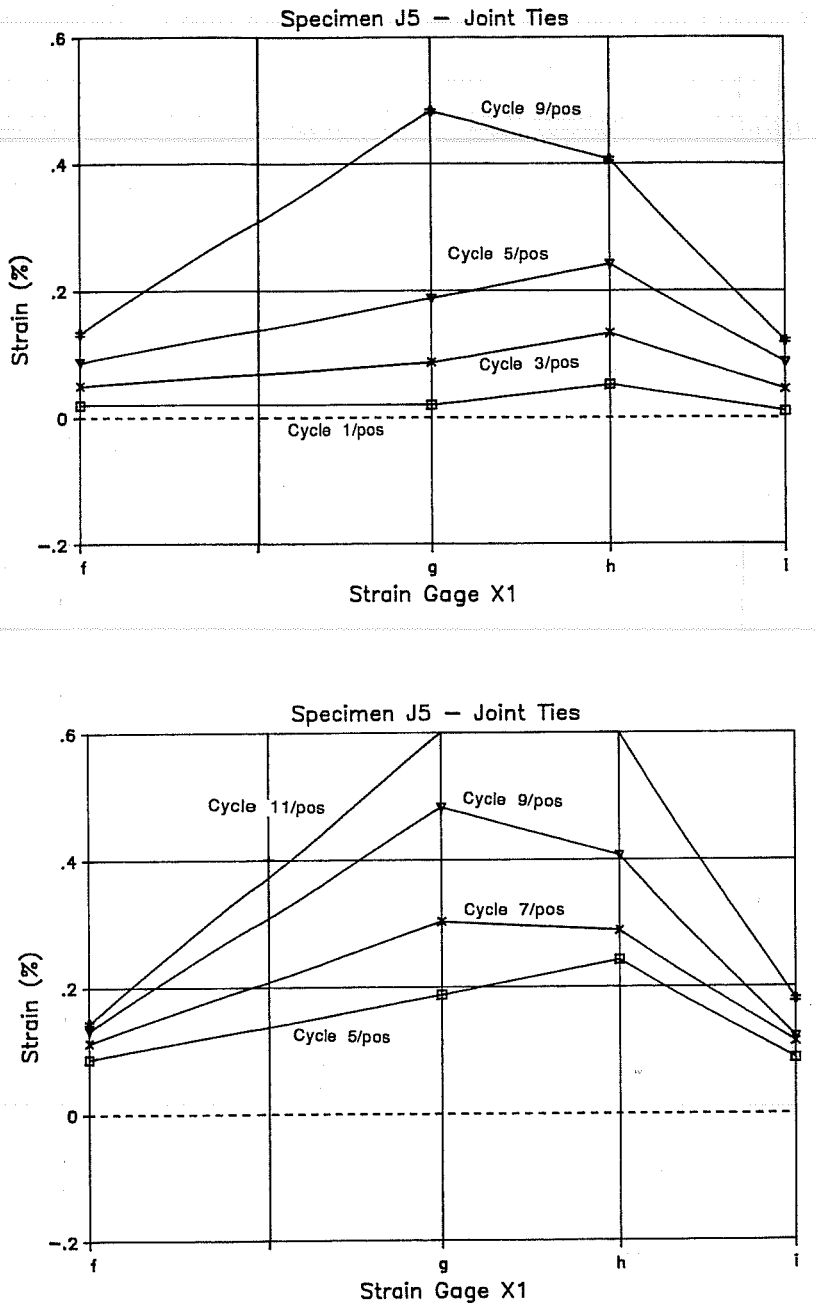

Figure 3.34 Strains in gage position X1 (Specimen J5)

The lower plot of Figure 3.34 shows strains measured at positive peaks of cycles 5, 7, 9 and 11. This plot illustrates the increase in strain during bidirectional loading cycles. In general, bidirectional loading increased strain in inner and outer joint ties. Results indicate the joint reinforcement is effective in confining the joint concrete.

3.4.2. Slab Bars. Strains were measured in top and bottom slab bars located in the southwest quadrant of the specimen. Figure 3.35 shows strain gage positions for slab bars. Position #1 is shown closest to the column, and position #8 is farthest from the column. Top slab bars were placed every 12 inches and bottom slab bars were placed every 24 inches. All slab reinforcement was Grade 60 steel.

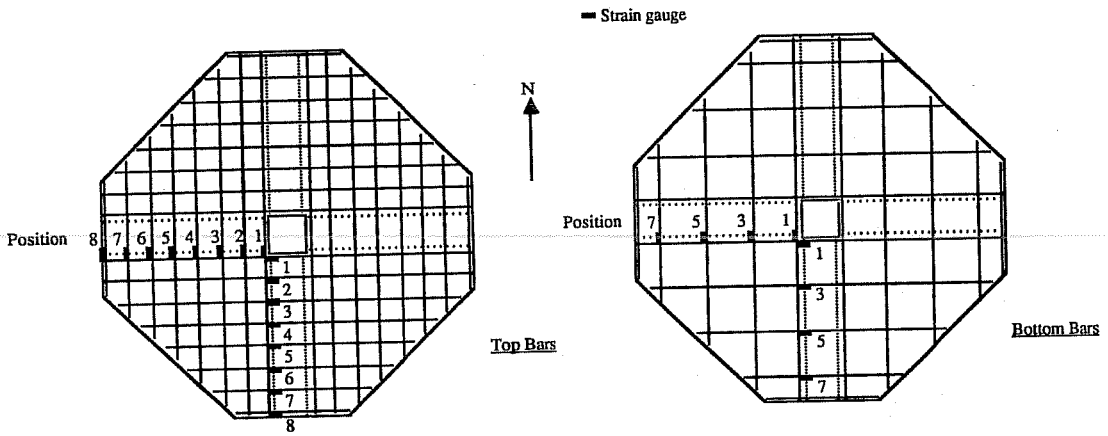

Figure 3.35 Strain Gage Positions for Slab Bars

In general, strain in slab bars increased with story drift angle. Both top and bottom slab bars exhibited tensile strains under positive and negative loadings. First yielding usually occurred in E-W bars located closest to the column (position #1).

In the E-W direction, first yielding occurred during cycle 5/pos for top bars and bottom bars. Exceptions are slab top bars of specimen J5 which yielded during cycle 3/pos and slab bottom bars of specimen J2 which yielded during cycle 9/pos.

E-W unidirectional loading affected strains in N-S slab bars, especially those located farthest from the column (position #8). First yield of top and bottom N-S slab bars

located at position #8 occurred during cycle 5/pos except for specimen J2 which occurred during cycle 9/pos. In general, first yielding of N-S slab bars located closest to the column occurred during 2% bidirectional drift after yielding of bars farthest from the column. Exceptions are for top slab bars for specimens J5 and J6 which yielded during cycle 4/pos.

Bidirectional interaction is clear from yielding of N-S slab bars. Yielding of N-S slab bars located at position #8 before bars located at position #1 yielded is probably due to tensile in-plane horizontal forces generated during E-W loading. In-plane forces generated at the face of the transverse beam imposed bending moments on the slab about the column vertical axis and produced tensile stresses perpendicular to the face of the E-W beam. These N-S slab forces were probably due to force transfer between the loading points (at the beam tips) and the beam-column-joint connection through the slab.

Figures 3.36 and 3.37 show story shear versus strain in slab reinforcement located at position #1 in the E-W direction for specimens J4 and J6. The top graph shows story shear versus strain for a top reinforcing bar and the bottom graph shows story shear versus strain for a bottom reinforcing bar. In this case, positive story shear indicates the slab is in tension (downward loading) and negative story shear indicates the slab is in compression (upward loading). Similar graphs can be shown for specimens J2 and J5.

The increase in strain was much larger during downward loading than during upward loading. Under downward loading, the bars were required to resist the tension forces in the slab. When the load was reversed, cracks closed and the concrete carried most of the compressive forces in the slab; only small compressive strains were measured in the slab reinforcement. With additional upward loading the concrete compression zone was generally above slab bottom bars. Therefore, tension strains were developed in bottom slab bars under both upward and downward loadings.

Larger tensile strains during downward loading indicate both top and bottom bars contributed to negative bending moment in the beams. Large plastic strains were common during 4% drift cycles.

Figures 3.38 through 3.41 show slab bar strains for specimen J4 measured at loading peaks. Top graphs show strains measured in top slab bars and bottom graphs show strains measured in bottom slab bars. Figures 3.38 and 3.39 show strains measured during cycles 1, 3, 5, and 9. Figures 3.40 and 3.41 show strains measured during cycles 4, 7, and 11. Similar figures can be shown for specimens J2, J5 and J6.

Strain increase with drift angle is illustrated. Large tensile strains are shown at 4% drift cycles. In general, strains are larger in slab top bars for a specified drift level. Under E-W unidirectional loading, strains in E-W slab top and bottom bars were largest at bars

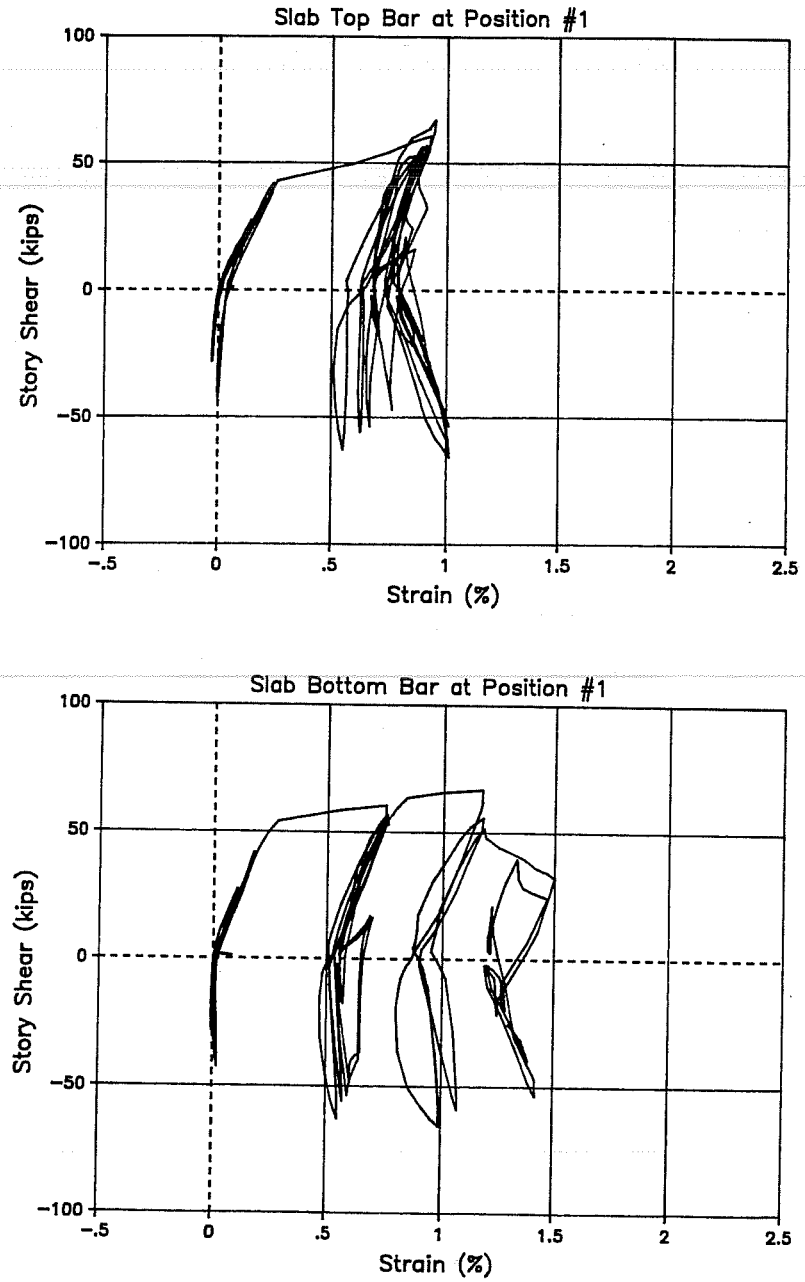

Figure 3.36 - Story Shear vs Strain in East-West Slab Bar (Specimen J4)

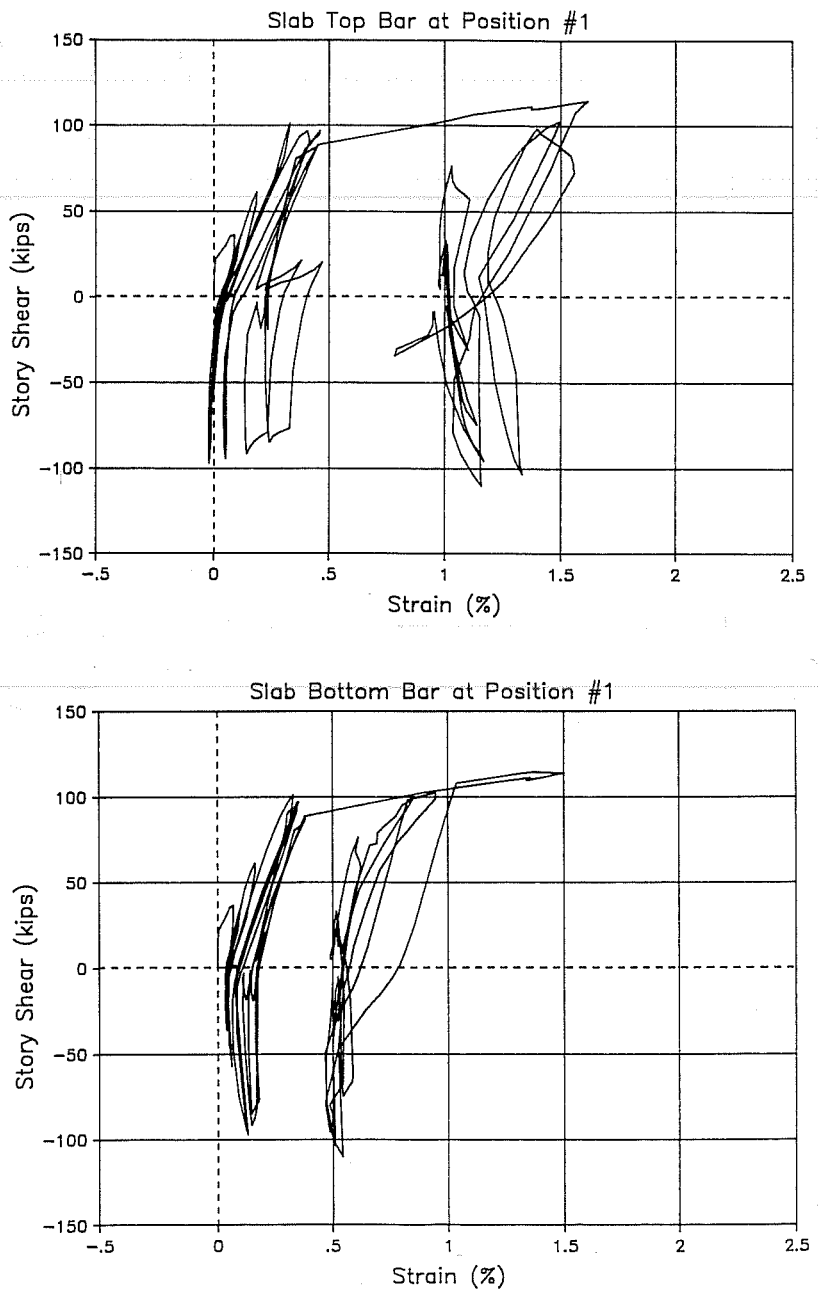

Figure 3.37 - Story Shear vs Strain in East-West Slab Bar (Specimen J6)

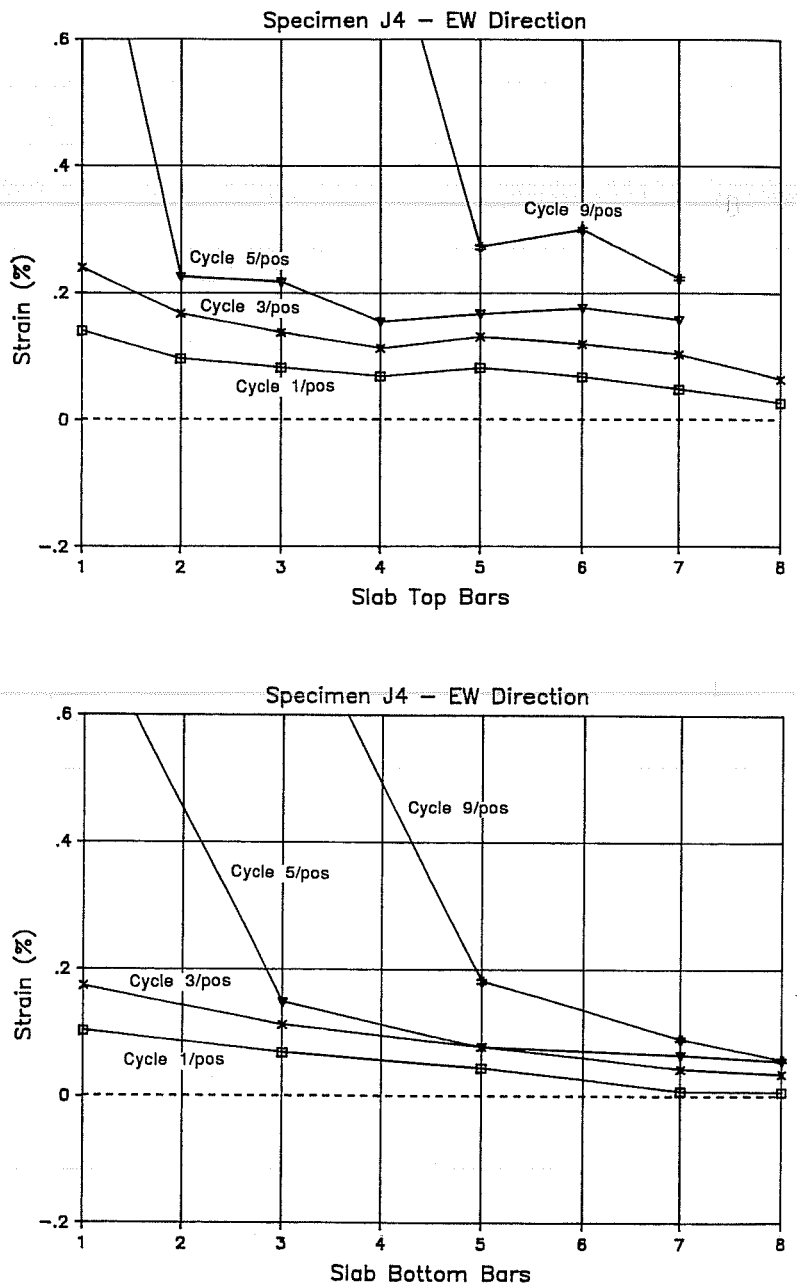

Figure 3.38 - East-West Slab Bar Strains
(Unidirectional Cycles)

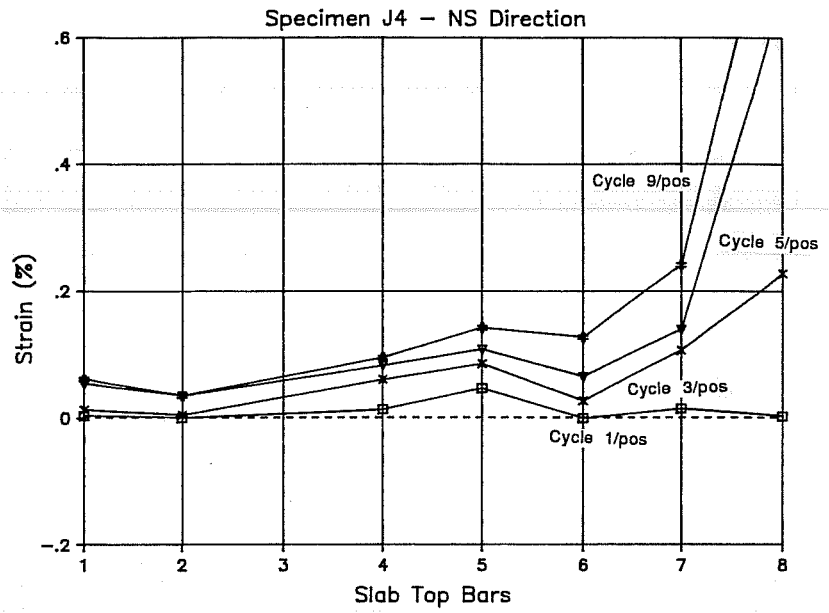

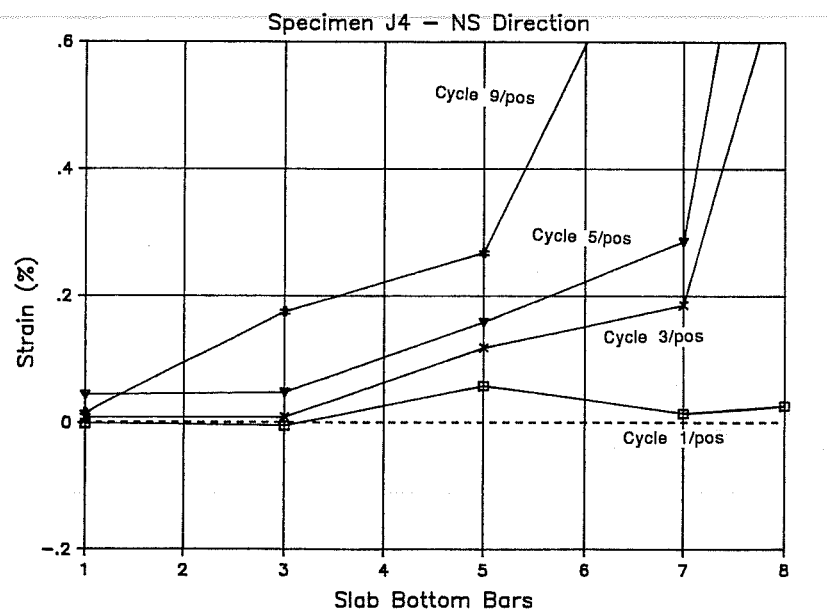

Figure 3.39 - North-South Slab Bar Strains
(Unidirectional Cycles)

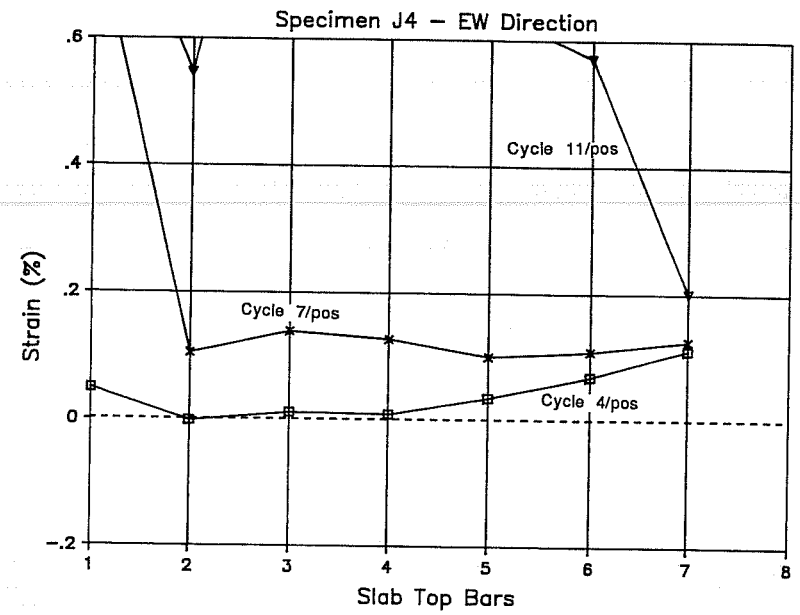

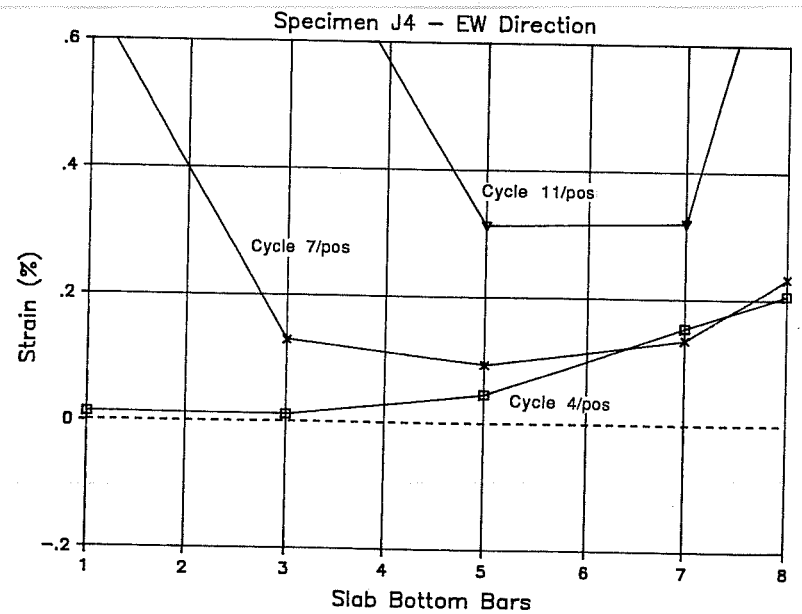

Figure 3.40 - East-West Slab Bar Strains
(Bidirectional Cycles)

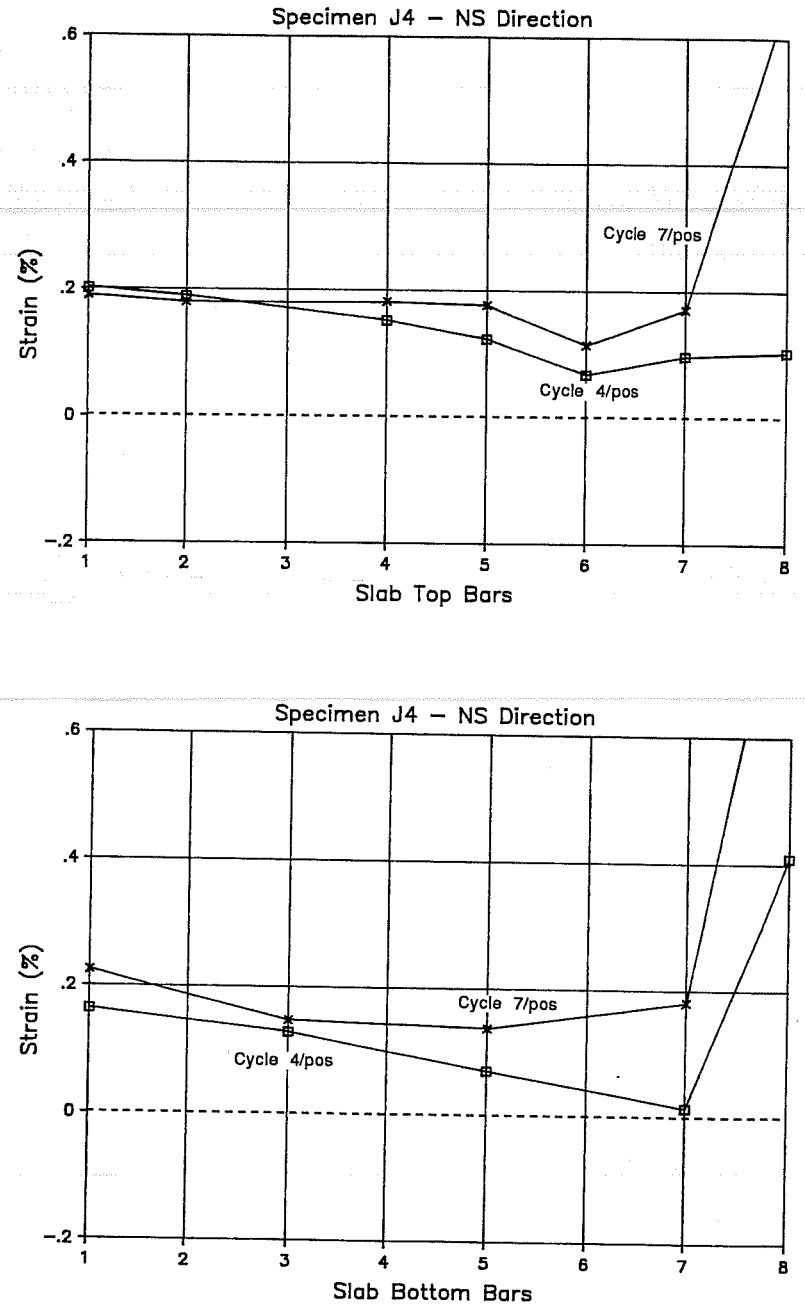

Figure 3.41 - North-South Slab Bar Strains (Bidirectional Cycles)

located near the column (Figure 3.38). Unidirectional E-W loading affected the strains in N-S slab bars. During unidirectional E-W loading, strains were highest in N-S slab bars farthest from the column (Figure 3.39). Highest strains under bidirectional loading occurred at bars located either closest or farthest from the column (Figures 3.40 and 3.41). Under bidirectional loading, slab bar strains were distributed almost uniformly. This is probably due to bidirectional interaction when in-plane forces mentioned previously are generated in one direction while loading in the other direction.

Figures 3.42 and 3.43 show stresses in E-W slab bars of specimens J4 and J6 measured at positive loading peaks of cycles 1, 3, 5, and 9 (slab is loaded downwards). Top graphs show strains measured in top slab bars and bottom graphs show strains measured in bottom slab bars. Similar graphs can be shown for specimens J2 and J5. Stresses were highest at bars closest to the column. Most slab bars had yielded during cycle 9/pos indicating large slab participation. High stresses in bottom slab bars indicate active participation of bottom bars in bending moment capacity. These slab bar stresses will be used later to evaluate slab contribution to beam bending moment capacity when the slab is in tension (Section 4.7).

3.4.3. Beam Bars. Strain gages were placed on top and bottom longitudinal beam bars as shown in Figures 2.22 for specimen J2 and 2.23 for specimen J6. Positioning of gages in specimens J4 and J5 is very similar to that of specimens J2 and J6.

Figure 3.44 shows nomenclature for strain gage positions in beam bars to be used in remaining figures of this section. Positions "a" through "h" refer to gages in top bars and positions "i" through "p" refer to gages in bottom bars. Positions "x" through "w" refer to gages located outside the joint. Some specimens have two layers of top bars. The uppermost layer is referred to as "top layer" and the second layer is referred to as "lower layer". If two layers of bottom bars exist, the layer closest to the beam bottom is referred to as "bottom layer" and the second layer is referred to as "upper layer".

Table 3.2 shows location of the longitudinal reinforcing bars. Location of slab and beam bars are indicated with respect to the top surface of the slab. This table is shown here because placement of the longitudinal bars with respect to position of the neutral axis is important for strain analysis.

Stress and strain analysis focused on E-W bars since E-W was the main loading direction. Results obtained for N-S longitudinal beam bars are very similar. Since N-S bars were placed below E-W bars, some differences occurred but were due primarily to the position of the longitudinal bars with respect to the neutral axis.

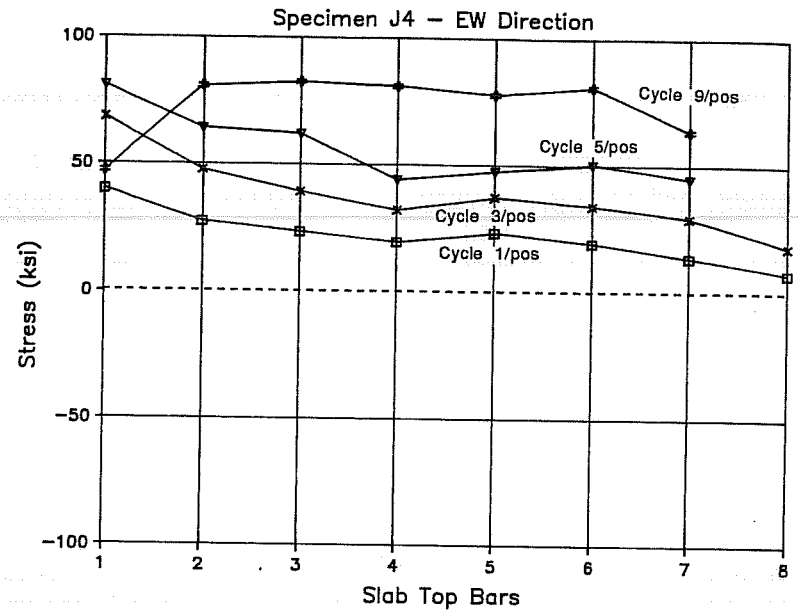

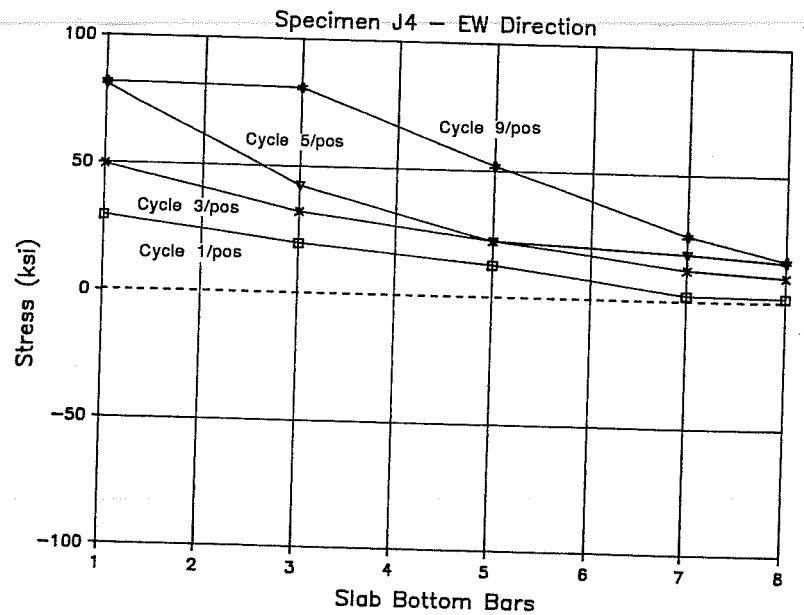

Figure 3.42 - East-West Slab Bar Stresses (Specimen J4)

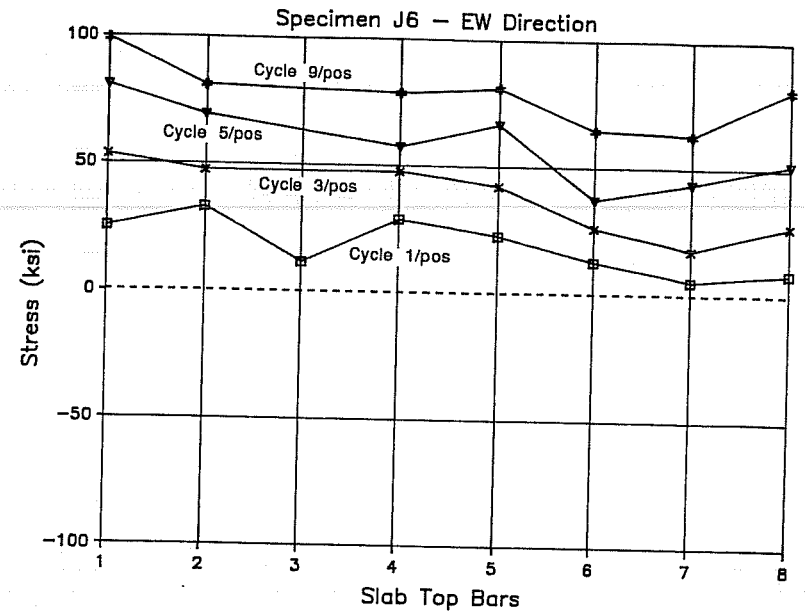

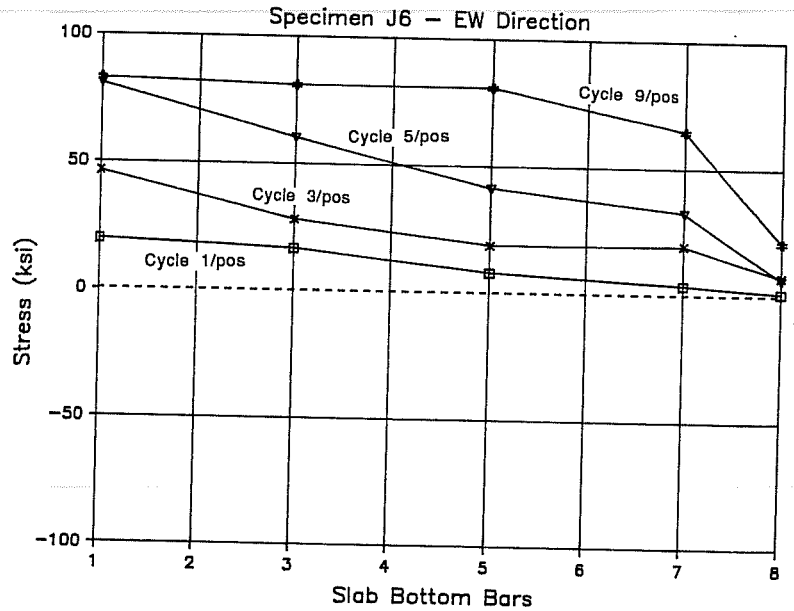

Figure 3.43 - East-West Slab Bar Stresses (Specimen J6)

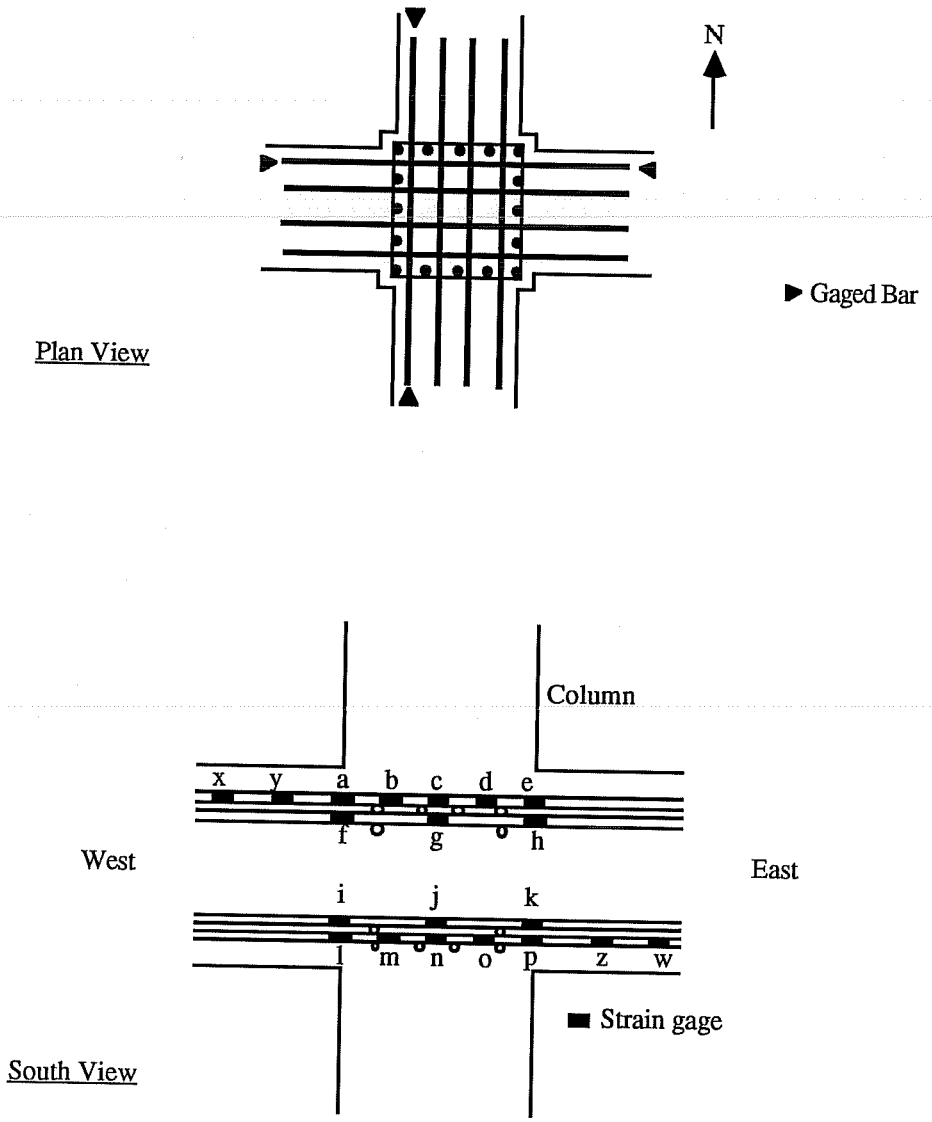

Figure 3.44 - Nomenclature for Strain Gage Positions on Beam Bars

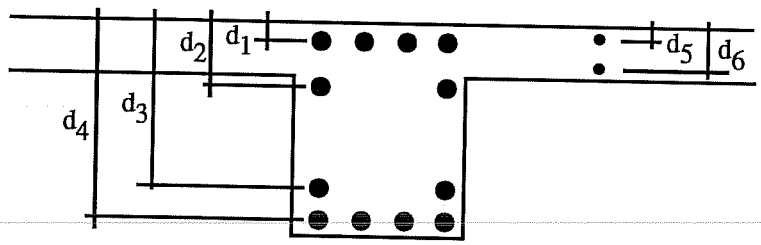

Specimen		Top Bars		Bottom Bars		Slab Bars	
		d_1	d_2	d_3	d_4	d_5	d_6
J2	EW	2.5	5.0	14.8	16.5	1.2	4.1
	NS	3.5	6.0	15.6	17.6	0.8	3.7
J4	EW	2.3	–	–	16.3	0.9	3.3
	NS	3.5	–	–	17.5	0.5	3.7
J5	EW	2.4	5.4	14.1	16.5	0.9	3.3
	NS	3.9	6.8	15.4	17.5	0.5	3.7
J6	EW	2.8	5.1	–	15.9	0.9	3.4
	NS	4.0	6.6	–	17.4	0.6	3.8

Table indicates distance from centroid of reinforcement to top surface of the slab (in inches)

Table 3.2 - Placement of Slab and Beam Bars

3.4.3.1. Beam Top Bars. First yielding of the top layer of E-W beam bars occurred during cycle 5 for all specimens. Bars placed in the lower layer of top bars first yielded during cycle 9 (4% drift) for specimens J2 and J5, and during cycle 6 (2% drift) for specimen J6.

Figure 3.45 shows west beam shear versus strain measured at gages located outside the joint. The top graph shows strain measured at gage position "x" (20 inches from the column face) and the bottom graph shows strain measured at gage position "y" (10 inches from the column face) for specimen J5. Positive west beam shear (downward loading) induced tension in top bars and compression in the bottom portion of the beam. Strains measured at position "x" do not indicate any yielding. However, yielding did occur at position "y". Under tension the bars were free to elongate and the increase in strain is obvious. When the load was reversed, the crack closed and concrete carried the induced compressive forces. Therefore, the strain of the bar is close to zero when compression is induced in the top part of the beam. The measured strains do not indicate bond deterioration outside the joint. Hysteresis loops obtained at position "y" indicate good bond conditions even after yielding.

Figure 3.46 shows west beam shear versus strain measured at gage position "a" for specimens J2 and J5. Plots for specimens J4 and J6 are similar to those of specimens J2 and J5 respectively. Tensile strains were measured under downward loading (positive beam shear) on specimen J2 and small compression strains were present under upward loading during cycles up to 2% drift. Again, concrete carried most of the compressive forces during upward loading. Because of crack closure no significant strain reversal took place. In 4% drift cycles, large tensile strains under downward loading decreased with unloading and residual tensile strains during upward loading remained.

For specimen J5, the strain behavior is different from that of specimen J2. The loops are saddle-shaped indicating tensile strains during both upward and downward loading, although the increase in strain during upward loading (negative beam shear) is less than during downward loading (positive beam shear). Strain increase during upward loading is due to position of the neutral axis. Specimens J5 and J6 were constructed using high strength concrete in the beams and slab, and the position of the neutral axis of the beam cross section tends to be higher than in normal strength concrete specimens. Participation of the slab concrete possibly raised the neutral axis above the beam bars. The threefold increase in concrete strength more than offsets the increase in beam shear measured for the high strength concrete specimens. Therefore, the top bars in the high strength specimens did not experience compressive strains because of the location of the neutral axis of the beam section. Therefore, the accumulated plastic strain is not recovered during upward loading and the cyclic strain history of the top reinforcing bars tends to center about an ever increasing tensile plastic strain.

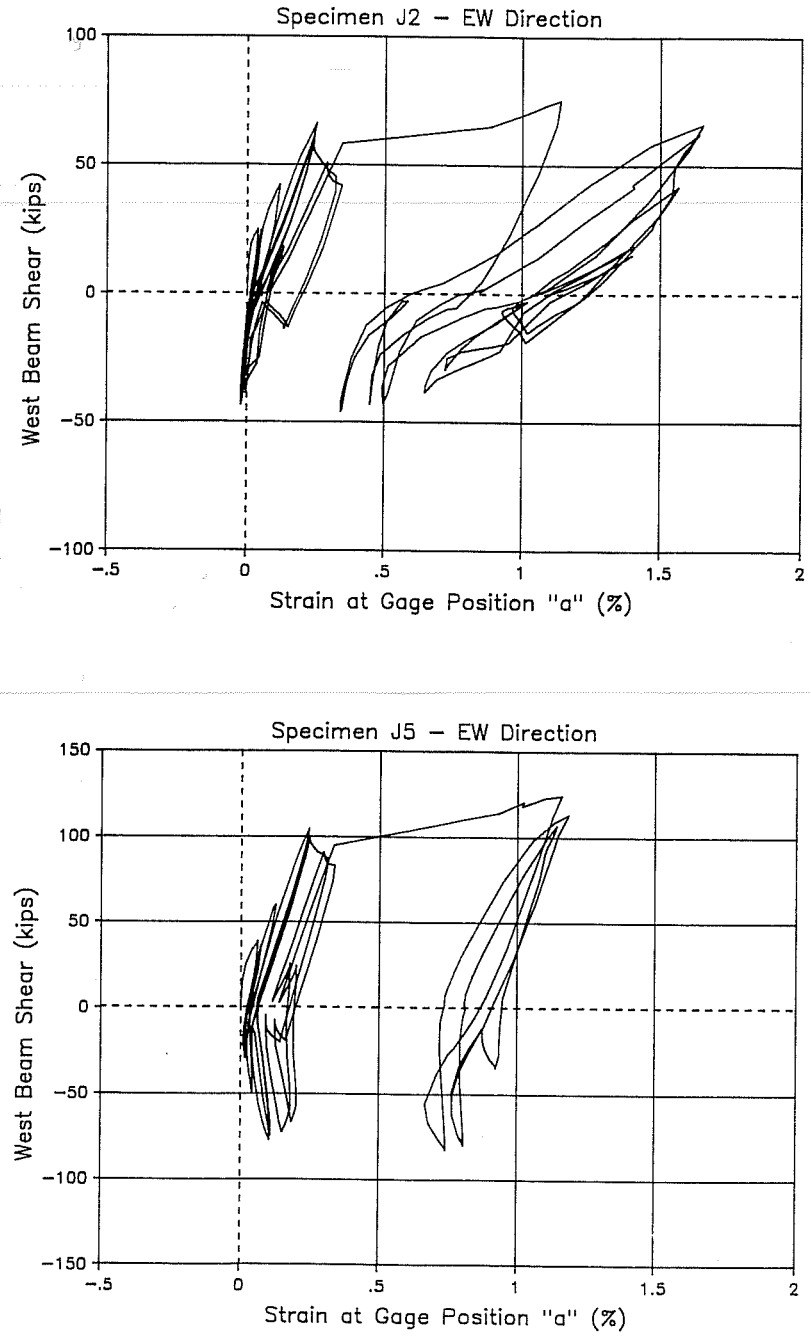

Figure 3.46 - West Beam Shear vs Strain at Gage Position "a"

Similar behavior can be observed in bottom slab bars. Table 3.2 shows that slab bottom bars and top beam bars of high strength specimens are less than one inch apart vertically. The bottom graph of Figure 3.37 shows the cyclic history of the slab bottom bar closest to the west beam of specimen J6. The curves shown in the bottom graph of Figure 3.37 and the bottom graph of Figure 3.46 are very similar. Therefore it is unlikely than the tensile strains measured during both upward and downward loading are indicative of bond deterioration. No apparent reason for slippage of slab reinforcement can be found. The position of the neutral axis is the probable cause of the cyclic strain history obtained.

Figure 3.47 shows west beam shear versus strain at gage position "f" for specimens J5 and J6. These are typical strain plots of gages located at the lower layer of bars next to the column face. The centroid of the lower layer of top bars was located about 5 inches from the surface of the slab (Table 3.2). The cyclic strain history of the lower layer of top bars shows saddle-shaped plots with tensile strains under downward and upward loading and tends to center about an ever increasing tensile plastic strain. Again, this is probably due to the location of the neutral axis of the cross section as explained previously.

Figures 3.48 and 3.49 show stress obtained at positions "a" through "e" for E-W top bars of specimens J2 and J5. No strain gages were placed at positions "b" and "d" for specimen J5. The top graph shows stress at peaks of positive loading cycles, and the bottom graph shows stress at peaks of negative loading cycles. Specimens J4 and J6 show stress distributions similar to those of specimens J2 and J5 respectively.

The top graph of Figure 3.48 shows stress distribution across the joint decreased from tension at the west side to approximately zero at the east side during positive loading up to 2% drift. At cycle 9, high negative stress was obtained at the east side (position"e"). The inverse occurred during negative loading as shown in the bottom graph. Zero stress obtained at the compression side of the joint indicates the neutral axis was close to the centroid of the steel bars, and contribution of the steel reinforcement to carry compression forces was not necessary. However, a high negative stress (about -50 ksi) was obtained at the compression side during cycle 9. This is probably due to high tensile residual strains that occurred after yielding. Also, the position of the neutral axis may have been lowered due to some spalling of the concrete at the top surface of the slab.

Figure 3.49 shows the stress distribution across the joint for E-W direction of specimen J5. Mostly tension stresses were obtained at both sides of the joint. Tension stresses were higher at the tension side. It is unlikely that in this case, tension across the joint indicates bond deterioration since tension stresses occurred very early in the loading history. Tension stresses on the compression side were probably caused by the higher position of the neutral axis due to participation of the high strength concrete slab. Again, negative

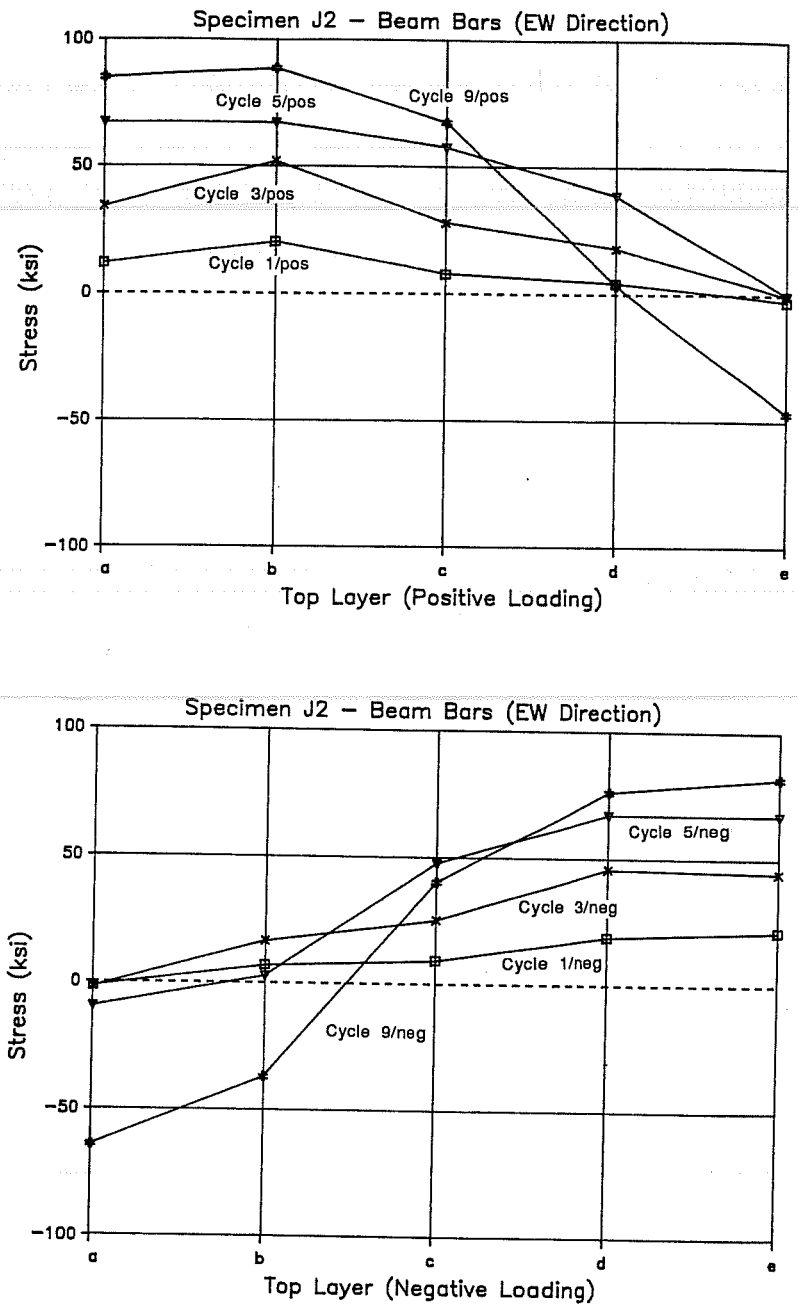

Figure 3.48 - Stress Distribution for Top Bars (Specimen J2)

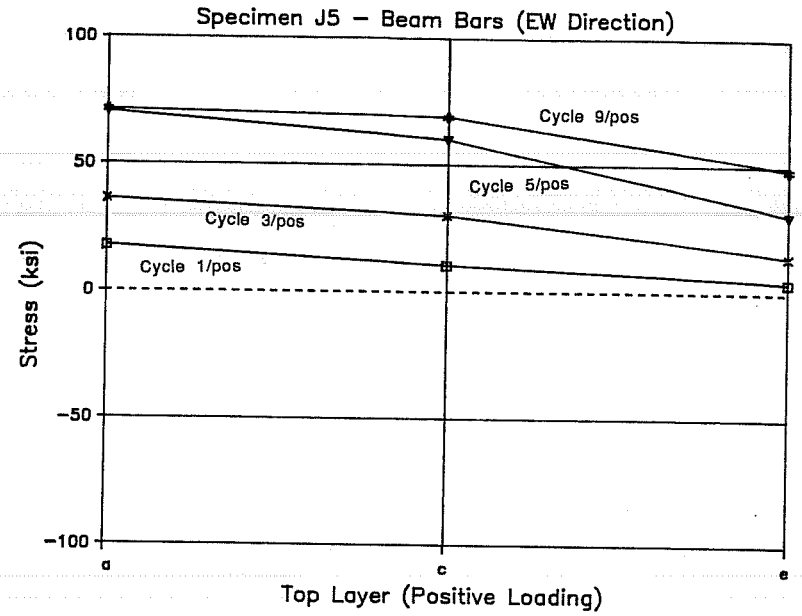

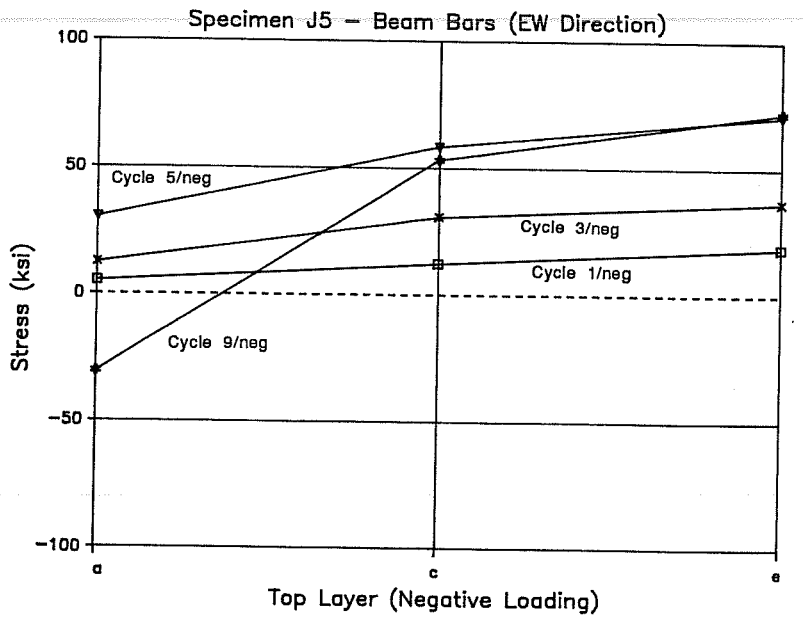

Figure 3.49 - Stress Distribution for Top Bars (Specimen J5)

stress obtained at the compression side during cycle 9/neg is probably due to high tensile residual strains that occurred previously.

Figure 3.50 shows stresses obtained at positions"f","g" and"h" for the lower layer of E-W top bars for specimens J2 and J5. Values were obtained at peaks of positive loading cycles. Behavior at negative loading peaks is very similar. Almost constant tension stresses are shown across the joint. As mentioned previously, this is due to location of the neutral axis above the lower layer of bars. The bars were placed at approximately 5 inches below the top surface of the slab. The neutral axis was probably never more that approximately 2.0 inches below the slab for any specimen at any time during the test.

In general, strains and stresses in top bars indicate good bond conditions. Bond deterioration probably occurred along the top layer after cycle 9. Residual strains caused high compression stresses on one side of the joint while high tension stresses were present at the other side. This is an important cause of bond deterioration [12,13].

3.4.3.2. Beam Bottom Bars. First yielding of both layers of E-W beam bottom bars occurred during cycle 5 for all specimens. Yielding of the second layer of bottom bars occurred during cycle 5, while yielding of the second layer of top bars occurred in later cycles (typically, during cycle 9). This is illustrative of the higher strains measured in bottom bars.

Figure 3.51 shows west beam shear versus strain measured at position"l" in E-W bottom bars for specimens J2 and J5. Specimens J4 and J6 show similar results. Tensile strains were measured under upward loading (negative story shear) and compressive strains under downward loading (positive story shear). Bottom bars were required to resist compressive forces due to the position of the neutral axis of the cross section and the greater amount of top reinforcement. The neutral axis is closer to the middepth of the beam since more beam concrete is required to resist compressive forces when the top is in tension. Therefore, compressive strains are more likely to be measured in bottom bars. In addition, the larger amount of top reinforcement induces higher compressive forces in the beam bottom during downward loading.

Although the tensile strains under upward loading decreased with unloading, the strain history exhibited small loops after reversal in the loading direction. Loops in the beam shear-strain relations during downward loading are evident in larger drift cycles. The loops were mainly caused by redistribution of compressive stresses from bottom beam bars to bottom beam concrete. At higher drift levels, large cracks formed at the beam bottom face during upward loading. When the loading was reversed, the bottom steel took most of the compressive forces and the bar strains decreased significantly. After the crack closed,

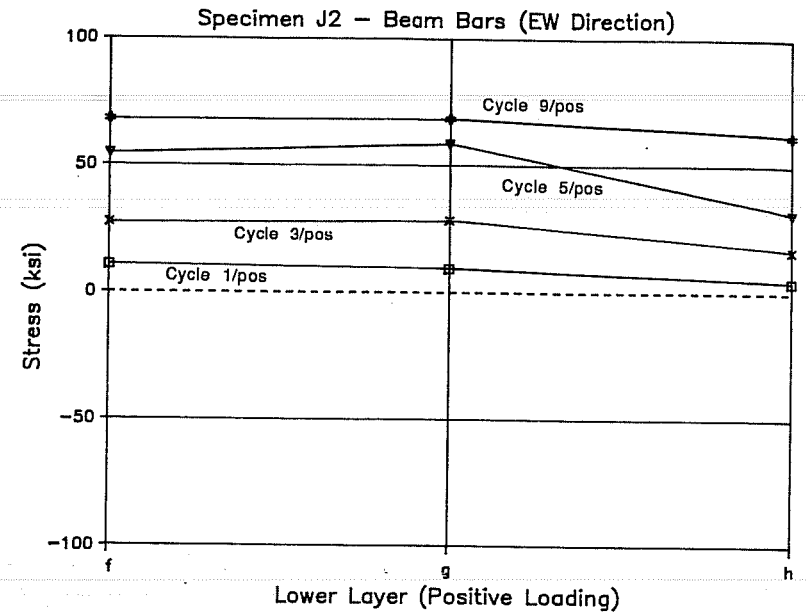

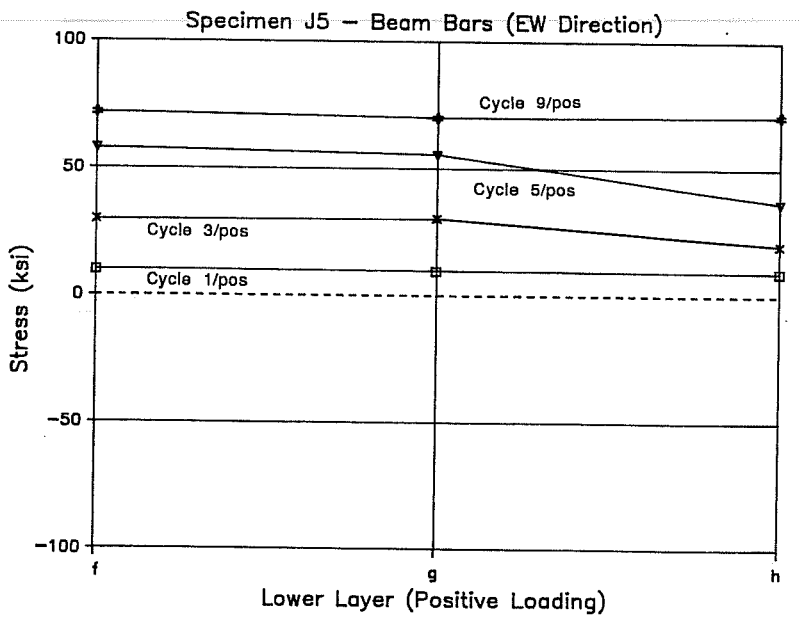

Figure 3.50 - Stress Distribution for Lower Layer of Top Bars

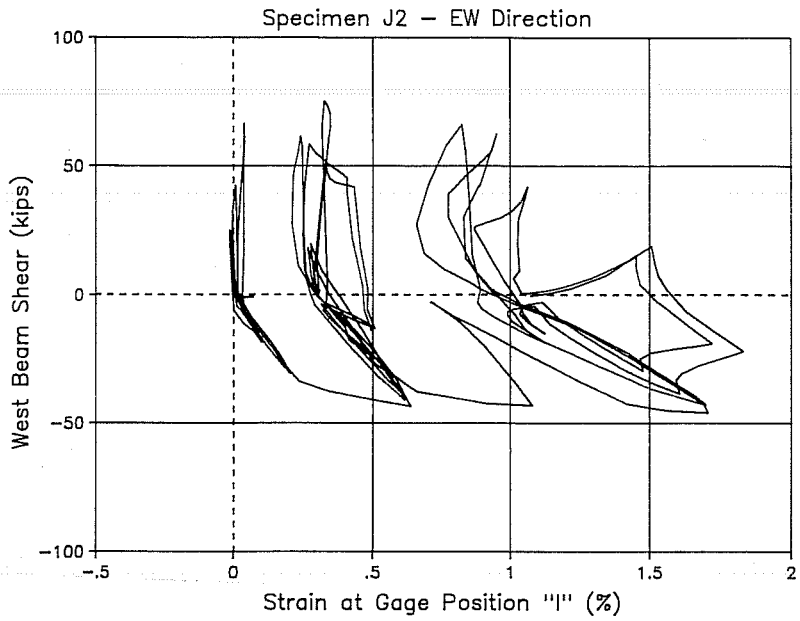

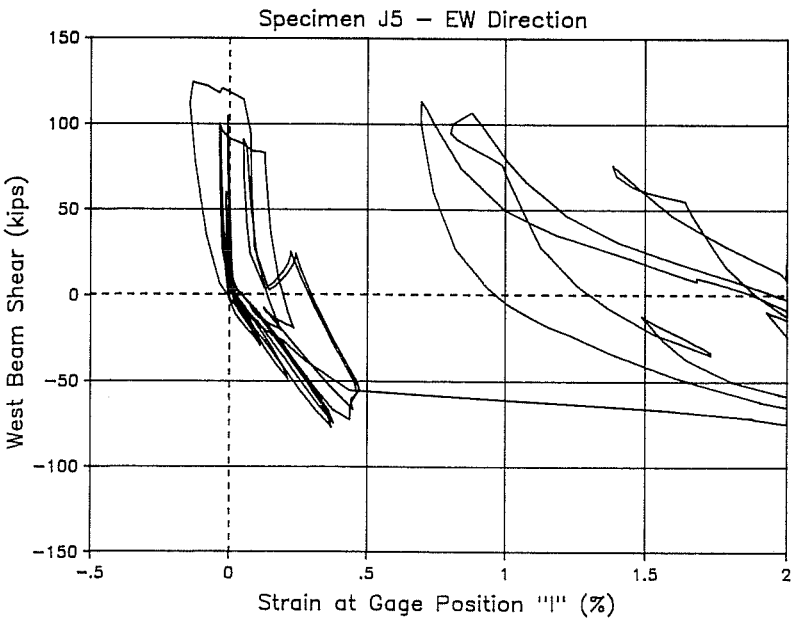

Figure 3.51 - West Beam Shear vs Strain at Gage Position "1"

stress redistribution occurred. Compressive forces in beam bottom bars decreased and bar strains increased which led to the small loops in beam shear-strain.

Figures 3.52 and 3.53 show stress obtained at positions"l" through"p" for E-W bottom bars of specimens J4 and J6. No strain gages were placed at positions"m" and"o" for specimen J6. The top graph shows stress at peaks of positive loading cycles and the bottom graph shows stress at peaks of negative loading cycles. Specimens J2 and J5 show similar stress distributions.

Stress distributions across the joint show mostly linearly decreasing tension stresses from the tension side of the joint to the compression side, especially up to cycle 5. Negative stresses were obtained on the compression side at cycle 5/neg and at cycle 9. Negative stresses at higher drift levels are due to a change in the location of the neutral axis due to bottom concrete spalling and crushing. The steel had to carry most of the compression forces. An additional factor is the high residual tensile strains across large crack openings.

The upper layer of beam bottom bars show stress distributions similar to the lower layer of beam top bars. Tension stresses predominated across the joint. Only at 4% drift cycles were compression stresses were obtained at the compression side of the joint. This was due to considerable spalling and crushing of the beam bottom concrete next to the column which significantly changed the position of the neutral axis.

In general, strains and stresses in bottom bars indicate good bond conditions. Bond deterioration probably occurred along the bottom layer after cycle 9. Bond behavior is discussed in more detail in Section 4.6.

3.4.4. Column Bars. Strain gages were placed on longitudinal column reinforcement inside and outside the joint. Only corner bars were gaged. Figure 3.54 shows strain gage positions on column longitudinal reinforcement. Positions 1 and 5 are ten inches above and below the joint respectively. Positions 2, 3 and 4 are inside the joint.

Due to the nature of the loading history, column bars subjected to the highest stresses during 2% bidirectional loading were located in the southwest and northeast corners of the column. During 4% bidirectional loading, the highest stressed bars were at the northwest and southeast corners.

In general, yielding of column bars occurred later than yielding of beam bars. Also, the strains measured in column bars were much lower than the strains measured in beam bars. Highest strains in column bars were rarely above 1%. This is to be expected due to the strong column-weak beam design philosophy.

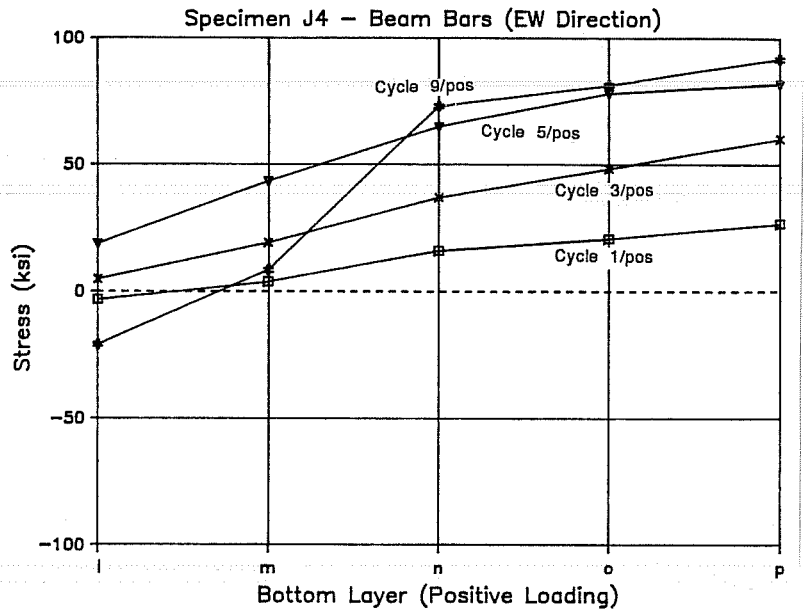

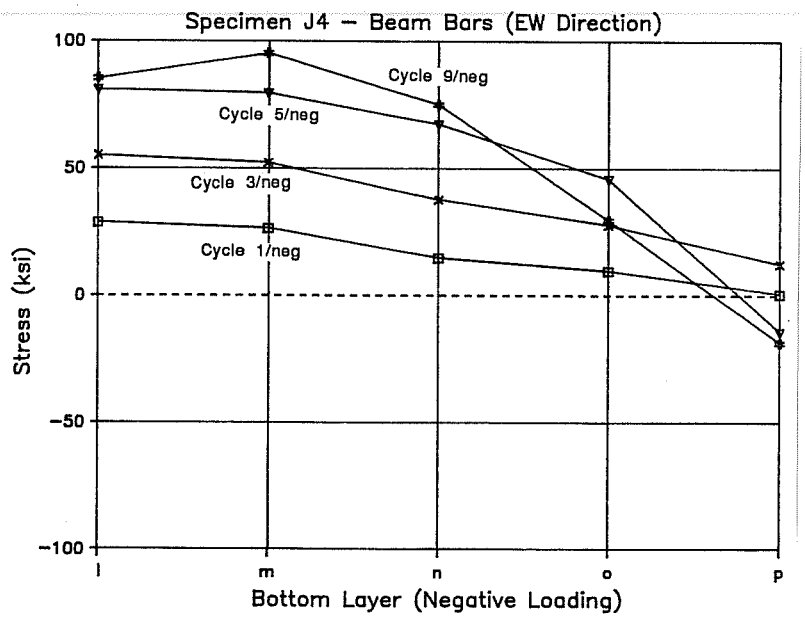

Figure 3.52 - Stress Distribution for Bottom Bars (Specimen J4)

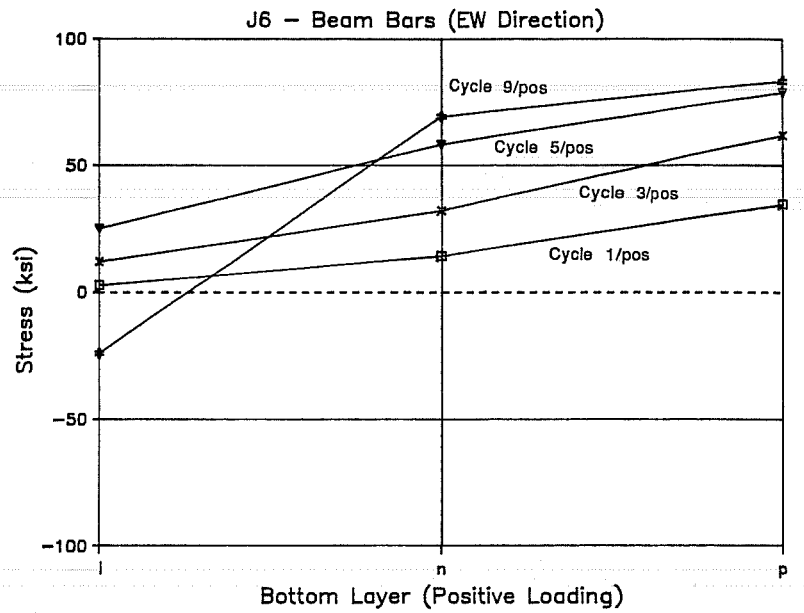

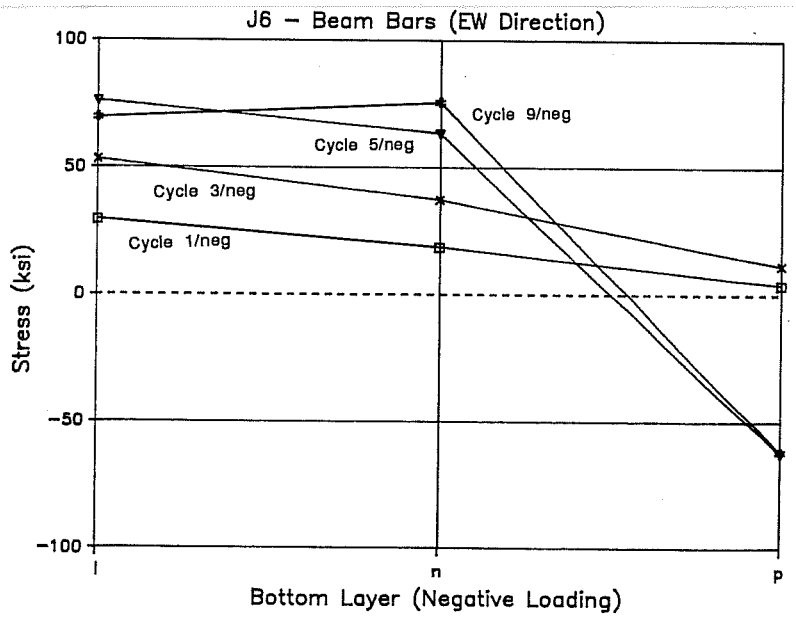

Figure 3.53 - Stress Distribution for Bottom Bars (Specimen J6)

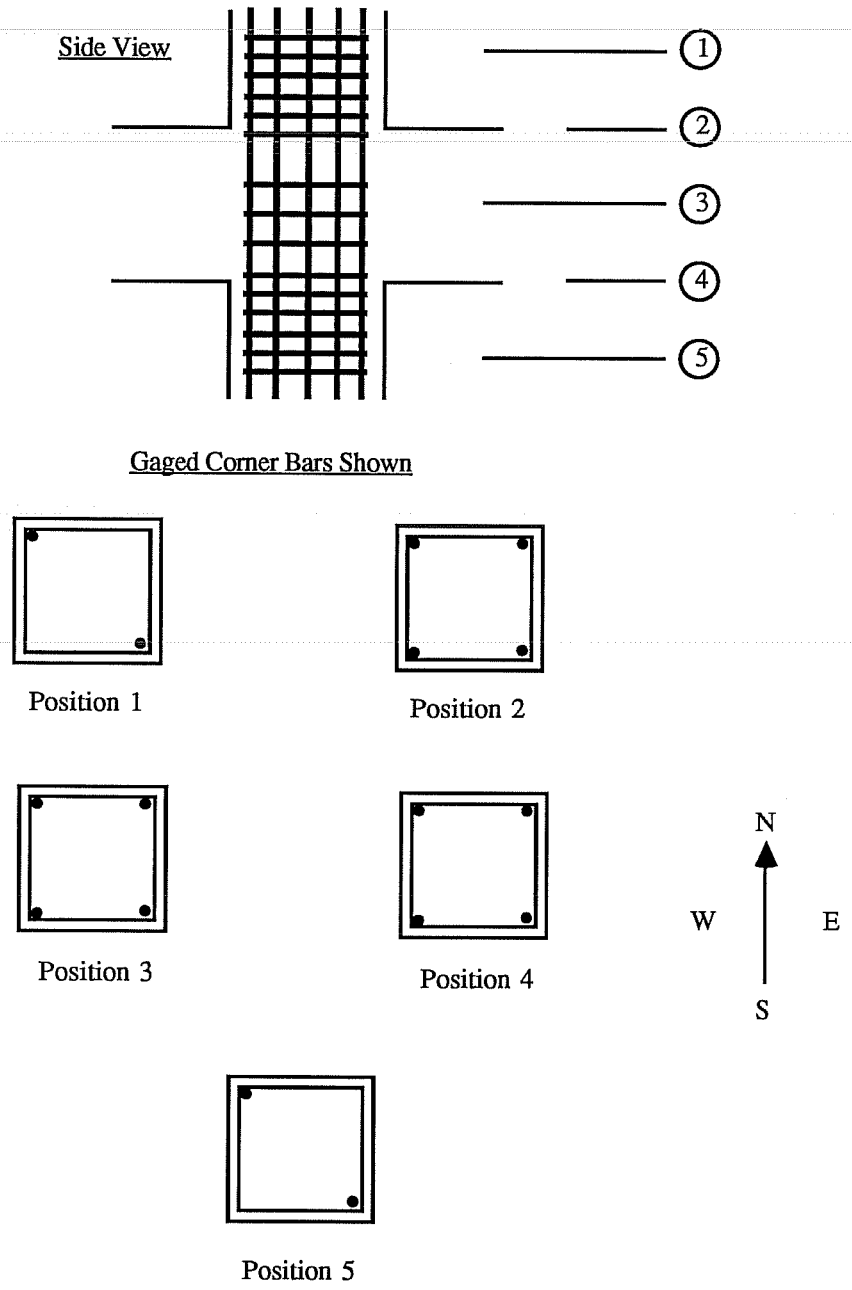

Figure 3.54 - Strain Gage Positions on Column Bars

Yielding of column bars occurred during the first bidirectional cycle at 2% story drift. First yielding was measured at position 2 of southwest corner bars. Yielding was first measured at position 3 and 4 during 4% story drift cycles. There is no apparent reason for yielding to occur at position 2 before occurring at position 4. Gages placed at positions 1 and 5 do not show any yielding before 4% drift bidirectional cycles.

Figure 3.55 shows E-W story shear versus strain at gage positions 1 and 5 for the northwest corner bar of specimen J4. These plots are typical of gages placed outside the joint. The plots show low strains, usually not exceeding 0.2%. Tensile strains were measured during positive story shear at gage position 1, and compressive strains during negative story shear. Conversely, compressive strains were measured during positive story shear at gage position 5, and tensile strains during negative story shear. Loops developed during 4% bidirectional loading, but the strain history indicates very good bond at gage positions 1 and 5.

Figures 3.56 and 3.57 show E-W story shear versus strain at gage positions 2 and 4 for the southwest corner bar of specimens J4 and J6. The southwest corner bar was chosen because it is on the highest stressed diagonal at 2% story drift.

Figure 3.58 shows E-W story shear versus strain at gage position 3 for the southeast corner bar of specimens J2 and J5. These plots are typical of any gage at position 3 in all of the specimens.

In general, plots shown in Figures 3.56 through 3.58 are saddle-shaped showing tensile strains in positive and negative story shear. This is especially true at gage position 3 where approximately the same strain was measured for equally opposite story shears, except during bidirectional loading.

Figures 3.56 and 3.57 show small compression strains at cycles 1 and 2, and during part of cycle 3. However, after cycle 3, tensile stresses predominated during positive and negative loading cycles. Small loops in the cyclic history occurred when compression forces were present in the surrounding concrete, i.e., during negative E-W story shear for gage position 2 and during positive E-W story shear for gage position 4. Larger loops occurred during bidirectional loading.

Figure 3.59 shows stress at gage positions 1 through 5 for the northwest corner bar of specimens J4 and J6. Stresses were obtained at peaks of E-W loading cycles 1, 3, 5 and 9. Except for cycle 1, only tensile stresses were obtained for the reinforcement inside the joint.

Bond loss and slippage probably occurred along column longitudinal reinforcement. Bond is discussed in more detail in Section 4.6.2.

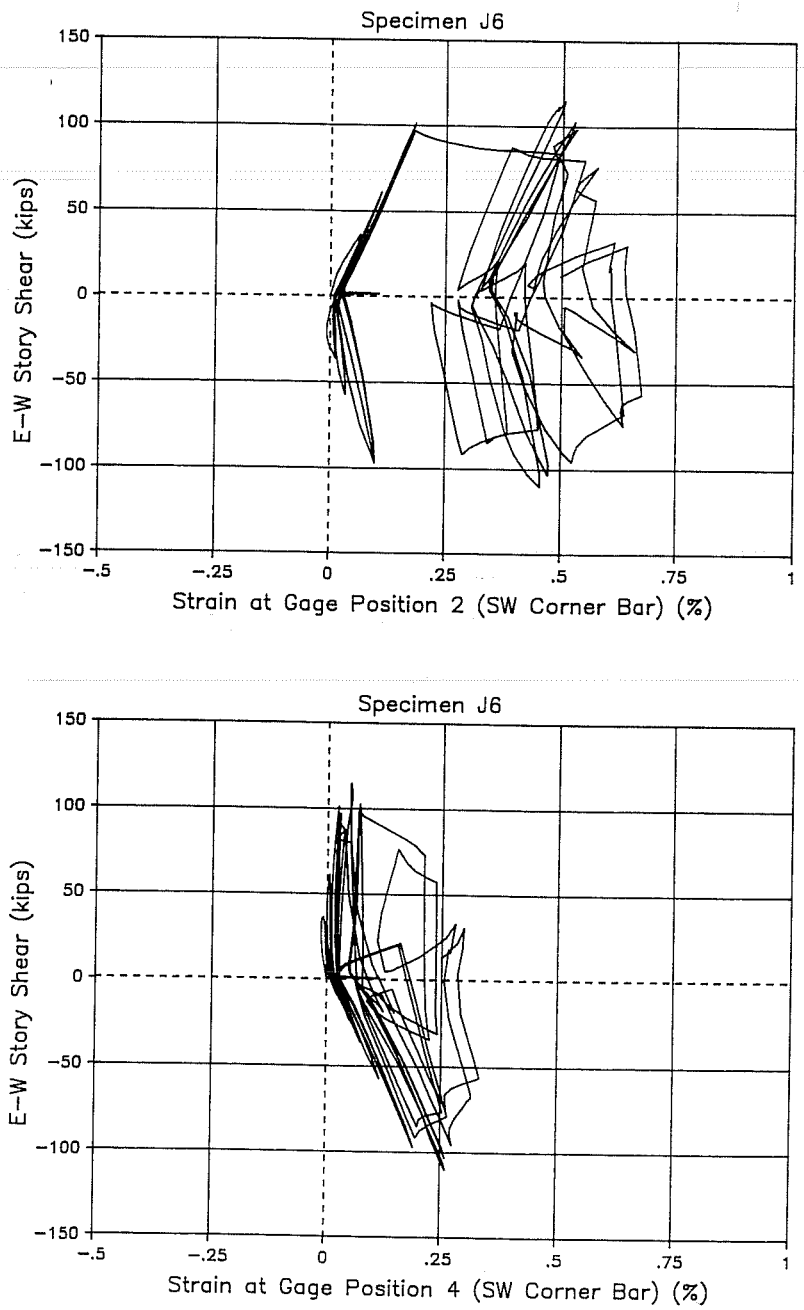

Figure 3.57 - Story Shear vs Strain in SW Corner Column Bar (Specimen J6)

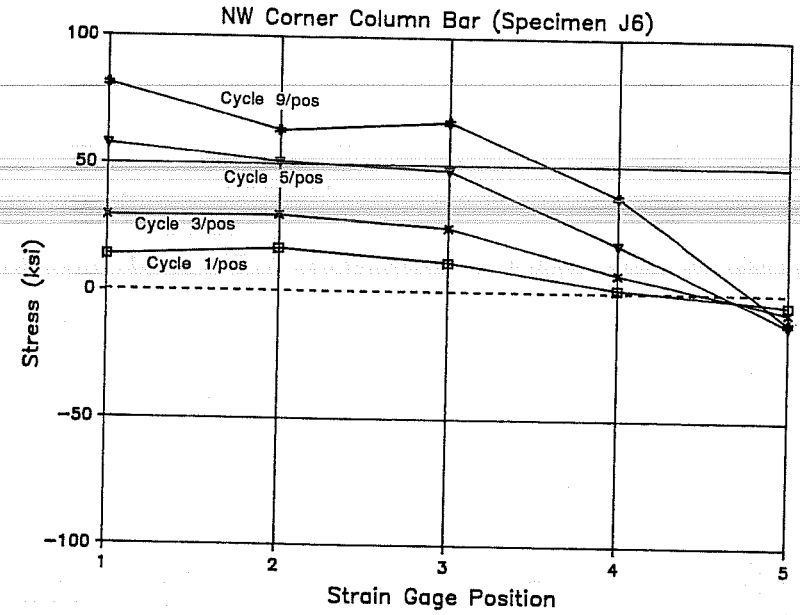

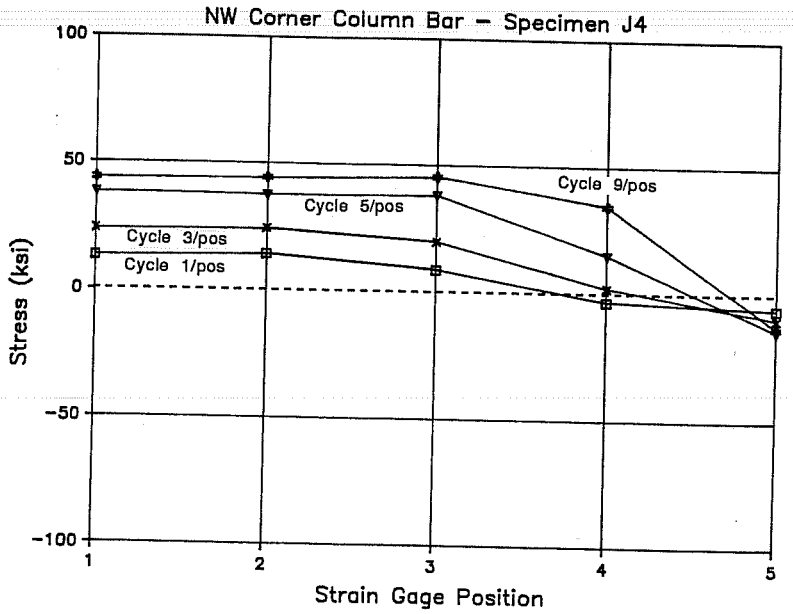

Figure 3.59 - Stress Distribution in NW Corner Column Bar

CHAPTER 4 - EVALUATION OF EXPERIMENTAL RESULTS

4.1 INTRODUCTION

In this chapter the performance of the tests described in the previous chapter will be examined in greater detail. Differences in specimen stiffness will be discussed. Hysteretic response and influence of bond will be analyzed. Contribution of each component to inter-story displacement will be calculated. Shear strengths predicted by current design guidelines will be compared with experimental values. The effect of the slab on the behavior of the specimens will be discussed. In the next chapter, design guidelines evolving from the evaluations of test results will be presented.

Again, focus of the discussion will be on differences in behavior of normal and high strength concrete specimens obtained during east-west loading. The behavior during bidirectional loading was evaluated and will be discussed when important.

As mentioned previously, evaluation of test data from specimens constructed with high strength steel and welded wire fabric reinforcing cages show insignificant differences in behavior from specimens constructed with normal strength steel. Therefore, discussion of the results will mention these differences only when illustrative.

4.2 STIFFNESS OF SPECIMENS

Stiffness of the subassembly can be defined through story shear- drift angle relations. Definitions of equivalent stiffness and peak-to-peak stiffness are shown in Figure 4.1.

Equivalent stiffness K_e is defined for each half cycle in each loading direction. As shown in Figure 4.1(a), a line connects points corresponding to the first zero story shear and maximum drift angle. The angle between this line and the x-axis is defined as equivalent stiffness. Since the loading cycles are displacement controlled, the point corresponding to first zero story shear would usually occur in the previous half cycle, unless zero story shear occurs with zero story drift.

Peak-to-peak stiffness K_p is defined for each cycle in each loading direction. Figure 4.1(b) shows a line connecting points corresponding to maximum positive and negative drift angles. The angle between this line and the x-axis is defined as peak-to-peak stiffness.

Due to the definitions of stiffness and nature of the hysteresis loops, values of peak-to-peak stiffnesses are larger than values of the equivalent stiffnesses. Equivalent stiffness allows comparisons between half cycles while peak-to-peak stiffness makes comparisons between full cycles easier.

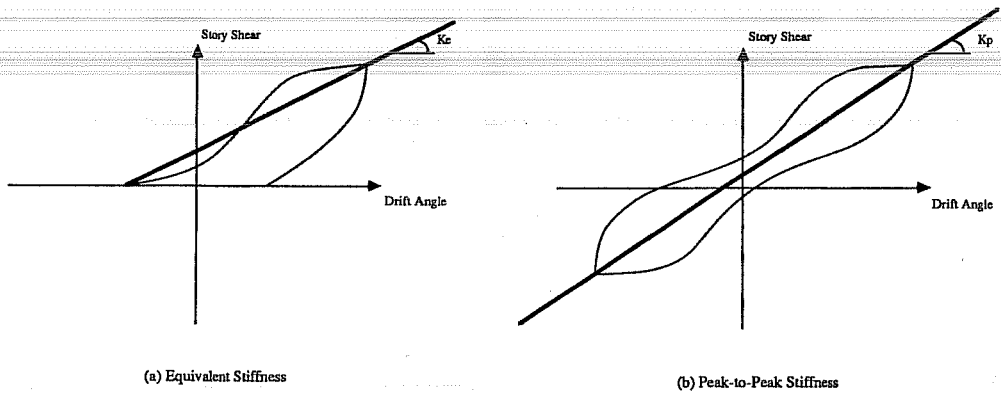

Figure 4.1 Definition of Stiffnesses

Figure 4.2 shows the notation used in remaining figures of this section. Figures 4.3 and 4.4 show equivalent stiffness against story drift for specimens J2 and J5 in E-W loading. Figure 4.5 shows peak-to-peak stiffness against story drift angle for E-W loading of specimens J2 and J5. Values of stiffness obtained from N-S loading cycles were very similar to the respective values of stiffness in E-W cycles. In addition, specimens J2 and J4, and specimens J5 and J6 have almost identical stiffnesses. Stiffnesses of specimen J4 were usually less than 5% lower than those of specimen J2. Specimen J6 showed values of stiffness about 8% lower than those obtained from specimen J5.

4.2.1. Equivalent Stiffness. Stiffness deterioration after each half cycle can be shown through equivalent stiffness vs. drift angle graphs in Figures 4.3 and 4.4 for specimens J2 and J5. Normal strength concrete specimens deteriorated faster than high strength concrete specimens. A parabolic curves best fits data from normal strength concrete specimens indicating more deterioration in stiffness in early stages of loading. High strength concrete specimens show a linear deterioration in stiffness with increase in story drift angle.

As expected, high strength concrete specimens were stiffer than normal strength concrete specimens. This was due to the increase in stiffness of the concrete with increase in concrete strength, and to higher amounts of longitudinal reinforcing steel used in the high

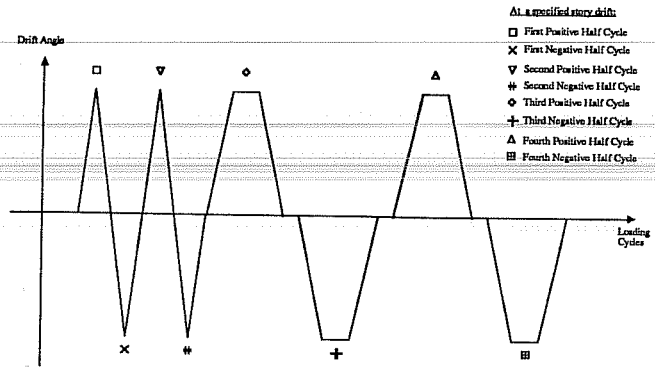

(a) Notation for Equivalent Stiffness

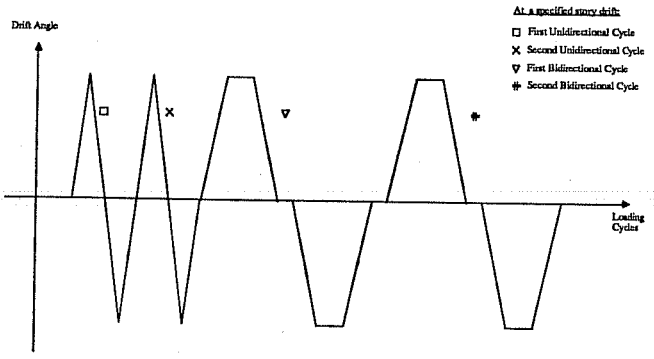

(b) Notation for Peak-to-Peak Stiffness

Figure 4.2 Notation for Figures 4.3 through 4.5

strength concrete specimens. The elastic modulus of elasticity was about 70% higher for the high strength concrete.

The specimens always showed greater equivalent stiffness in the first positive half cycles. This was due to less residual displacement at the start of the cycle at a given deflection level. Residual deformations at zero story shear were usually smaller at the beginning of cycling at a specified drift level. Stiffness did not change significantly after the first cycle at a specified deformation level. Although there was loss of stiffness during bidirectional cycles, most of the deterioration came with the increase in the specified story drift.

4.2.2. Peak-to-Peak Stiffness. Figure 4.5 shows peak-to-peak stiffnesses against story drift angle for specimens J2 and J5. Again, these graphs show that high strength

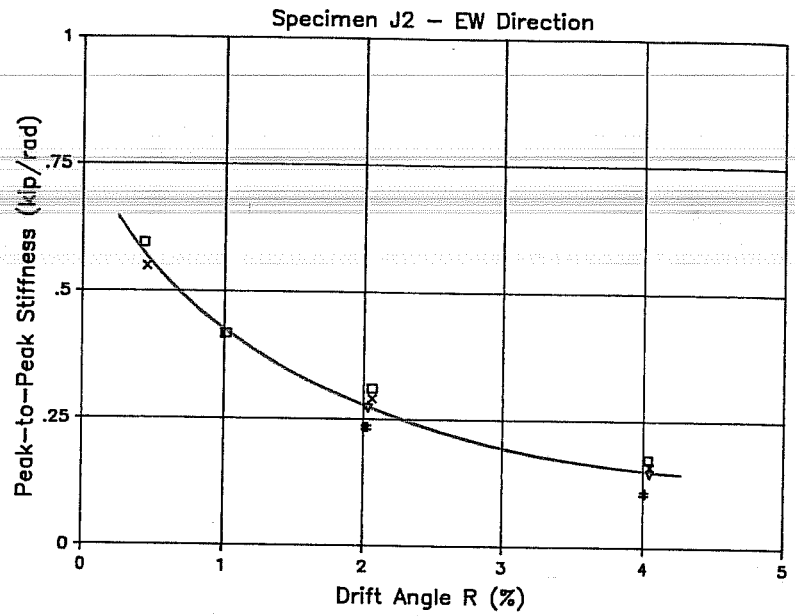

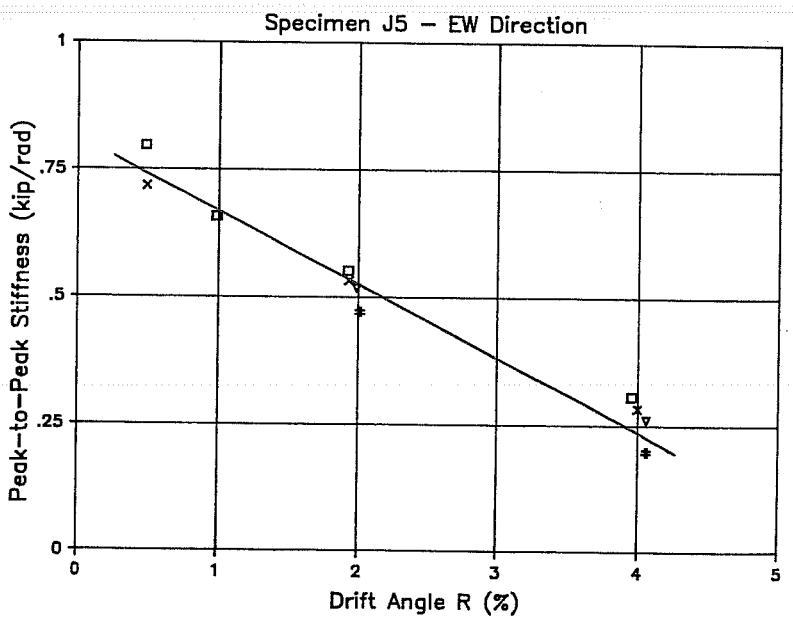

Figure 4.5 - Peak-to-Peak Stiffness for Specimens J2 and J5

concrete specimens were stiffer than normal strength concrete specimens. The stiffness of the high strength concrete specimens was about 45% greater at 0.5% story drift and about 70% at 4% story drift.

Linear stiffness deterioration is shown for specimen J5 which is also typical for specimen J6. Stiffness deterioration for specimen J2 (as well as specimen J4) follows a parabolic shape with greater losses in the first cycles of loading. Between 0.5% and 2% drift levels, loss of stiffness in normal strength concrete specimens is approximately 45%. For high strength concrete specimens, this loss is 28%. Between 2% and 4% drift levels, degradation in stiffness is about the same for all specimens. Normal strength concrete specimens were about 48% stiffer at 2% story drift than at 4% story drift, and high strength concrete specimens were about 52% stiffer.

The first loading cycle at a given deformation level always showed slightly higher stiffness. This was due to a small decrease in maximum load in subsequent cycles. Only small losses in stiffness were observed after the first cycle at the same story drift, including the bidirectional cycles. Greater deterioration accompanied increases in the deformation level.

Degradation in stiffness occurred mainly due to cracking, spalling and crushing of the concrete. More cracking and concrete spalling was observed in normal strength concrete specimens especially up to 2% story drift and led to loss in stiffness observed in specimens J2 and J4. Specimens J5 and J6 showed crushing and spalling only at later cycles in the loading history. Bond deterioration and the Bauschinger effect on the steel stress-strain relationship did not seem to significantly affect overall stiffness degradation of the specimens.

Deterioration in stiffness of the specimens can be illustrated by observing the crushing of normal and high strength concrete cylinders in a universal testing machine. During testing of high strength concrete cylinders, there is less deformation of the cylinder and concrete spalling and crushing does not occur until the very last moment prior to an explosive failure of the cylinder. In a similar way, the high strength concrete specimens J5 and J6 did not deteriorate significantly until later stages of loading as concrete sections were abruptly detached from adjoining sections and sudden spalling of the concrete cover occurred.

4.2.3. Specimen Flexibility. Table 4.1 shows calculated ultimate story shears and calculated story drift angles at first yielding for all specimens. Ultimate story shears were calculated from maximum joint shear strength according to ACI 352 Committee Report recommendations [2].

Deflection at first yielding R_y is obtained as suggested for the U.S.-Japan-New Zealand Project [17,18]. The following is the procedure used to obtain story drift angle at first yielding.

Table 4.1 Calculated Ultimate Story Shears and Calculated Story Drift Angles at Yielding

Specimen	Story Shear V_u (kips)	R @ $0.75V_u$ (%)	R_y (%)
J2	48.7	0.80	1.07
J4	54.6	0.98	1.31
J5	80.2	0.91	1.21
J6	88.1	1.18	1.57

Step 1. Calculate ultimate story shear V_u using design recommendations (capacity reduction factors should be equal to one) and actual material and geometric properties of the specimen. Ultimate moments at the critical section of beams should be considered. These values are shown in the second column of Table 4.1.

Step 2. During loading cycle 3 obtain the story drift angle corresponding to three-quarters of the calculated ultimate story shear V_u. The specimen must be loaded at least up to three-quarters of the calculated ultimate story shear.

Step 3. The story drift angle at first yielding R_y is defined as four-thirds of the story drift angle corresponding to three-quarters of the calculated ultimate story shear (from step 2).

$$R_y = (4/3) * R \; at \; (3/4)V_u$$

The maximum earthquake imposed story drift angle that could be considered to be realistic is of the order of 3%. Displacements beyond this limit are likely to lead to serious overall frame instability [16]. According to Table 4.1, yield deflection varied from about 1% to about 1.5%. This is considered high compared to the realistic maximum limit of 3% since frame structures in earthquake zones are expected to go far beyond yield deflection. Such high yield deflections indicate high specimen flexibility compared with code-designed structures. Although the specimens are generally flexible, no single component (beams, column or joint) is responsible for such flexibility. This is discussed in more detail in Section 4.4.1.

4.3 HYSTERETIC BEHAVIOR

4.3.1. Energy Dissipation. Large amounts of energy are released during an earthquake. Some of this energy is transformed into potential energy which is absorbed by the structure as strain energy. Deformations of the structure are responsible for most of the

energy absorption-dissipation mechanisms. It is important to assess the energy dissipation characteristics of the specimens to study their performance under large cyclic deformations.

4.3.1.1. Total Cumulative Energy Dissipation. The total amount of energy dissipated for each specimen is obtained by calculating the area of hysteresis loops described by story shear- interstory drift curves. Since the displacement at beam tips is the same due to the nature of the loading history, the total cumulative energy dissipated by the specimen can be calculated by integration of the story shear-interstory drift curves.

Figures 4.6 and 4.7 show cumulative energy dissipated in the E-W and N-S directions for each specimen. Figure 4.8 shows total (sum of both directions) cumulative energy dissipated for each specimen. These figures show values obtained at positive peaks of each loading cycle. The curves would be shifted downwards slightly if values obtained at the end of each loading cycle were used.

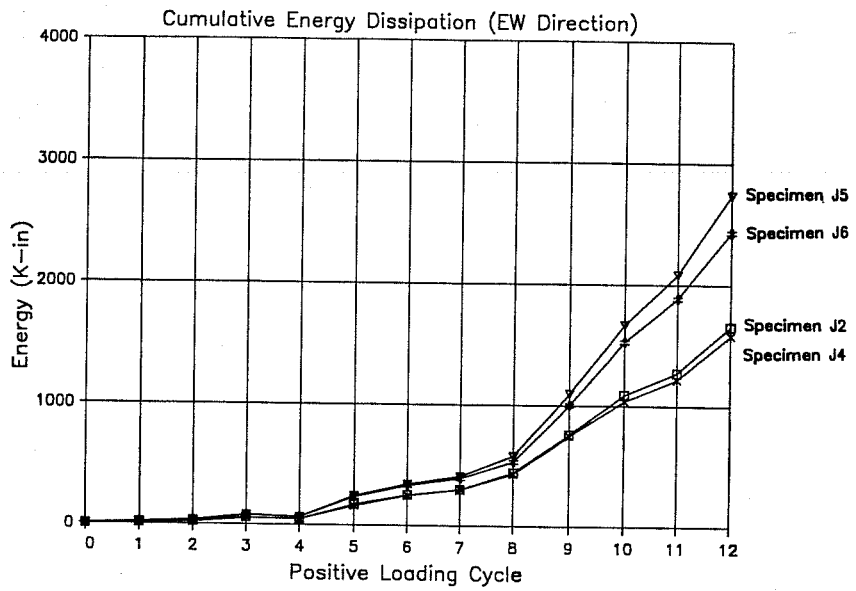

Figure 4.6 Cumulative Energy Dissipated (EW Direction)

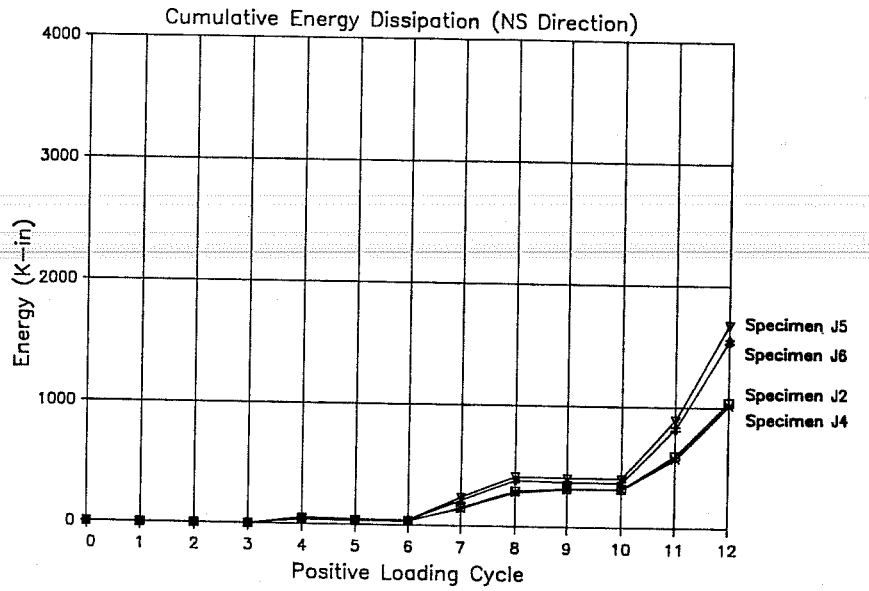

Figure 4.7 Cumulative Energy Dissipated (NS Direction)

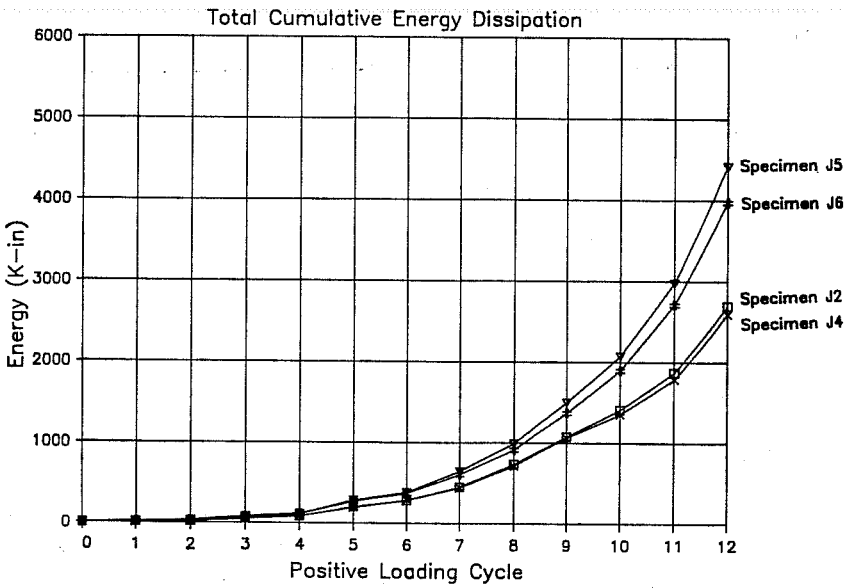

Figure 4.8 Total Cumulative Energy Dissipated

As expected, the high strength concrete specimens dissipated more energy than the normal strength concrete specimens due to higher story shears. Also, most of the loading occurred in the E-W direction, so more energy was dissipated in this direction. High strength steel specimens J4 and J6 showed very similar curves to those of specimens J2 and J5, respectively, but slightly less energy was dissipated since lower story shears were reached.

Most of the energy was dissipated during 4% story drift cycles. Specimen J2 dissipated 2.7 times more energy during 4% drift loading than from the start of testing through 2% story drift cycles. Specimen J5 dissipated 3.7 times more energy after cycle 9 than before cycle 9.

4.3.1.2. Contribution to Energy Dissipation. The basic elements contributing to the total energy dissipation mechanism are beams and slab, column, and joint. The following equation relates the contribution of these elements to story drift angle (explained in detail in Section 3.3).

$$R = \left(1 - \frac{h_b}{H} - \frac{h_c}{L}\right) * \gamma + \theta_b + \theta_c$$

Where:

R = interstory drift angle

$\left(1 - \frac{h_b}{H} - \frac{h_c}{L}\right) * \gamma$ =joint contribution to the drift angle

θ_b = beam tip deflection angle; beam contribution

θ_c = column tip deflection angle; column contribution

Multiplying each side of this equation by the column height H, each contribution to interstory drift can be obtained.

$$I.D. = R * H = H * \left(1 - \frac{h_b}{H} - \frac{h_c}{L}\right) * \gamma + \theta_b H + \theta_c H$$

Curves showing the relation of each of the three components to story shear can be easily obtained. The area of hysteresis loops described by each curve can be calculated by integration and the contribution of beams (and slab), column, and joint to the total energy dissipation mechanism is obtained.

Figures 4.9 through 4.12 show the percent contribution of each element to the total cumulative energy dissipated for specimens J2, J4, J5 and J6. Contribution to total cumulative energy dissipation was obtained at peaks of positive and negative half cycles. Values

plotted are averages between positive and negative peaks of each loading cycle. Contributions are shown for E-W (top) and N-S (bottom) loadings.

In general, the joint contribution increased steadily throughout the test. The beam contribution was usually the largest. The column contribution was small and decreased after 2% drift cycles.

The joint contribution for specimen J2 (Figure 4.9) increased from about 20% in the first loading cycles to about 40% at the end of the test. Column contribution decreased steadily from about 20% to less than 7%. Beam contribution maintained at about 60% throughout the test with a small decrease for the N-S direction. Although the beams and slab dissipated most of the energy, the joint contribution is important since it nearly doubled. A large increase in joint shear distortion is apparent since the hysteresis loops were pinched (Section 3.3.1). Formation of plastic hinging in the beams is not clearly shown as an increase in the beam contribution since a relative increase in joint contribution occurred at the same time.

The joint contribution for specimen J4 (Figure 4.10) increased from about 10% to 40% for E-W loading cycles and from approximately 20% to 50% for N-S loading cycles. The increase was significant until cycle 8 but joint contribution remained constant afterwards. The column contribution remained at about 20% throughout most of the test. Beam and slab contributions decreased from about 60% to 40% for E-W loading, and to about 30% for N-S loading.

As in specimen J2, the relative increase in joint contribution in specimen J4 indicates an increase in joint shear distortion. Although joint shear distortion increased after cycle 8 (Section 3.3.1.), it was accompanied by an increase in the beam tip deflection angle due to plastic hinge formation. Therefore, both joint and beams dissipated more energy after cycle 8, but their relative contribution to the total energy dissipated did not change. Contrary to specimen J2, joint contribution in J4 increased with a decrease in beam contribution before cycle 9. In addition, maximum joint shear for bidirectional loading occurred in cycle 7/pos. For specimen J2, maximum bidirectional story shear was measured in cycle 11/pos (Table 3.1). This is indicative of greater joint distress for specimen J4 occurring in 2% bidirectional cycles followed by plastic hinging of the beams at cycle 9. However, in specimen J2 both joint deterioration and plastic hinging seemed to occur after cycle 8.

For specimen J5 (Figure 4.11), joint contribution in the E-W direction increased from less than 15% in cycle 1 to about 45% in cycle 8, and decreased to 30% at the end of the test. In the N-S direction, the joint contribution increased from about 20% at cycle 4 to 40% at the end of the test. The column contribution in the E-W direction decreased from

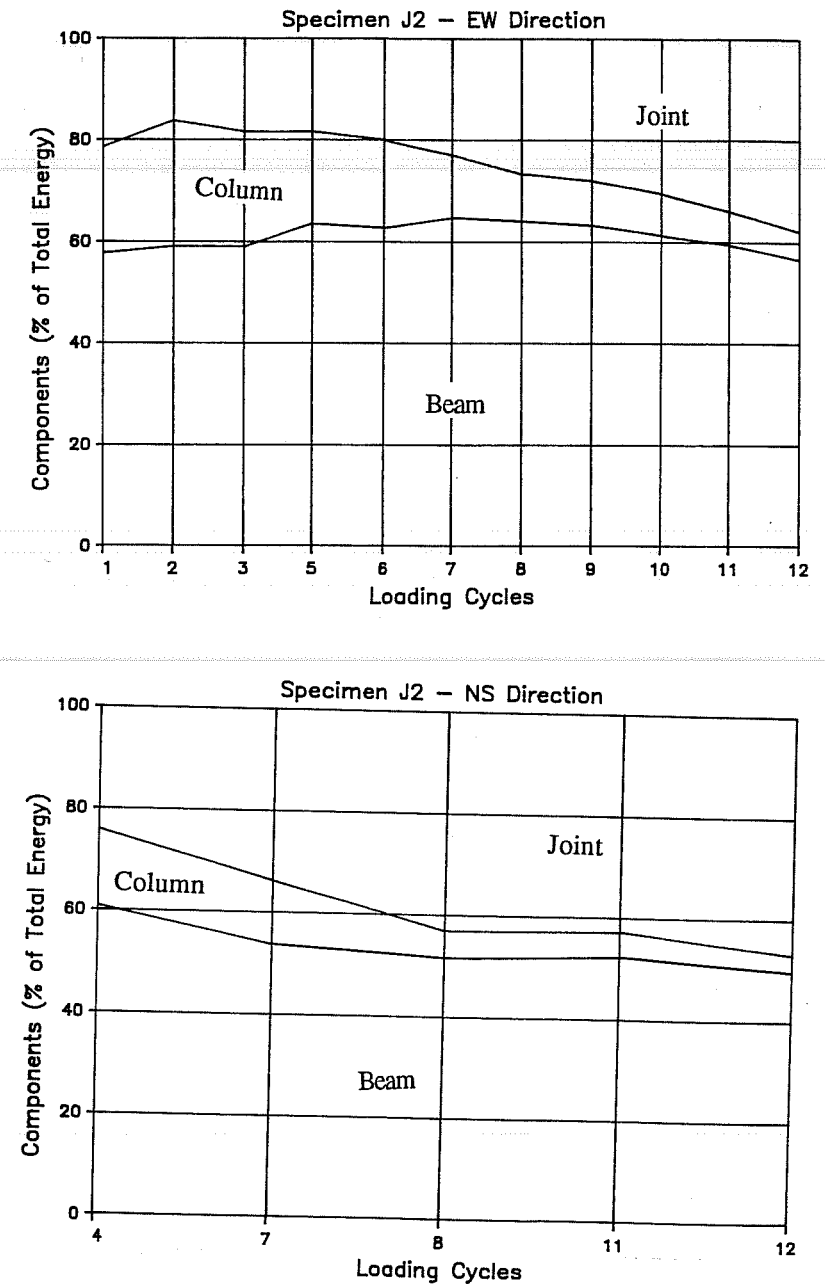

Figure 4.9 **Beam, Column and Joint Contributions to Total Energy Dissipation for Specimen J2**

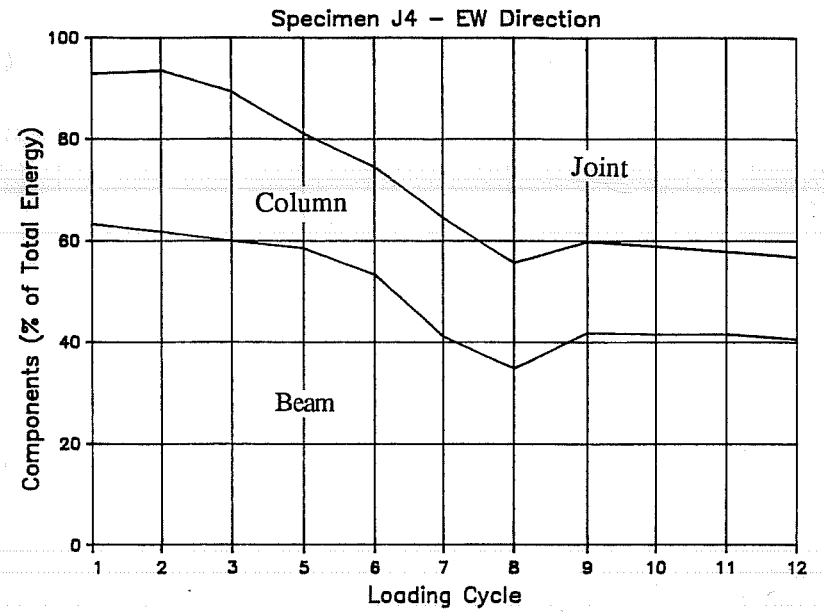

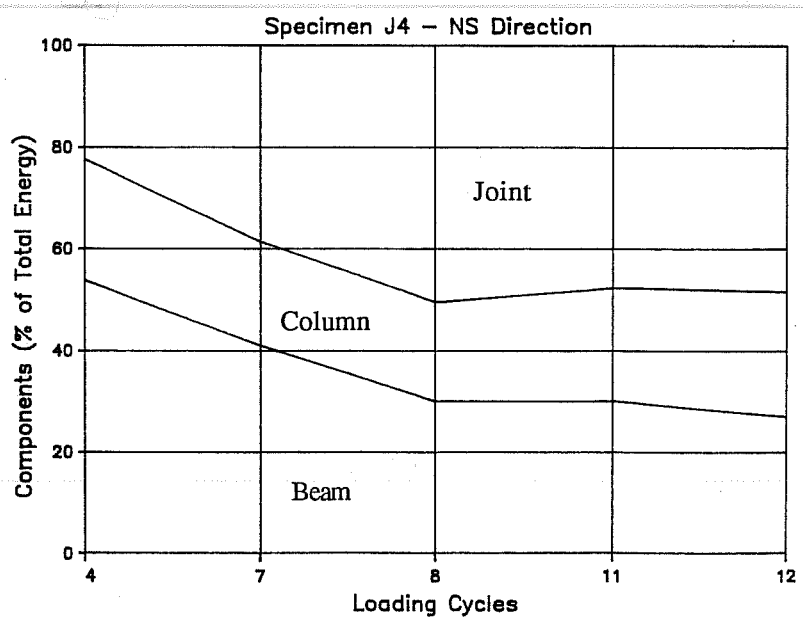

Figure 4.10 **Beam, Column and Joint Contributions to Total Energy Dissipation for Specimen J4**

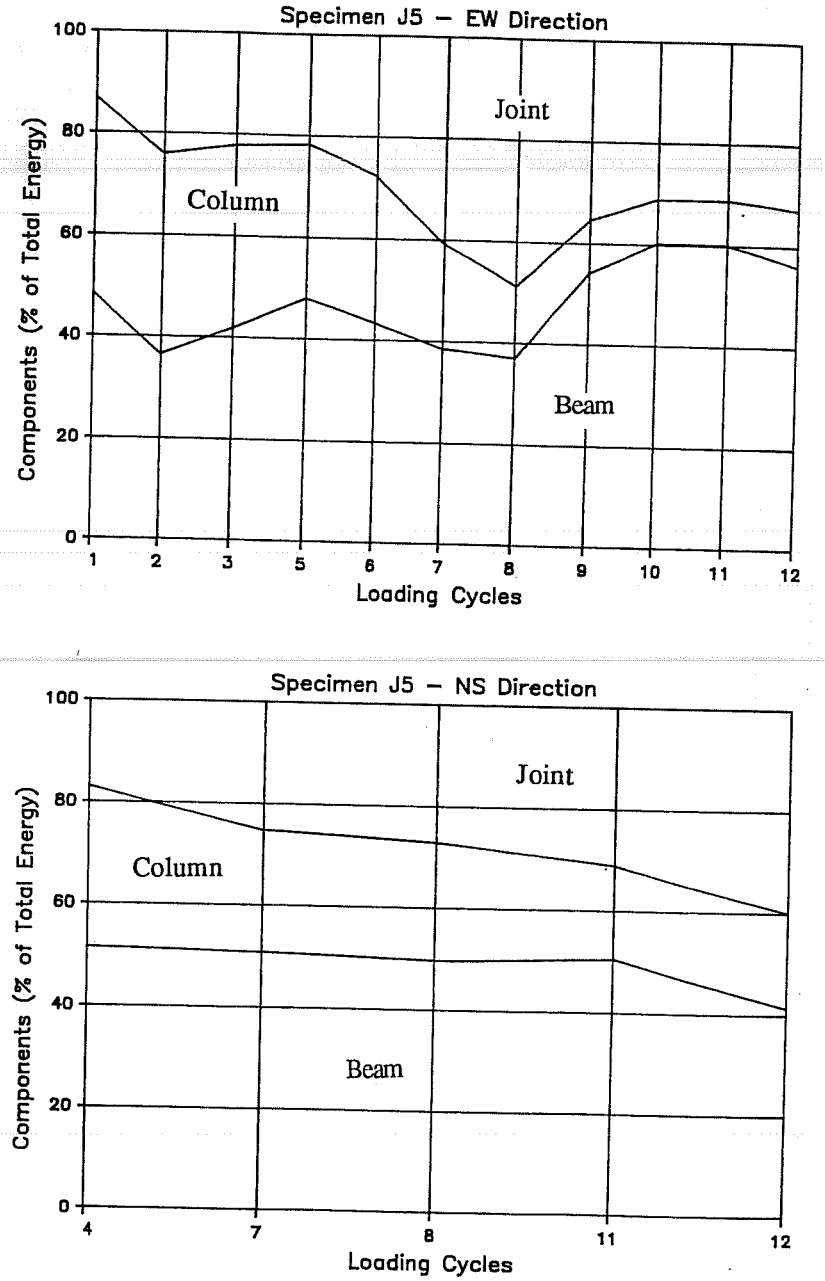

Figure 4.11 **Beam, Column and Joint Contributions to Total Energy Dissipation for Specimen J5**

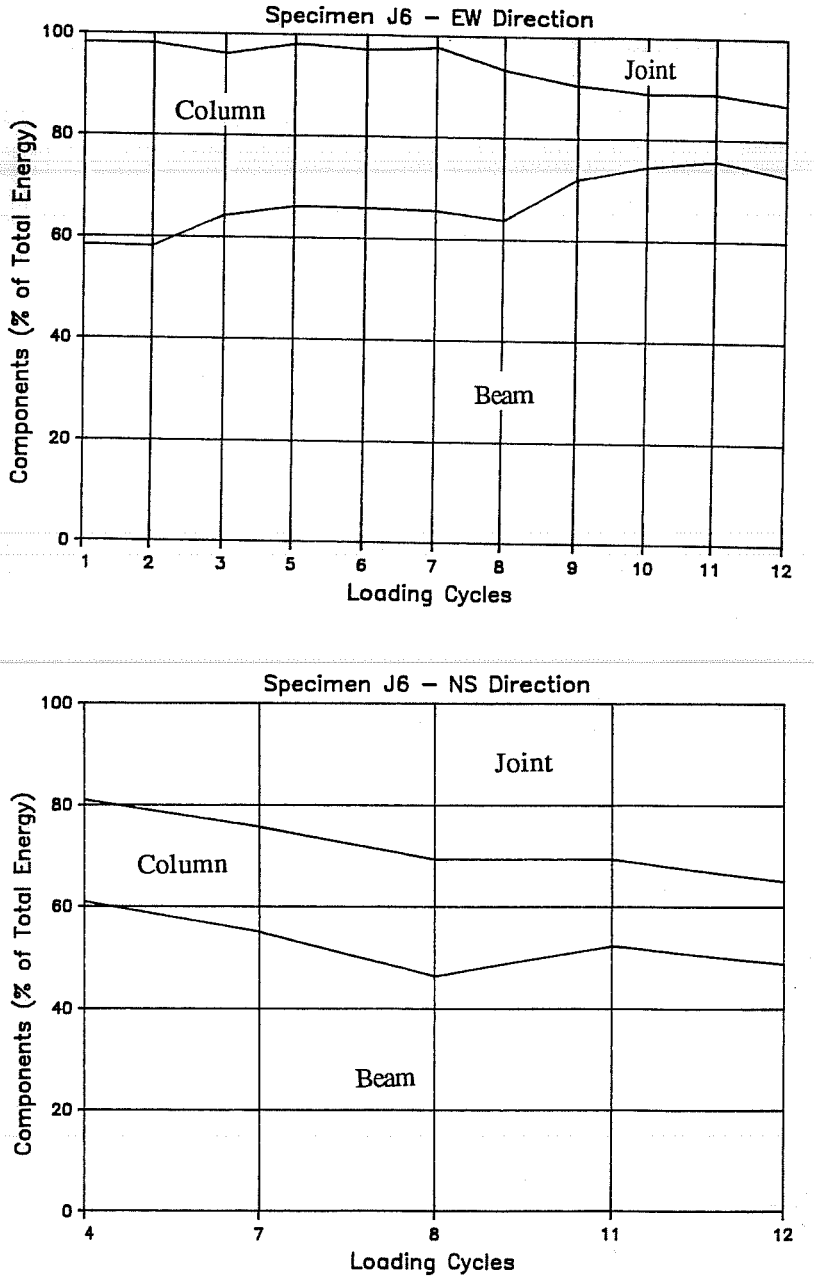

Figure 4.12 **Beam, Column and Joint Contributions to Total Energy Dissipation for Specimen J6**

approximately 35% to less than 10%, and to about 20% in the N-S direction. The beam contribution in the E-W direction remained at about 40% until cycle 8 when it increased sharply to about 60%. In the N-S direction, the beam contribution was nearly constant at approximately 50%.

Plastic hinge formation in specimen J5 is evident from the increase in beam contribution after cycle 8, especially in the E-W direction. As for specimen J4, maximum story shear in bidirectional loading occurred in cycle 7/pos (Table 3.1). Again, this indicates joint distress in 2% bidirectional cycles, while formation of beam plastic hinges occurred in 4% story drift cycles.

Both joint and beam contributions increased in specimen J6, especially during E-W loading (Figure 4.12). Joint contribution in E-W loading increased throughout the test from less than 5% to about 15%, and in N-S loading from about 20% to about 35%. The beam contribution increased from 60% to 75% in E-W loading but remained under 60% for N-S loading. The column contribution decreased sharply in E-W loading from almost 40% to about 10%, and was approximately 20% during N-S loading.

As for specimen J2, maximum story shears for specimen J6 occurred at 4% story drift. While formation of plastic hinges during cycle 9 is more evident than in specimen J2, it is not as clear as in specimen J5. Although plastic beam hinging did occur in specimen J6, it was accompanied by an increase in joint distress in the 4% story drift cycles. This is especially true during E-W loading, where the column contribution decreased sharply.

4.3.2. Pinching in the Hysteresis Loops. Energy dissipating capacity is characterized by the shape of hysteresis loops. In general, pinching indicates low energy dissipating capacity which is undesirable in structural design in earthquake zones.

Pinching of the hysteresis loops occurred for all four specimens, especially when loading at higher drift levels. In general, this was associated with several factors:

a. Shear distress in the joint. High shear forces in the joint led to deterioration of the joint concrete. Extensive diagonal cracking and concrete crushing inside the joint occurred during reversed cyclic loading. Since the specimens were designed so joint shear failure would occur, significant joint distress was expected as failure approached.

b. Difference in top and bottom beam reinforcement. Top longitudinal reinforcement was greater than bottom reinforcement by 85% in specimen J2 and by 30% in specimen J5 (Table 2.3). This difference is further increased if slab reinforcement is considered. Calculated beam moment capacities show beams stronger in negative bending (top reinforcement in tension) than in positive bending. On average,

negative moment capacities were 85% higher for specimen J2 and 57% higher for specimen J5.

Since the beams were taken to the same deflection level in positive and negative bending, strains and stresses in the bottom steel were greater than in the top steel. Therefore, bottom reinforcing bars were more likely to have plastic deformations and to lose anchorage first. This was reflected in the shape of the hysteresis loops. Less pinching occurs when positive and negative beam moment capacities are equal.

c. Presence of slab. The slab not only provided more top longitudinal reinforcement but also confined the top part of the joint, reducing the amount of cracking and spalling at the top. Bond conditions of the top reinforcement were better due to the slab confinement.

The slab also provided more concrete to carry the compression forces and influenced the position of the neutral axis. Participation of the top steel in carrying these forces is reduced. Therefore, lower bond stresses were necessary and inelastic deformation of the top bars in compression is less likely. Anchorage loss was not as critical as in bottom bars.

Less cracking and concrete crushing was expected at the top of the connection as well as less reinforcing bar strain. Differences in behavior between lower and upper parts of the beams were enhanced even further.

d. Cracking and crushing of concrete in the beams. Due to higher stresses in bottom bars in tension, and the position of the neutral axis, larger cracks were expected to form in the bottom part of beams. After formation of large cracks and plastic deformation of the bars, the bottom reinforcement carried all compression forces when the load was reversed. This caused further deterioration of bond along bottom bars. The bar was in compression on one side of the joint and in tension on the other side. Until the beam concrete came into contact with the column, the compressive force was carried entirely by the beam steel and bond damage occurred. In addition, the stiffness of the section was lower than when concrete is carrying compression. Further pinching of the load deflection curves occurred.

Due to lack of concrete confinement and greater stresses in the concrete of the beam bottom, crushing and spalling was more likely to occur first. After spalling of the bottom concrete cover in the beams next to the column face, bottom reinforcing bars carried all compression forces. The situation described earlier worsened because there was less beam concrete to carry compression when cracks closed. Loss of stiffness resulted in more pinching of hysteresis loops.

e. Beam bar slip through the joint. The loss of bond and slippage of beam bars through the joint was reflected in the beam tip deflection angle. When bond deterioration occurred, the beam shear force produced a larger displacement at the beam tip than occurred with no bar slippage. Subsequently, only a small force was required at the beam tip to pull the bars through the joint, creating pinching in the curves.

The quantitative influence of the five factors described above on the shape of the load-deflection curves is not easily obtained. The difficulty of assessing each effect is further increased due to their interdependency.

Figure 4.13 illustrates pinching in the load-deflection curves of specimen J5. West beam shear is plotted against beam end rotation in region 1 (Figure 3.23). Loops corresponding to cycles 9 and 10 are indicated. Negative beam shear was measured at positive loading cycles (top bars in tension). At the start of cycle 9, the stiffness was higher than in cycle 10 since there was no major concrete cracking or spalling. The specimen reached its peak unidirectional load at 4% story drift after yielding of the west beam top bars. West beam shear is higher in positive loading when the top longitudinal bars are in tension. Towards the positive peak of cycle 9, significant spalling and crushing of the concrete occurred, especially at the bottom of the west beam next to the column face. Since bottom concrete spalled, most of the compression forces were carried by bottom bars. Considerable bond deterioration may have occurred in the bottom bars since they were in tension on the east side of the joint and in compression on the west side. Large inelastic deformations occurred after the positive peak in cycle 9. Loss of stiffness and pinching was evident during cycle 10. Due to a large crack opening and concrete spalling, the beam shear-beam curvature relation exhibited low stiffness since the joint moment was resisted by a steel force couple at the top and bottom reinforcing layers. Stiffness was further reduced due to the likelihood of bar slippage through the joint.

4.3.3. Equivalent Viscous Damping Ratio. Damping is one of the most important parameters influencing the ability of a structure to dissipate energy under dynamic excitation. The equivalent viscous damping ratio H_{eq} can be obtained by computing the ratio of dissipated energy to the strain energy of an equivalent linear system divided by a constant 2π [11]. This definition is shown in Figure 4.14. It can be calculated from story shear-drift angle curves or story shear-interstory drift curves. Equivalent viscous damping ratio is used to normalize viscous damping of the system and reflects the amount of pinching in the hysteresis loops. Overall energy dissipation characteristics of the specimens are easier to compare.

The equivalent viscous damping ratio H_{eq} for a perfectly elasto-plastic system is shown in Figure 4.15. Displacement ductility ratio μ is defined as the ratio of displacement

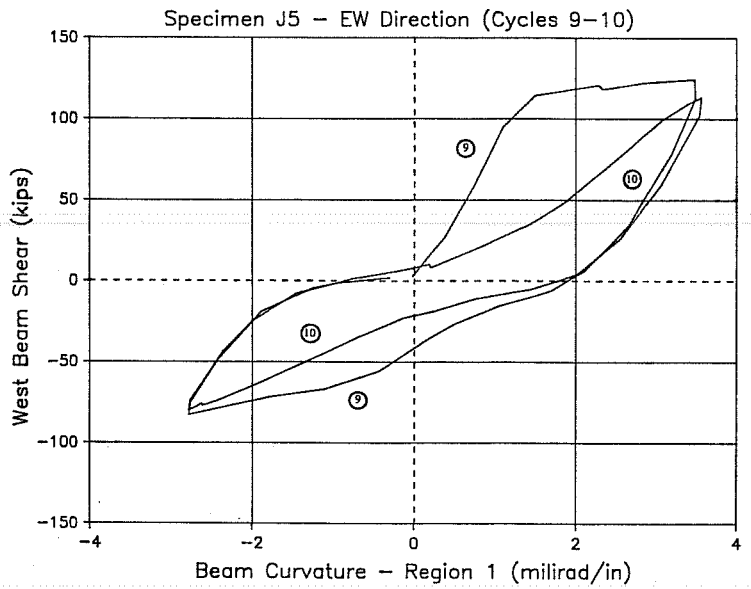

Figure 4.13 West Beam Shear vs Beam End Curvature for Specimen J5 (Cycles 9-10)

at ultimate to displacement at yielding. The table below shows equivalent viscous damping ratios H_{eq} for different displacement ductilities μ of an elasto-plastic system.

μ	H_{eq}
2	0.16
3	0.21
4	0.24
5	0.26
6	0.27

Figures 4.16 and 4.17 show equivalent viscous damping ratio H_{eq} against story drift angle for specimens J2 and J5 in the E-W direction. Figure 4.18 shows the same for the N-S direction. Equivalent viscous damping ratios for specimens J4 and J6 are almost identical to those for specimens J2 and J5 respectively. Notation for Figures 4.16 through 4.18 is the same as shown in Figure 4.2(a).

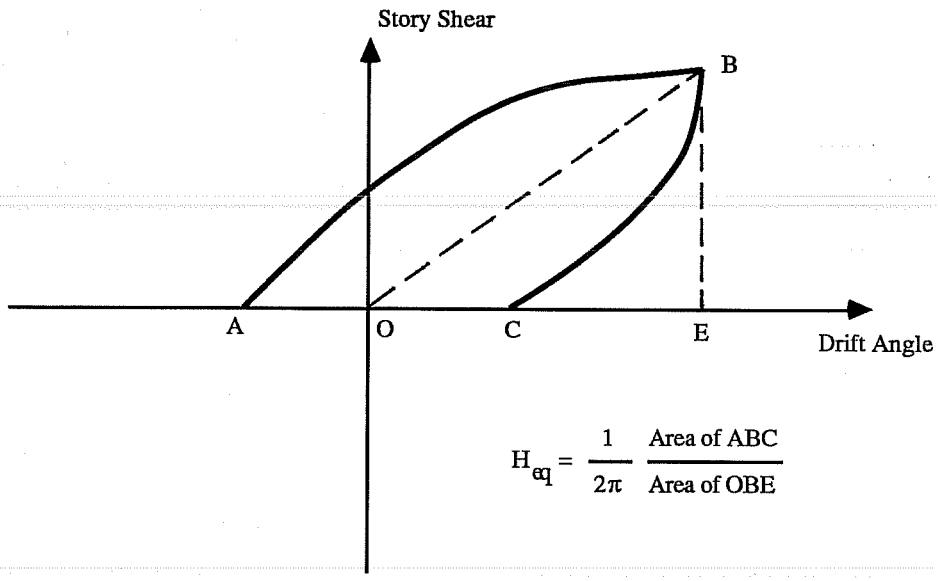

Figure 4.14 Equivalent Viscous Damping Ratio H_{eq}

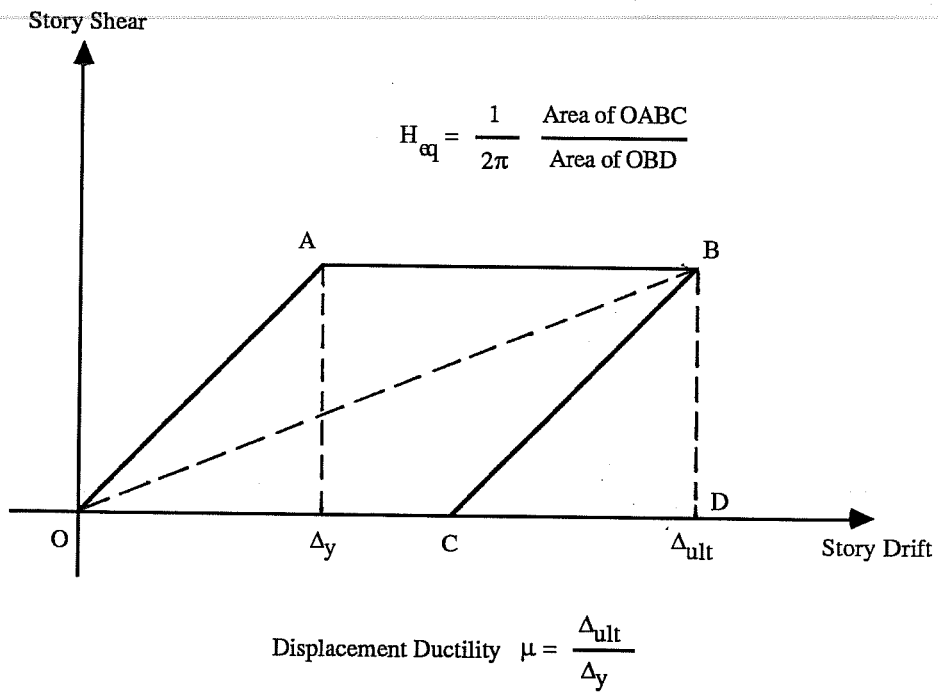

Figure 4.15 Displacement Ductility for Elasto-Plastic Model

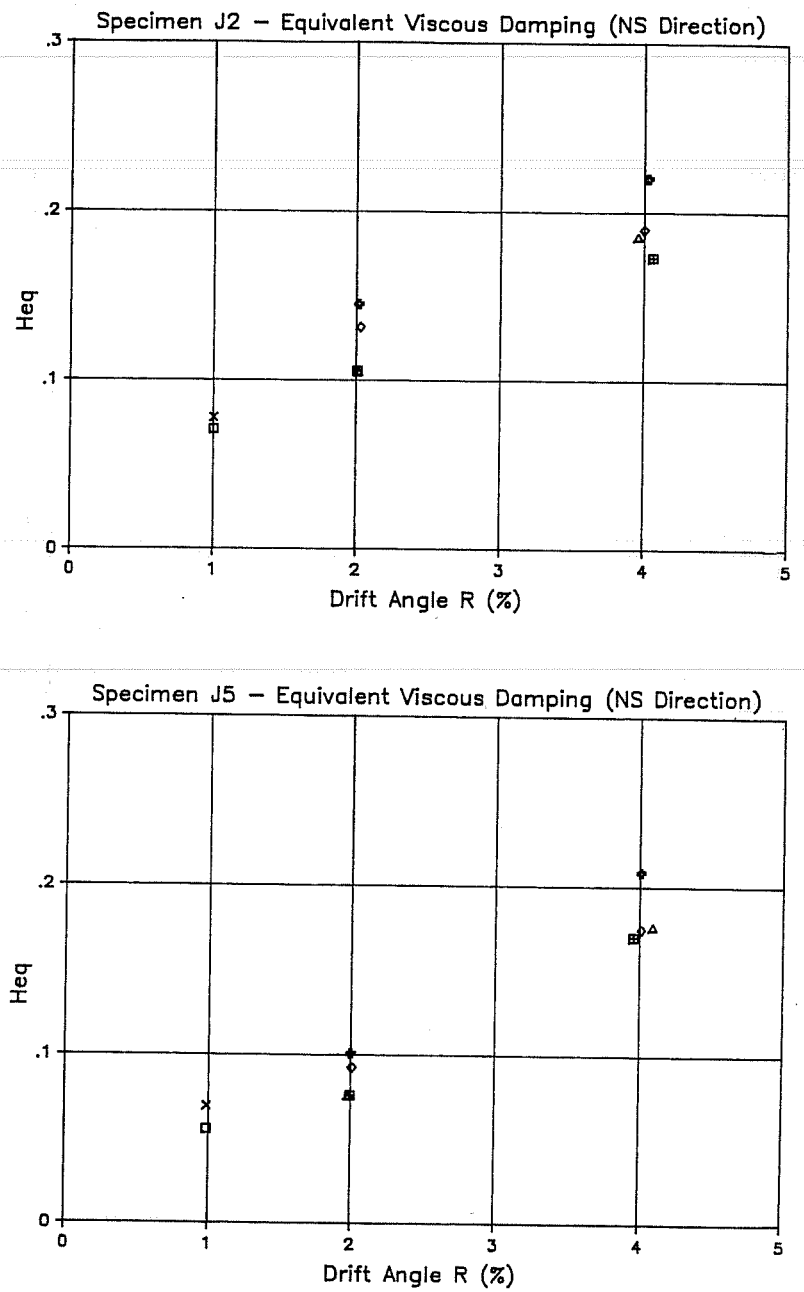

Figure 4.18 **Equivalent Viscous Damping Ratio for Specimens J2 and J5 (NS Direction)**

In general, equivalent damping ratios were low. Typically, values were below 0.1 through cycles at 2% story drift and below 0.2 for 4% story drift cycles. Displacement ductility ratios corresponding to these values would not be more than three for a perfect elasto- plastic system (Figure 4.15). The table below is a summary of the range of equivalent damping ratios. Highest values were reached during bidirectional cycles.

	Unidirectional	Bidirectional	
Story Drift	Specimens J2/J5	Specimen J2	Specimen J5
0.5%-2%	0.04-0.10	0.09-0.14	0.07-0.10
4%	0.08-0.15	0.11-0.22	0.13-0.21

In unidirectional E-W loading, high strength and normal strength concrete specimens showed very similar equivalent damping ratios. Values were quite low, especially up to 2% drift cycles. High strength concrete specimens showed lower values at 2% story drift due to the predominantly elastic nature of the hysteresis curves. In unidirectional loading, higher equivalent damping ratios were always obtained in the first cycle at a specified drift level. Typically, the first negative half cycle gave highest ratios.

In the bidirectional cycles, equivalent damping ratios obtained for the E-W direction were similar for all specimens. Also, equivalent damping ratios obtained for the N-S direction were similar for all specimens. Ratios were higher than those obtained for unidirectional cycles, but were typically below 0.2. Again, high strength concrete specimens showed lower values at 2% story drift due to the predominantly elastic nature of the hysteresis curves. In E-W bidirectional loading, the lowest equivalent viscous damping ratios were obtained in the first positive half cycle for a specified drift level. In N-S bidirectional loading, the highest ratios were obtained at the first negative half cycle for a specified drift level.

Figure 4.19 shows story shear against story drift angle for cycles 9 through 12 of E-W loading of specimen J5. This figure will be used for a qualitative explanation of some of the values of damping ratios.

In general, the first negative half cycle showed higher equivalent damping ratios than the first positive half cycle for unidirectional E-W loading and for bidirectional N-S loading. For example, specimen J5 showed a higher damping ratio for half cycle 9/neg than for half cycle 9/pos (E-W unidirectional loading), and a higher ratio for half cycle 11/neg than for half cycle 11/pos (N- S bidirectional loading). This is due to the large deformations

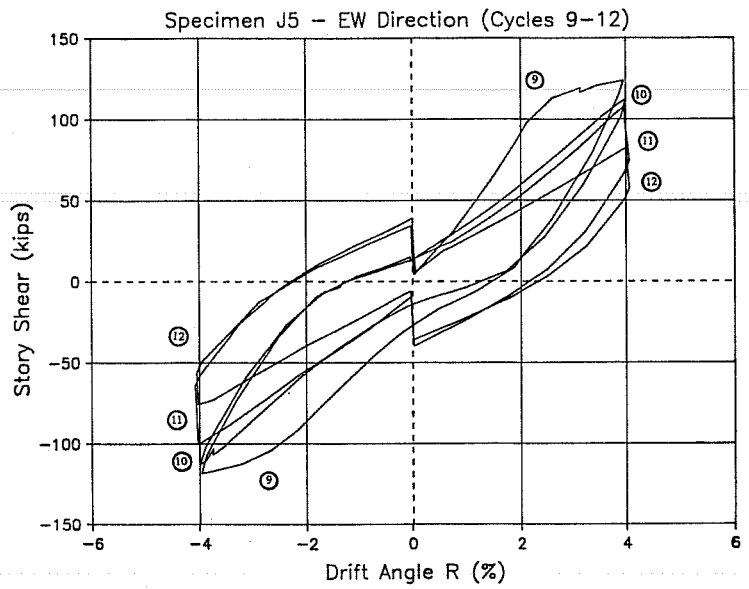

Figure 4.19 Story Shear vs Drift Angle for Specimen J5 (Cycles 9-12)

at the start of the first negative half cycle which were not present at the start of the first positive half cycle (Figure 4.19). This did not occur for E-W bidirectional loading since large deformations were already present at the start of the first positive half cycle.

In E-W bidirectional loading, the first positive half cycle showed the lowest damping ratios. This is illustrated in Figure 4.19 by cycles 11 and 12. Due to bidirectional loading interaction, vertical offsets in the story shear-drift angle curves were produced. The offsets occurred at both zero and 4% story shear. However, vertical offsets did not occur at the beginning of bidirectional loading, i.e., at the start of the first positive half cycle (cycle 11/pos). As a result less energy was dissipated during that half cycle and the equivalent damping ratio was lowest.

Although equivalent viscous damping ratios were low, the flexibility of the specimens as shown in Table 4.1 must be considered. Yield deflection was high, ranging from about 1% to 1.5%. Therefore, thin hysteresis loops occurred at the first loading cycles and high damping ratios were precluded. However, at cycles of higher story drift, low damping ratios reflect low energy dissipating capabilities. Higher damping ratios during bidirectional loading cannot be attributed to better energy dissipating characteristics but rather to the nature of bidirectional loading interaction.

4.4 INTERSTORY DISPLACEMENT COMPONENTS

4.4.1. Contribution to Interstory Drift Angle. The elements contributing to interstory drift are the beams, column, and joint. The contribution of each of these elements can be related to story drift angle R as shown in Section 3.3. It is important to assess the contribution of each element to determine where most of the deformation and distress occurred.

Figures 4.20 through 4.23 show the beam, column, and joint contribution to story drift angle for specimens J2, J4, J5 and J6. Each contribution is expressed as a percentage of the drift angle. Values for E-W loading cycles are shown on the upper graph and for N-S loading cycles on the lower graph. For each loading cycle, the percent contribution shown is an average between values calculated at the peaks of positive and negative half cycles.

Figures 4.20 through 4.23 are similar to Figures 4.9 through 4.12 where contributions to cumulative energy dissipation are shown. Similar trends for joint, column and beam contributions can be observed. In general, the joint contribution increased. The column contribution was the lowest and steadily decreased. The beam contribution was highest reaching more than 60% after formation of plastic hinges.

Plastic hinging in E-W beams of specimens J4, J5 and J6 was clear from the increase in beam contribution from cycle 8 to cycle 9 during E-W loading. In specimens J4 and J5, beam hinging was accompanied with a decrease in the joint contribution, a trend which was not observed in specimen J6. For specimen J2, plastic beam hinging is not clear from Figure 4.20 due to the steady increase in the joint contribution occurring at the same time. Figure 3.21 shows beam hinging in specimen J2 during the large increase in beam tip deflection angle during cycle 9.

Joint deterioration is clear in E-W loading cycles. A large increase in the joint contribution occurred in cycle 7 for specimens J4 and J5. Also, maximum joint shear for bidirectional loading occurred in cycle 7/pos for specimens J4 and J5 (Table 3.1). However, for specimens J2 and J6, major joint distress did not occur before 4% story drift cycles were reached.

The joint contribution during N-S loading increased steadily while the beam contribution did not show any large increases. Evidence of plastic beam hinging was not clear since the beam contribution remained almost constant throughout. In addition, clear evidence of plastic hinging in N-S beams during cycle 11 (first 4% story drift cycle in N-S direction) cannot be found in story shear-beam tip deflection angle curves. The beam tip deflection angle showed large increases only during the last loading cycle. In general, crack patterns

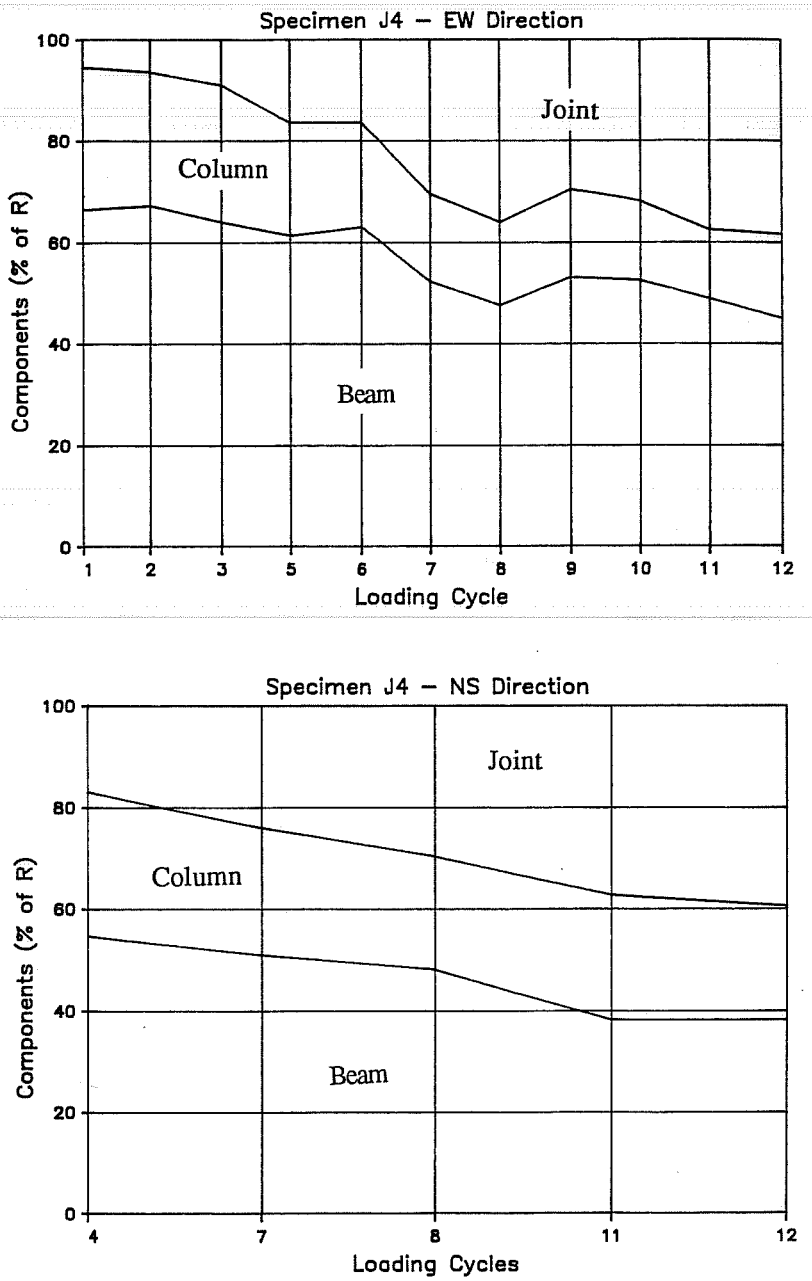

Figure 4.21 **Beam, Column, and Joint Contributions to Interstory Drift Angle for Specimen J4**

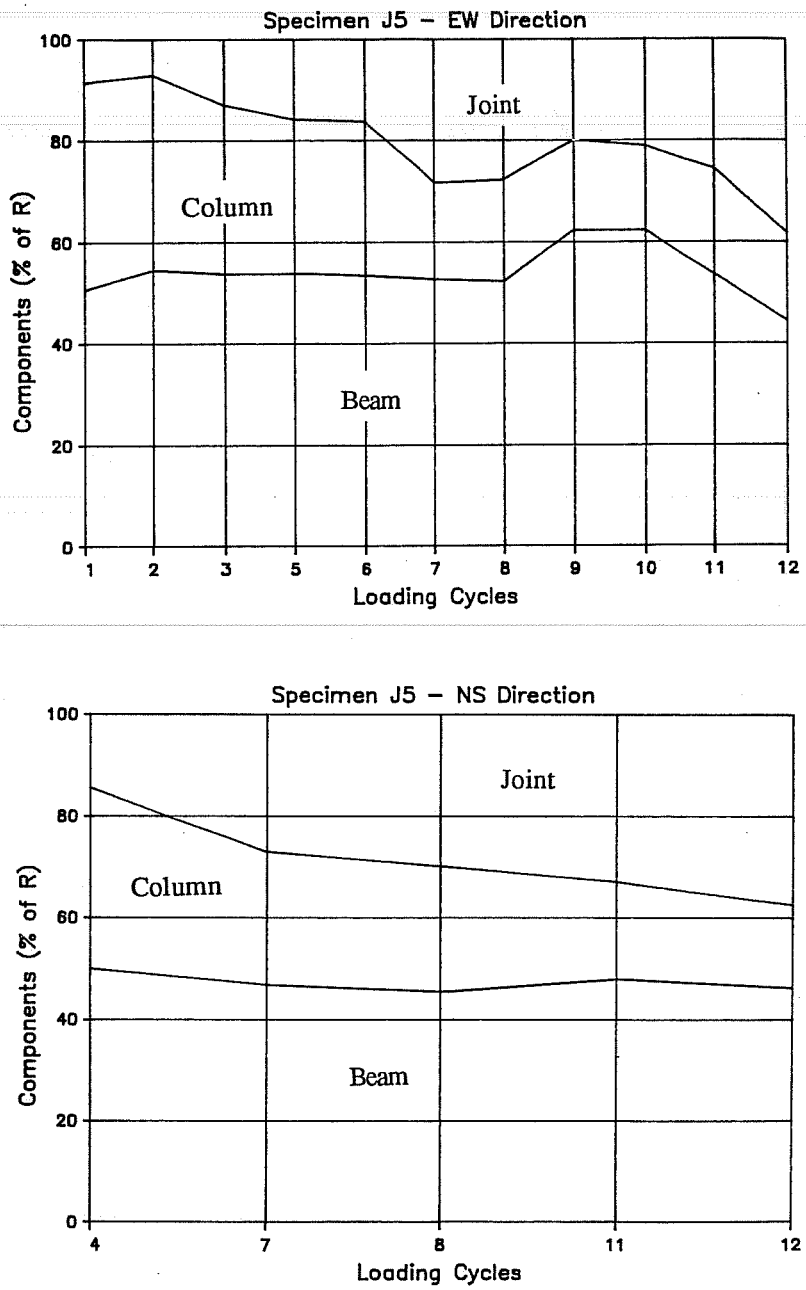

Figure 4.22 **Beam, Column, and Joint Contributions to Interstory Drift Angle for Specimen J5**

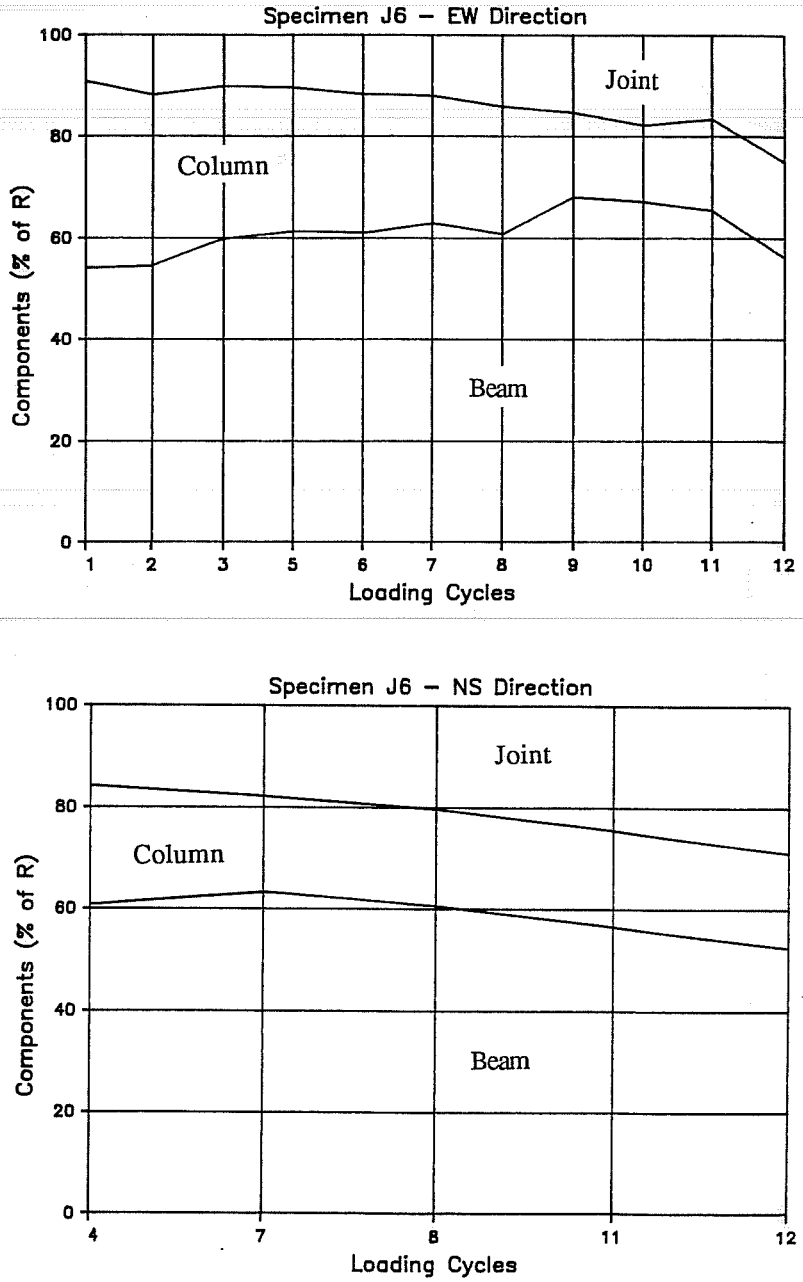

Figure 4.23 **Beam, Column, and Joint Contributions to Interstory Drift Angle for Specimen J6**

show concrete crushing and spalling in N-S beams, but this occurred towards the end of the test.

In summary, significant joint distress occurred for all specimens in both loading directions. Joint distress was more significant during bidirectional cycles. For example, large increases in the joint contribution can be seen during cycle 7 in E-W loading of specimens J4 and J5, cycle 11 in E-W loading of specimen J2, cycle 12 in E-W loading of specimens J5 and J6, cycle 7 in N-S loading of specimens J2 and J5. However, joint shear failure probably occurred during the 4% story drift unidirectional cycles since a large increase in joint shear distortion was observed. In addition, maximum story shears in unidirectional loading occurred at 4% story drift. Plastic hinging of E-W beams occurred during 4% drift unidirectional cycles. Formation of plastic beam hinging is sometimes unclear due to joint distress occurring at the same time. This is especially true during N-S bidirectional loading cycles.

4.4.2. Contribution to Beam Tip Deflection Angle. Beam deformations were controlled by the region next to the column. In order to assess the formation of plastic beam hinging it is important to identify the contribution of beam deformations next to the column to the beam tip deflection angle. Therefore, a comparison between member end rotation and beam tip deflection angle is appropriate. Member end rotations in region 1 (Figure 3.23) were measured in all beams. According to the assumed deformation pattern shown in Figure 2.16, the beam tip deflection angle should be larger than the beam end rotation.

In Table 4.2, beam end rotations in region 1 are tabulated as a percentage of beam tip deflection angle. Percentages shown are averages between values obtained at peaks of positive and negative half cycles. Some measurements obtained for N-S beams may be distorted due to concrete spalling in 4% drift bidirectional cycles.

Typically, most of the beam deformations occurred in the first 4 inches from the column face (region 1). In addition, the contribution of beam end rotation in region 1 increased with story drift angle. In general, a large relative increase can be observed during cycle 9 for E-W loading and during cycle 11 for N-S loading. Formation of beam plastic hinges during 4% story drift cycles is evident since the percentages increased substantially.

4.5 SPECIMEN DETAILS

Joint shear strength can be studied through interstory shears. Ultimate story shears can be calculated using joint shear strength obtained from design recommendations. Beam hinging is assumed next to the column. The following expression can be used to calculate unidirectional story shear.

Table 4.2 Beam End Rotation in Region 1
(Percentage of Beam Tip Deflection Angle)

	Specimen			
	J2	J4	J5	J6
East-West Cycle				
3	44	48	50	46
5	47	56	52	49
7	49	57	54	51
9	69	88	65	71
11	72	89	65	71
North-South Cycle				
4	45	56	52	45
7	56	64	61	46
11	98	94	N/A	84

$$V_u = \frac{b_j * h_j * j_b * v_j}{H(1 - h_j/L - j_b/H)}$$

Where:

V_u =calculated ultimate unidirectional story shear

v_j =maximum joint shear stress according to design recommendations

H = column height

L = beam span

b_j =joint width

h_j =joint depth

j_b =beam moment arm

Tables 4.3 and 4.4 show measured maximum story shear compared with calculated ultimate story shear. Measured story shears in Table 4.3 were obtained at 2% story drift, and measured story shears in Table 4.4 were obtained at 4% story drift. Calculated story shears are independent of story drift angle. Unidirectional ultimate story shears were calculated from the expression above using three design guidelines: ACI Committee Report 352 [2], AIJ Standard for Reinforced Concrete Structures [3], and NZS Code of Practice 3101 [4].

		J2		J4		J5		J6	
		Uniaxial	Biaxial	Uniaxial	Biaxial	Uniaxial	Biaxial	Uniaxial	Biaxial
Measured Story Shear (kips)		64.3	72.1 [EW = 42.7] [NS = 58.1]	62.9	69.6 [EW= 42.65] [NS = 55.0]	106.7	136.9 [EW = 86.9] [NS = 105.8]	101.4	128.5 [EW = 85.0] [NS = 96.4]
Calculated Story Shear (kips)	a) ACI 352	48.7 (1.32)	48.7 (1.48)	54.6 (1.15)	54.6 (1.27)	80.2 (1.33)	80.2 (1.72)	88.1 (1.15)	88.1 (1.46)
	b) AIJ-SRC	45.6 (1.41)	45.6 (1.58)	47.0 (1.34)	47.0 (1.47)	68.3 (1.56)	68.3 (2.02)	70.4 (1.44)	70.4 (1.83)
	c) NZS-3101	15.3 (4.20)	15.3 (4.72)	12.5 (5.03)	12.5 (5.52)	20.0 (5.33)	20.0 (6.88)	21.0 (4.83)	21.0 (6.12)

( ) Ratio of measured story shear to calculated story shear

Table 4.3 - Measured Maximum Story Shear Compared with Calculated Story Shear at 2% Story Drift

		J2		J4		J5		J6	
		Uniaxial	Biaxial	Uniaxial	Biaxial	Uniaxial	Biaxial	Uniaxial	Biaxial
Measured Story Shear (kips)		72.0	73.4 [EW = 37.6] [NS = 63.0]	67.1	66.1 [EW= 32.05] [NS = 57.80]	123.9	134.3 [EW = 74.85] [NS = 111.49]	114.7	129.7 [EW = 72.4] [NS = 107.6]
Calculated Story Shear (kips)	a) ACI 352	48.7 (1.48)	48.7 (1.51)	54.6 (1.23)	54.6 (1.21)	80.2 (1.54)	80.2 (1.67)	88.1 (1.30)	88.1 (1.47)
	b) AIJ-SRC	45.6 (1.58)	45.6 (1.61)	47.0 (1.43)	47.0 (1.41)	68.3 (1.81)	68.3 (1.97)	70.4 (1.64)	70.4 (1.85)
	c) NZS-3101	15.3 (4.70)	15.3 (4.79)	12.5 (5.37)	12.5 (5.29)	20.0 (6.18)	20.0 (6.71)	21.0 (5.47)	21.0 (6.16)

( ) Ratio of measured story shear to calculated story shear

Table 4.4 - Measured Maximum Story Shear Compared with Calculated Story Shear at 4% Story Drift

The provisions for ultimate shear strength of interior joints of these three recommendations are outlined in Appendix B. Ratios of measured to calculated story shears are shown in parenthesis.

Definitions of joint width b_j and joint depth h_j vary according to each recommendation as follows. Joint width b_j is the average of the beam and column widths for ACI 352 and AIJ-SRC, and is equal to the column width for NZS 3101. Joint depth h_j is equal to column depth for ACI 352 and NZS 3101, and is equal to 7/8 of effective beam depth for AIJ-SRC. The beam moment arm j_b was always taken as 7/8 of effective beam depth for consistency.

Bidirectional story shears are also shown in Tables 4.3 and 4.4. Measured bidirectional story shears were obtained as the square root of the sum of the squares of the peak E-W and N-S story shears during bidirectional loading. Maximum measured bidirectional story shears at 2% and 4% story drift are shown in the tables.

There are no design recommendations for calculating bidirectional story shear from joint shear strength. Unidirectional story shears were calculated for E-W and N-S directions, and circular or elliptical interaction curves were assumed for bidirectional strengths. Story shears in orthogonal directions do not differ by more than 2%. This difference occurs in specimens J5 and J6 due to slightly unequal beam effective depths. Therefore, elliptical interaction curves were used for specimens J5 and J6. Ratios of measured to calculated bidirectional story shears shown in Tables 4.3 and 4.4 are given by the expression below.

$$ratio = \sqrt{\frac{(V_{m1})^2}{(V_{u1})^2} + \frac{(V_{m2})^2}{(V_{u2})^2}}$$

Where:

V_m =measured unidirectional story shear

V_u =calculated unidirectional story shear

$_{1,2}$ =subscripts indicate E-W and N-S loading directions

In all cases, measured story shears at 2% and 4% story drifts exceeded calculated story shears. Calculated ultimate strengths were exceeded under unidirectional and bidirectional loadings. Calculated story shears using the New Zealand Standard were lowest since the concrete contribution is neglected. The lowest ratios of measured to calculated story shear were obtained using the ACI 352 recommendations which assigns all joint shear strength to the concrete. Japanese guidelines (AIJ-SRC) assign joint shear strength to both concrete and transverse steel. Ratios obtained using AIJ- SRC guidelines were higher than

those obtained using the ACI 352 Report and both were much lower than ratios obtained using the New Zealand Standard.

Higher ratios of measured to calculated story shear were obtained for high strength concrete specimens indicating that current design recommendations provide a safe estimate of the shear strength of the two high strength concrete joints. There is no evidence of a significant influence of high strength steel reinforcement on joint shear strength. These tests indicate joint shear strength depends more on concrete compressive strength than on the amount and strength of the joint reinforcement.

The table below shows a summary of the ratios of measured to calculated story shears from Tables 4.3 and 4.4. For each of the three design guidelines, the range of values of the ratios and the average ratio for unidirectional and bidirectional loading is shown.

	2% Story Drift		
	Range	Average	
		Unidirectional	Bidirectional
ACI 352	1.15-1.72	1.24	1.48
AIJ-SRC	1.34-2.02	1.44	1.73
NZS 3101	4.20-6.88	4.85	5.81
	4% Story Drift		
	Range	Average	
		Unidirectional	Bidirectional
ACI 352	1.21-1.67	1.39	1.47
AIJ-SRC	1.41-1.97	1.62	1.71
NZS 3101	4.70-6.71	5.43	5.74

Ratios of ultimate to measured story shears were always greater than one. For unidirectional loading, average ratios were about 12% greater at 4% drift than at 2% drift. For bidirectional loading, average ratios changed only 1%.

Maximum story shears were measured at 4% story drift except for bidirectional loading of specimens J4 and J5, which were maximum at 2% story drift. For specimens

J2 and J6, bidirectional story shears increased less than 2% when the drift angle increased from 2% to 4%. Bidirectional story shears decreased for specimens J4 and J5 but not by more than 5%. Essentially, the ratios of measured to calculated bidirectional story shears remained unchanged from 2% to 4% drift cycles. Basically, bidirectional shear strength was as high at 2% story drift as it was at 4% story drift.

Unidirectional E-W story shears were highest at 4% story drift. The increase in measured unidirectional story shear ranged from 7% for specimen J4 to 15% for specimen J5. Typically, ratios obtained for unidirectional loading are less than those obtained for bidirectional loading, especially at 2% story drift.

E-W beam hinging occurred during cycle 9 when maximum unidirectional story shears were measured. Higher story shears might have been reached if plastic hinging had not occurred. It is possible that beam flexural strength governed E-W unidirectional story shears.

4.6 BOND BEHAVIOR OF LONGITUDINAL REINFORCEMENT

4.6.1. Beam Bars. Average bond stresses for beam longitudinal reinforcement were calculated at 0.5% and 1% story drift. Average bond stresses were calculated using bar stresses obtained at the ends of the joint (over a 20-inch column depth). These stresses were usually low, rarely exceeding 400 psi. However, low bond stresses are not necessarily indicative of bond deterioration. They are low because bar stresses are low since beam shears (and story shear) are not high at this stage. Also, bar positioning was such that the neutral axis of the cross section was usually above the longitudinal reinforcement.

At 2% story drift beam shears increased significantly and so did story shear. As mentioned previously in Section 4.5, story shear measured at 2% story drift did not differ significantly from maximum story shears. Therefore, bar stresses were higher than in previous cycles. Average bond stresses were also calculated at 2% story drift and maximum values are shown in Table 4.5. Typically, the maximum values at 2% story drift were obtained during cycle 5/neg. In addition, Table 4.5 includes ratios of column depth to bar diameter and design bond stresses. Design bond stress is an average bond stress over the basic development length of a bar as specified by Section 12.2.2 of ACI Building Code Requirements 318-83 [1].

As shown in Table 4.5 measured bond stress at 2% story drift increased from previous cycles, and maximum values ranged from 635 psi for top bars of specimen J5 to 1820 psi for bottom bars of specimen J6. Measured bond stresses were about the same for top and bottom beam bars of specimen J2 and J4. Bond stresses in top bars of specimens

Position	Specimen	Bar Size	h/d_b	Design Bond Stress (psi)	Measured Bond Stress (psi) at 2% Drift
Beam Top Bar	J2	#8	20.0	504	962
	J4	#8	20.0	539	1,023
	J5	#10	16.0	676	635
	J6	#9	17.8	818	844
Beam Bottom Bar	J2	#6	26.7	671	822
	J4	#7	22.9	616	1,043
	J5	#8	20.0	845	1,468
	J6	#9	17.8	818	1,820

Where : h = column depth

d_b = bar diameter

Design bond stress = $\sqrt{f'_c} / (0.04 \pi d_b)$

Measured bond stress = $(f_2 - f_1) * d_b / 4h$

f_1, f_2 = beam bar stresses measured at column face

Table 4.5 - Bond Stresses for Beam Bars

J5 and J6 were less than half the bond stresses in bottom bars. In all cases, measured bond stresses exceeded design bond values.

Bond deterioration probably did not occur during 2% drift cycles. Evidence of this can be found in bar stress distribution and in analysis of beam end rotations. Figures in Section 3.4.3 showing stress distributions along the top and bottom layers of beam bars indicate a decrease in stress across the joint. This decrease was fairly linear up to cycle 5 (2% story drift). The constant decrease in stress from tension to compression across the joint indicates good bond along the bars. However, during cycle 9, the stress distribution is almost constant up to the joint midlength and the decrease occurs mainly outside the middle of the joint. High stresses from the tension side to the joint midlength indicate yield penetration and probably bond loss occurred.

Figures in Section 3.3.4 showing beam end curvatures against beam shear also indicate good bond behavior up to 2% drift levels (See Figures 3.24 through 3.27). Bond deterioration and bar slip could be partially responsible for large increases in beam end curvature. However, large increases in beam end rotations did not occur until cycle 9 (4% story drift). This was especially true for the high strength concrete specimens which show generally elastic curves up through 2% drift cycles. In addition, pinching of the loops before cycle 9 is minor. This is evidence of good bond behavior of beam bars during 2% story drift cycles, even though beam shears were close to maximum.

Lower ratios of column depth to bar diameter shown in Table 4.5 tends to indicate that bond was more critical in top beam bars. This is supported by the lower bond stresses obtained for specimens J5 and J6. However, it is believed than bond deterioration was more critical in bottom bars for the following reasons. (Some of these factors have been discussed previously in Sections 3.4.3. and 4.3.2.)

1. Bond for top bars was enhanced by the confining effect of the slab. Horizontal splitting cracks formed on the side face of east and west beams of specimens J5 and J6 near the location of bottom reinforcement (Figures 3.13 and 3.14). Certainly the confining effect of the slab prevented such cracks from forming near the location of the beam top reinforcement.

2. Participation of the slab concrete altered the position of the neutral axis of the cross section. Generally, the top bars were at or below the neutral axis. The slab provided a much larger effective width than the beam width. Therefore, beam top bars did not have to contribute much to resist compression forces. One of the major sources of bond deterioration are high compression forces on one side of the

joint and high tension forces on the other side. Since the slab resisted most of the compression force, top beam bars were not subjected to large stress reversals.

3. Differences in the amount of top and bottom reinforcement may help bond deterioration [12,13]. The amount of top reinforcement (including slab steel) was much larger than the amount of bottom reinforcement for any of the specimens. This leads to higher strains in bottom reinforcement during upward loading. Therefore, tensile residual strains may lead to high compressive stresses during stress reversals with unloading. In addition, higher compressive forces are induced in the bottom part of the beam.

4. Higher forces occurred during downward loading than during upward loading due to the difference in top and bottom reinforcement and the position of the neutral axis. This led to higher compressive forces in the bottom part of the beam causing significant spalling and crushing of the beam bottom forces. In addition, the confining effect of the slab reduced spalling of the top beam concrete. This led to high compressive forces at the bottom bars at one side of the joint while high tension forces occurred on the other side. This was an important cause for bond deterioration in bottom bars at cycles of 4% story drift when most of the concrete spalling occurred.

Conditions for bond deterioration and bar slip at 4% story drift levels were good: large inelastic deformations, plastic hinging at the beam ends, high compressive and tension stresses at opposite ends of the joint, spalling of the beam bottom concrete causing the steel bars to carry most of the compressive forces, large crack opening especially at the beam bottom. Large increases in beam end curvatures (Figures 3.24 through 3.27) and pinching of the loops were probably not only caused by bond deterioration, but also by large strains in the reinforcement and large crack opening.

Bar stresses obtained at 4% story drift show very high average bond stresses. These bond stresses were often in excess of 2000 psi. Much higher bond stresses can be obtained if the average stress is calculated using two joint midlengths (10 inches each). While very low bond stresses are obtained on the tension side of the joint (usually less than 500 psi), very high stresses are obtained on the compression side (some as high as 3500 psi). Bond deterioration occurred at this stage, although bond damage across the joint was not total. The formation of the concrete compression strut inside the joint was probably responsible for the high bond values obtained on the compression side. High compressive forces inside the joint, in addition to the compressive forces coming from the beam and column caused crack closing, and contact between bar steel and concrete was obtained on the compressive side of the joint. Although this does not reduce pinching in the hysteresis loops, it does allow joint

strength to develop at 4% story drift cycles. Only after breakdown of the compression strut due to joint shear failure does total bond damage across the entire joint occur.

No significant difference in bond behavior could be found between normal and high strength reinforcement.

4.6.2. Column Bars. Indications of bar slippage and bond deterioration in longitudinal column reinforcement were evident from an analysis of strains and stresses in column bars. In addition, ratios of beam depth to column bar diameter were below 20 for all specimens. A ratio of 17.8 was obtained for specimens J2 and J4, and a ratio of 16.0 was obtained for specimens J5 and J6. Therefore, bond deterioration of column bars could have been expected.

Strains and stresses in corner column bars were analyzed in Section 3.4.4. Several features found in the analysis of strain cyclic history and stress distribution tend to indicate slippage in column bars.

Except for the initial loading cycles, only tensile strains were measured during the rest of the loading history. Cyclic strain history of gages located inside the joint mainly produced saddle- shaped curves which tended to center about an ever increasing tensile strain which was an indication of bar slippage [13,14]. Bond seemed to have further deteriorated after yielding of the column bars during 2% bidirectional drift cycles.

During bidirectional loading, diagonally opposed corners of the column are highly stressed. For example, during positive half cycles at 2% bidirectional drift (cycles 7/pos and 8/pos), the southwest and northeast column corners will be subjected to combined stresses from the south and west beams are loaded downwards, and from the north and east beams are loaded upwards. The southwest column corner concrete below the beams will be subjected to high compression stresses. During cycles 7/neg and 8/neg, the southwest column corner concrete above the slab will be subjected to high compression stresses. It is believed that when such a state of compressive stress occurs bond of the longitudinal corner bar will be assured. However, strain history curves of corner column bars (Figures 3.56 and 3.57) show tensile loops during bidirectional cycles. This indicates that even when the surrounding concrete was subjected to high compression stresses, it was not enough to prevent an increase in column bar strain. Probably, bond loss had occurred along the corner column bar passing through the joint.

During 4% drift cycles, concrete at the corner of the joint crushed and spalled. Probably more bar slippage occurred at this stage. High tensile strains were measured under both positive and negative loadings. Stress distributions show high tensile stresses in the column bars within the beam depth.

No significant difference was found in the bond behavior of normal (Grade 60) and high strength (Grade 75) reinforcing steel.

4.7 EFFECTIVE SLAB WIDTH

An important parameter for design purposes is the amount of slab effectively participating with the beam in T-beam action. Current code provisions for evaluation of effective slab width were based on tests with the slab in compression. There are no code provisions which consider the amount of slab steel contributing to the flexural capacity when the slab is in tension. The effective slab width when the slab is in tension will be evaluated for the test specimens.

The total slab width of the specimens was 204 inches (Figure 2.1). The width B on each side of the beam was 94 inches. The effective slab width b_e is defined here as the effective flange overhang on each side of the beam. Effective slab width is shown in Figure 4.24. All slab bars are #3 Grade 60 steel.

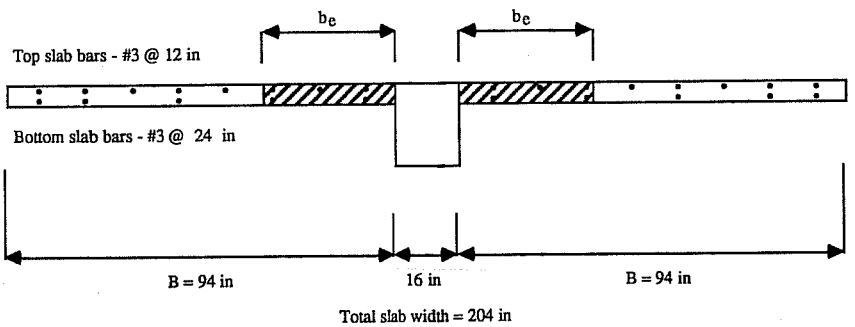

Figure 4.24 Effective Slab Width

The effective slab width b_e contributing to negative bending moment capacity can be evaluated through slab bar stresses such as those shown in Figures 3.42 and 3.43. One measure of effective slab width b_e is to calculate the ratio of tensile force in the slab reinforcement to the force if all slab bars reach yielded. The tensile force in the slab reinforcement is obtained from stresses calculated from measured strains at peaks of loading cycles. The equation below was used to calculate the effective slab width b_e.

$$b_e = B * \sum \frac{A_s * \sigma_s}{A_s * f_y}$$

Where:

b_e =effective slab width

B = slab width on one side of the beam

A_s =area of slab reinforcing bar

σ_s =reinforcing bar stress

f_y =reinforcing bar yield strength

Figure 4.25 shows effective slab width against story drift angle. Effective slab width b_e is shown as a percentage of slab width B. Values were calculated using the equation above with stresses obtained at positive peaks of loading cycles 1, 3, 5, and 9 (west slab in tension). No values were calculated for specimen J5 at 4% story drift. Several slab strain gages for specimen J5 were malfunctioning at this stage and the effective slab width calculated using these strains were unrealistic. The top graph shows effective slab width calculated using stress in top slab bars only. Both top and bottom slab bar stresses were used to obtain values in the bottom graph. In all specimens, bottom bars were continuous over the support. However, in many cases, bottom slab bar design is based on gravity loading and sufficient anchorage for seismic loads may not be provided at the support. Therefore, only top slab bars can be considered effective in those cases.

Effective slab width increased with drift angle. At 2% story drift, effective slab width was about 70% when only top bars were considered and about 60% when top and bottom bars were considered. At 4% story drift, these percentages increased to about 94% when only top bars were considered and to about 80% when all bars were considered. Figure 4.25 indicates that the bending moment capacity can be significantly enhanced by the slab steel. No major difference can be observed in slab effective width between specimens constructed with normal and high strength materials.

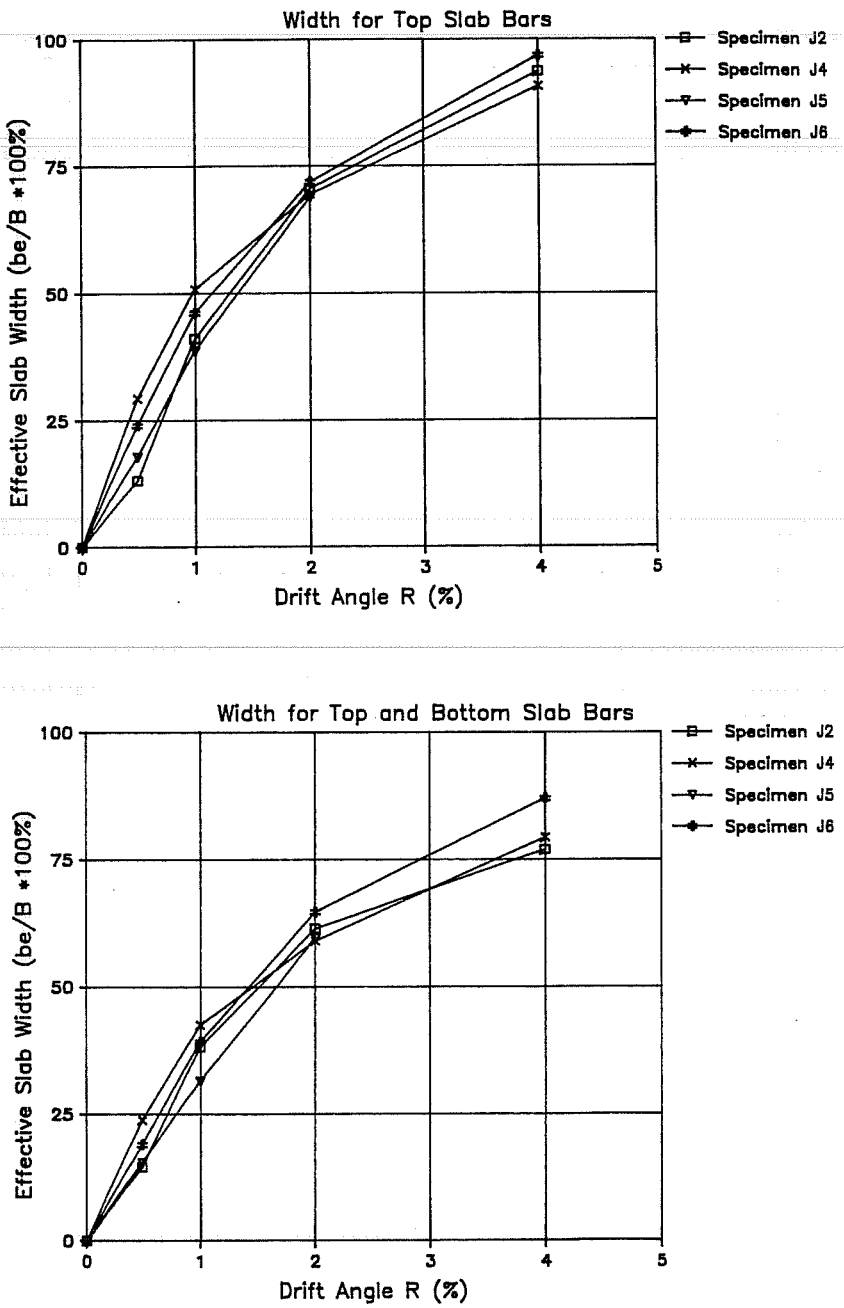

Figure 4.25 Effective Slab Width vs Story Drift Angle

Beam	Moment	Positive Bending					Negative Bending				
		M_{test} (k-in)	R_{calc} (k-in)	$\frac{M_{test}}{R_{calc}}$	T_{calc} (k-in)	$\frac{M_{test}}{T_{calc}}$	M_{test} (k-in)	R_{calc} (k-in)	$\frac{M_{test}}{R_{calc}}$	T_{calc} (k-in)	$\frac{M_{test}}{T_{calc}}$
J2	East-West	3,770	2,766	1.36	2,990	1.26	5,580	4,379	1.27	5,357	1.04
	North-South	3,739	2,969	1.26	3,193	1.17	4,938	4,060	1.22	5,072	0.97
J4	East-West	3,601	2,809	1.28	2,994	1.20	5,533	3,975	1.39	5,166	1.07
	North-South	3,764	3,047	1.24	3,233	1.16	4,506	3,659	1.23	4,856	0.93
J5	East-West	6,713	5,462	1.23	5,769	1.16	9,056	7,739	1.17	9,028	1.00
	North-South	7,476	5,891	1.27	6,198	1.21	8,014	6,985	1.15	8,279	0.97
J6	East-West	6,001	4,562	1.32	4,723	1.27	8,709	6,915	1.26	8,276	1.05
	North-South	6,838	5,017	1.36	5,178	1.32	7,407	6,309	1.17	7,677	0.96

M_{test} : measured maximum beam moment at joint end

R_{calc} : calculated moment capacity as rectangular beam

T_{calc} : calculated moment capacity as T-beam (b_e= 0.19B for positive bending)
(b_e= 0.30B for negative bending)

Table 4.6 - Measured Beam Moments @ 2% Story Drift vs. Calculated Moment Capacity

Beam \ Moment		Positive Bending					Negative Bending				
		M_{test} (k-in)	R_{calc} (k-in)	$\frac{M_{test}}{R_{calc}}$	T_{calc} (k-in)	$\frac{M_{test}}{T_{calc}}$	M_{test} (k-in)	R_{calc} (k-in)	$\frac{M_{test}}{R_{calc}}$	T_{calc} (k-in)	$\frac{M_{test}}{T_{calc}}$
J2	East-West	4,061	2,766	1.47	2,990	1.36	6,317	4,379	1.44	5,885	1.07
	North-South	3,674	2,969	1.24	3,193	1.15	5,235	4,060	1.29	5,619	0.93
J4	East-West	3,732	2,809	1.33	2,994	1.25	6,079	3,975	1.53	5,828	1.04
	North-South	3,704	3,047	1.22	3,233	1.15	4,755	3,659	1.30	5,524	0.86
J5	East-West	7,369	5,462	1.35	5,769	1.28	10,544	7,739	1.36	9,785	1.08
	North-South	7,354	5,891	1.25	6,198	1.19	8,919	6,985	1.28	9,042	0.99
J6	East-West	6,599	4,562	1.45	4,723	1.40	10,045	6,915	1.45	9,081	1.11
	North-South	6,968	5,017	1.39	5,178	1.35	8,642	6,309	1.37	8,488	1.02

M_{test} : measured maximum beam moment at joint end

R_{calc} : calculated moment capacity as rectangular beam

T_{calc} : calculated moment capacity as T-beam (be= 0.19B for positive bending)
(be= 0.60B for negative bending)

Table 4.7 - Measured Beam Moments @ 4% Story Drift vs. Calculated Moment Capacity

Effective slab width can also be evaluated by comparing calculated and measured beam moment capacities. Table 4.6 shows measured maximum beam moments at 2% story drift compared with calculated moment capacities. Table 4.7 shows the same for measured beam moments at 4% story drift. Beam moments were calculated with and without slab participation. Rectangular beam moments (no slab participation) are indicated in Tables 4.6 and 4.7 by R_{calc}. Beam moments calculated using T-beam action are indicated by T_{calc}. In positive bending (slab in compression), the effective slab width b_e was taken following recommendations of the ACI Building Code 318-83 [1]. In this case, the effective slab width b_e corresponds to 0.19B. Calculated beam moments in positive bending are independent of story drift.

In negative bending (slab in tension), there are no code guidelines for effective slab width. Both top and bottom slab bars were considered to contribute to the beam moment capacity. Effective slab width b_e was taken equal to 0.30B for calculation of beam moments at 2% story drift, and was taken equal to 0.60B for calculation of beam moments at 4% story drift. Beam negative moments T_{calc} shown in Tables 4.6 and 4.7 were based on these values.

In positive bending, ratios of measured to calculated rectangular beam moments ranged from 1.23 to 1.36 at 2% story drift. For calculated T-beam moments, ratios were from 1.16 to 1.32. In general, ratios obtained at 4% story drift were slightly higher due to an increase in measured beam moments. Higher values of b_e were used to calculate T-beam moments. However, the difference between calculated moments using different values of b_e is negligible because the position of the neutral axis changes only slightly within the slab. Therefore, the bending moment arm is always about the same.

In negative bending, ratios of measured to calculated rectangular beam moments ranged from 1.15 to 1.39 at 2% story drift, and from 1.28 to 1.53 at 4% story drift. Ratios obtained at 4% story drift were higher due to higher measured negative bending moments. To evaluate T-beam action, several values of effective slab width b_e were used to obtain ratios of measured to calculated moment capacity. Values of b_e =0.30B for 2% story drift and of b_e = 0.60B for 4% story drift came closest to the measured maximum moments at each specified drift level. At 2% story drift, ratios of measured to calculated T-beam moments were between 0.93 and 1.07. At 4% story drift, ratios of measured to calculated T-beam moments were between 0.93 and 1.08. Calculated values are in very close agreement with test results.

The slab influence on beam moment capacity is clear from Tables 4.6 and 4.7. Capacities calculated without the slab contribution considerably underestimated measured bending moments. Presence of slab steel significantly affected negative bending moments.

High strength materials appeared to have no affect on effective slab width because no difference was observed between ratios obtained for specimens constructed with high strength materials.

One should keep in mind that all slab reinforcement was #3 Grade 60 steel placed the same way in all specimens. However, more beam longitudinal reinforcement was used in the high strength concrete specimens. Therefore, the relative contribution of the slab moment to the total bending moment capacity is smaller in the high strength concrete specimens. The effective slab width does not appear to depend on the amount of beam reinforcement.

CHAPTER 5 - DESIGN AND CONSTRUCTION RECOMMENDATIONS

5.1 INTRODUCTION

In evaluating the test results in Chapter 4, the joint shear strength, the performance of high strength materials, stiffness degradation and bond behavior of longitudinal reinforcement under bidirectional loading, and the role of the slab on the beam-column-joint failure mechanism were studied. In this chapter, the impact of the test results on an understanding of the behavior of interior beam-column joints constructed using high strength materials will be assessed. Finally, specific design recommendations will be made.

5.2 BEHAVIOR OF INTERIOR BEAM-COLUMN JOINTS CONSTRUCTED USING HIGH STRENGTH MATERIALS

5.2.1. Joint Shear Strength. One of the main objectives of these tests was to study joint shear strength of specimens constructed with high strength materials. Therefore, the specimens were designed for high joint shears, near the limiting ACI value, to be reached. All specimens failed in joint shear at 4% drift after formation of plastic beam hinges next to the column face. In fact, specimens resisted story shears higher than those calculated using current design recommendations for joint shear strength. Maximum story shears were obtained at 4% story drift for unidirectional loading. However, story shears at 2% story drift did not differ from story shears obtained at 4% drift by more than 15%, and were still higher than calculated story shears. Bidirectional loading resulted in virtually no difference between story shears obtained at 2% and 4% bidirectional drift cycles.

Figure 5.1 shows maximum measured joint shear stresses at 2% drift. The stresses were determined using beam geometry definitions of ACI Committee 352. Joint shear stress in the E-W direction is plotted against joint shear stress in the N-S direction. Points on the horizontal axis indicate unidirectional joint shear stresses. In ACI 352, it is recommended that unidirectional joint shear stresses should not exceed 20 $\sqrt{f'_c}$, but there are no guidelines for bidirectional joint shear stress. A circular interaction diagram for bidirectional shear interaction was assumed using the unidirectional value of 20 $\sqrt{f'_c}$ as the radius of the circle.

The test results indicate that current ACI 352 recommendations provide a safe estimate for unidirectional shear strength of interior joints constructed with normal and high strength materials. A unidirectional joint shear strength of 20 $\sqrt{f'_c}$ can be safely used in designing joints constructed using high strength materials. In addition, a circular interaction diagram provides a conservative estimate of bidirectional joint shear strength.

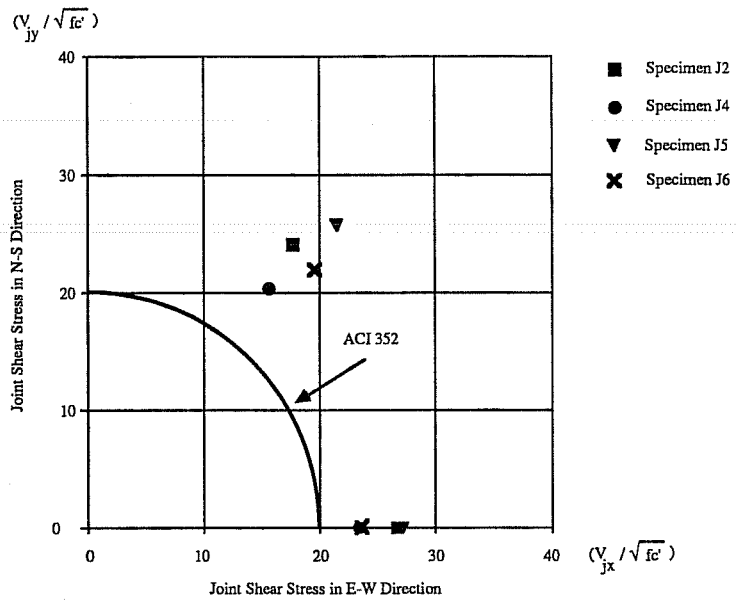

Figure 5.1 Joint Shear Stress at 2% Drift

5.2.2. Joint Transverse Steel Reinforcement. High strength welded wire fabric was used as transverse joint reinforcement in two specimens (J4 and J6). Size, spacing, and amount of joint ties were calculated according to ACI 318 recommendations based on a yield strength of 80 ksi. Normal strength steel was used as transverse joint reinforcement in the other two specimens (J2 and J5). Design of joint ties was then based on a yield strength of 60 ksi.

Strains in joint ties indicated that both normal and high strength joint transverse reinforcement were effective in confining the joint concrete. It appears that the confinement provided by the high strength welded wire fabric is as effective as that of the normal strength steel reinforcement. The joint shear strength was unaffected by the variation in strength of the transverse steel or by use of welded wire fabric.

5.2.3. Stiffness. Equivalent and peak-to-peak stiffnesses were calculated at every loading cycle. In general, the specimens became less stiff with increase in drift angle. Increase in drift angle was more significant in decreasing the stiffness of the specimen than additional loading cycles at the same drift level, especially for the high strength concrete specimens.

High strength concrete specimens were much stiffer than normal strength concrete specimens. However, no difference in stiffness was observed between the specimens constructed of different steel grades because the total steel force ($A_s f_y$) was kept constant in companion specimens.

In early cycles, the reduction in stiffness of normal strength concrete specimens was higher than the reduction in stiffness of high strength concrete specimens. Cracking and spalling of the concrete seemed to be the factors that most contributed to stiffness reduction.

In order to design the specimens to reach high joint shear stresses, the beams were required to develop high internal force couples (large amounts of longitudinal steel) and relatively small column cross sections were necessary. The result was a flexible specimen with large flexural deformations at first yielding of the longitudinal beam. First yielding of beam and column bars occurring during the 2% drift cycles and low displacement ductilities were determined because of the high yield deflection. Although the design satisfied ACI 318 requirements, it is not considered typical of the overall geometry of structures constructed in zones of high seismic risk.

As the analysis of deformation components in Section 4.4 showed, no single component was responsible for the flexibility of the specimen. In early cycles, the beam deformation was the major component of the specimen deformation, with the column and the joint contributing nearly equally. In the high strength concrete specimens, the joint contribution was small. As the test progressed, the joint deformation increased and the beam and/or column contribution usually decreased.

5.2.4. Energy Dissipation. Energy dissipation characteristics of the specimens were studied using equivalent viscous damping ratio, and by determining the contribution of beams, column, and joint to the total energy dissipated in each specimen.

Energy dissipation characteristics were not influenced by the use of high strength steel reinforcement. High strength concrete affected energy dissipation mostly up through 2% drift cycles. Due to generally elastic behavior before 4% drift, equivalent viscous damping ratios for the high strength concrete specimens were lower than for the normal strength concrete specimens.

The high strength concrete specimens dissipated considerable more energy than the normal strength concrete specimens since higher loads were reached at specified drifts. In general, the beams contributed most to the energy dissipated, and the column contributed the least. The joint contribution increased considerably during the test as joint shear distress increased. Formation of beam plastic hinges next to the column faces was evident during 4%

drift cycles for all specimens. Beam plastic hinging and joint shear cracking were responsible for most of the dissipated energy in later loading cycles.

Pinching in the hysteresis loops indicated low energy dissipation in all specimens. This can be associated with several factors: shear distress in the joint, difference in top and bottom longitudinal reinforcement, bar slip through the joint, concrete cracking and crushing, and presence of slab. These factors influenced energy dissipation in all specimens, regardless of the material strengths used.

Hysteretic pinching was reflected in equivalent viscous damping ratios. Highest damping ratios were not usually above 0.20 and occurred during 4% drift cycles. High damping ratios in earlier cycles cannot be expected because the specimens were flexible and generally "thin" elastic loops were generated before yielding of the reinforcement, especially for high strength concrete specimens.

5.2.5. Bond Behavior. Strains measured in beam and column longitudinal reinforcement gave valuable insight to bond deterioration along these bars.

In general, beam top bars showed less bond deterioration than other longitudinal reinforcement. This was probably due to a smaller amount of beam bottom reinforcement and to the presence of the slab. Bond loss in beam bottom bars and column corner bars was more evident. Bond deterioration of beam bottom bars may have started during 2% bidirectional drift cycles and definitely increased during 4% drift cycles. Several factors contributed to more bond deterioration in beam bottom bars: larger amount of top reinforcement, position of the neutral axis, more spalling and crushing of beam bottom concrete, large inelastic bottom bar strains.

Japanese researchers [15] have compared beam bar bond index with equivalent viscous damping ratios. Such relationships gave insight for selecting minimum limits of column depth to beam bar diameter ratios to prevent bond deterioration. Beam bar bond index indicates the possibility of bond degradation along the beam reinforcement. The average bond stress u_b over the column width for simultaneous bar yielding in tension and compression at the two joint faces is given as

$$u_b = \frac{f_y}{2}\left(\frac{d_b}{h_c}\right)$$

Where:

f_y = yield strength of beam bars, psi

d_b = beam bar diameter, in

h_c = column width, in

If the bond strength is assumed proportional to the square root of the concrete compressive strength, f'_c, bond index can be defined as

$$BI = \frac{u_b}{\sqrt{f'_c}}$$

Bond deterioration is more likely to occur for a high bond index.

Kitayama et al [15] have plotted equivalent viscous damping ratios Heq at a drift angle of 1/46 rad (about 2%) against beam bar bond index for plane beam-column subassemblages tested at the University of Tokyo. The tests were conducted on specimens constructed using normal strength materials. Their results are reproduced in Figure 5.2 where the Japanese tests are indicated by small squares. In addition, equivalent viscous damping ratios at 2% drift are plotted against bond index for the beam bottom bars of specimens J2, J4, J5 and J6 (indicated by inverted triangles). The solid line was derived from the least squares method to fit the Japanese data.

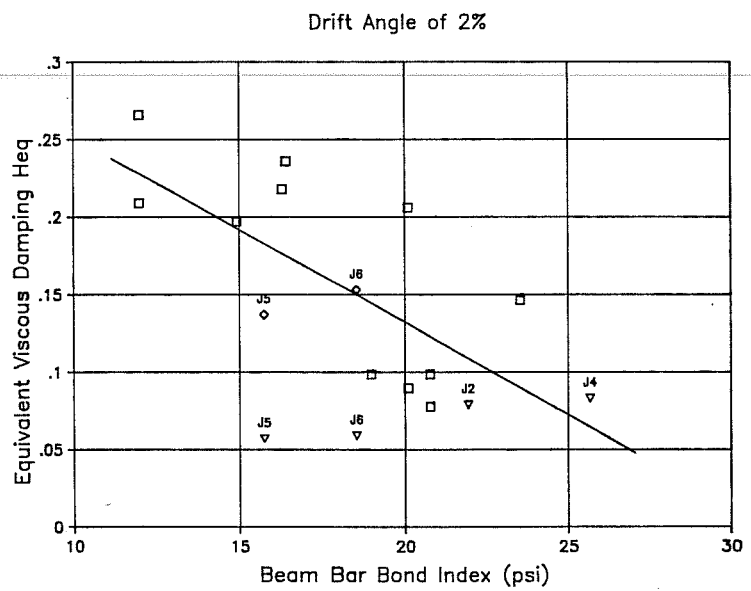

Figure 5.2 Equivalent Viscous Damping vs Beam Bar Bond Index

Based on the Japanese test results shown in Figure 5.2, Kitayama et al recommend a minimum limit of column depth to beam bar diameter ratio of

$$(\frac{h_c}{d_b}) > \frac{f_y}{(38.2\sqrt{f'_c})}.$$

Results from specimens J2 and J4 agree well with trends observed in the Japanese data. It appears that results from normal strength concrete specimens J2 and J4 support the use of the above equation. Points corresponding to the results from the high strength concrete specimens J5 and J6 lie well below the solid line in Figure 5.2, indicating poor correlation with the above equation. This is due to the generally elastic behavior observed in the high strength concrete ($f'_c = 12{,}000$ psi) specimens up to 2% drift. Low values of equivalent viscous damping ratios for the high strength concrete specimens resulted from thin hysteretic loops in story shear-drift angle curves (Figures 3.3 and 3.4). Low equivalent viscous damping for the high strength concrete specimens up to 2% drift was not due to bond degradation of beam bars. From this comparison, a limit of column depth to beam bar diameter could not be determined for the two high strength concrete specimens since the viscous damping ratios were not related to bond deterioration up to 2% drift in specimens J5 and J6. However, as shown in analysis of bond behavior of beam bars in Section 4.6.1., bond deterioration probably occurred at 4% drift levels. Pinching of the hysteresis loops of story shear-drift angle curves for specimens J5 and J6 is clear at 4% drift. Equivalent viscous damping ratios for the two high strength concrete specimens are also plotted against bottom beam bar bond index in Figure 5.2 and are indicated by the small diamonds. Correlation with the solid line is significantly better when equivalent viscous damping ratios at 4% drift are used for the high strength concrete specimens.

Strain gages placed in column corner bars were used to monitor bond behavior in column longitudinal reinforcement. Apparently, column corner bars started to slip early in the test, probably during 1% story drift. Bond deterioration increased considerably after yielding during 2% bidirectional drift cycles. However, strains in column longitudinal reinforcement were not as large as strains in beam longitudinal reinforcement during later loading cycles. Although, bar slip may have occurred earlier for column bars, the amount of slip in beam bars was higher in later loading cycles. Bond deterioration in bottom beam and column bars did not prevent the formation of a concrete compression strut to resist joint shear forces. As previously mentioned, story shears measured during 2% and 4% drift cycles did not differ significantly. There was no discernible difference in bond behavior of Grade 60 and Grade 75 bars passing through the joint.

5.2.6. Slab Participation. A quantitative estimate of slab participation was obtained by evaluating slab effective width under negative (slab in tension) moment. The

influence of the slab in T-beam moment capacities when the slab is in compression is well known. However, design recommendations do not offer guidelines which consider slab steel contributing to the beam bending moment capacity when the slab is in tension.

The effective slab width be (Figure 4.24) was evaluated using two methods. In the first method, effective slab width was calculated using slab bar stresses. Effective slab width be was more than 60% of the slab width B at 2% drift and increased to about 80% at 4% drift.

Effective slab width can also be evaluated by comparing calculated and measured beam moment capacities. Measured maximum and calculated beam moment capacities were compared at 2% and 4% story drifts. Different beam moment capacities were calculated by assuming different amounts of slab steel participating in the negative moment capacity. Test results at 2% story drift best compared with calculated values when 30% of the slab was used as effective slab width. Slab participation increased to 60% at 4% story drift.

Obtaining effective slab width through slab bar stresses is probably more representative of actual behavior than obtaining effective slab width through comparison of measured with calculated beam negative moment capacities. In calculating negative moment capacities, contribution of beam top bars is assumed to be the same at 2% and 4% story drift and all beam top bars were assumed to be at the same yield stress. Therefore, the increase in negative moment as story drift increased from 2% to 4% would come exclusively from slab bars which is unlikely. Strain hardening of the beam steel probably contributed to higher bending moment capacities at 4% story drifts.

5.2.7. High Strength Materials. The tests conducted showed the influence of variations in material strength on the behavior of beam- column-joint connections. In general, high strength concrete had greater influence on joint behavior than high strength steel and welded wire fabric.

No difference in behavior of beam-column joints could be found between the use of high strength (Grade 75) steel longitudinal reinforcement or high strength (f_y = 80 ksi) welded wire fabric for transverse reinforcement and Grade 60 bars.

Effect of high strength concrete (f'_c = 12,000 psi) on behavior was notable, especially up to 2% story drift cycles. High strength concrete specimens were stiffer, cracked and spalled less, and had thinner hysteresis loops than comparable normal strength concrete (f'_c = 4,000 psi) specimens.

Joint shear strength, bidirectional interaction, and effective slab width did not appear to be affected by variations in material strength.

5.3 DESIGN RECOMMENDATIONS

Design recommendations contained in this section were based on the four tests conducted on specimens J2, J4, J5 and J6. The recommendations apply to monolithic beam-column-joint connections in primary moment resisting frames. It is anticipated that maximum interstory drift will be limited to about 2%. Members connected to the joint should be designed to develop hinging in the beams following the "strong column-weak beam" design philosophy. These recommendations cover only interior joints as classified by the ACI 352 Committee Report. In addition, it is assumed that monolithic slabs are included in the beam-column-joint connection.

The results of this experimental work led to the following design recommendations for interior joints constructed with normal and high strength materials:

1. ACI 352 Committee Report recommendations can be extended to include the use of high strength concrete (f'_c up to 12,000 psi) and Grade 75 steel in interior beam-column joints. Such application includes the use of welded wire fabric (f_y up to 80 ksi) as joint transverse reinforcement.

2. Resistance to joint shear forces during bidirectional loading can be assumed to be reached if the unidirectional joint shear stress does not exceed the unidirectional shear strength in each direction independently. Therefore, checking joint shear strength in each direction will assure bidirectional joint shear strength. The following two equations should be satisfied.

$$v_1 \leq 20\sqrt{f'_c}$$

$$v_2 \leq 20\sqrt{f'_c}$$

Where:

v_1, v_2 = horizontal joint shear stress in perpendicular directions generated by beam plastic hinges under unidirectional load conditions. Unidirectional joint shear stress should be determined as outlined in the ACI 352 recommendations.

3. The presence of the slab should be taken into account when computing beam moment capacities. When calculating beam negative moment capacities a total slab overhang equal to half the transverse span can be used. The effective slab width would then include the slab overhang and the beam width. Both top and

bottom slab bars can be used in calculating beam negative moment capacities, as long as sufficient anchorage of the slab bars is provided.

4. Bond conditions along the longitudinal reinforcement can be improved if a minimum limit is imposed on member depth-bar diameter ratios. The use of the equation below developed by Kitayama et al [15] for column depth to beam bar diameter is suggested for bars passing through joints constructed using normal strength concrete. Beam top bars may be exempt from this requirement but further investigation is needed.

$$(\frac{h_c}{d_b}) > \frac{f_y}{(38.2\sqrt{f'_c})}.$$

Not enough data is available to recommend a limit for bars passing through joints constructed using high strength concrete. The use of the above equation for bottom beam bars of specimens J5 and J6 resulted in column depth to beam bar diameter ratios of 16.5 and 17.2 respectively. Actual column depth to bottom beam bar diameter ratios for specimens J5 and J6 were 20 and 17.8. Therefore, the above equation could not be considered conservative when applied to the two high strength concrete (f'_c = 12,000 psi) specimens.

5.4 IMPLICATIONS OF USE OF HIGH STRENGTH MATERIALS IN BEAM-COLUMN JOINT CONSTRUCTION

Several favorable aspects of using high strength materials as opposed to normal strength materials were observed during construction of the specimens. The most important are outlined below.

1) A significant improvement in labor productivity and construction quality was obtained by use of welded wire fabric reinforcing cages. Construction tolerances were improved. The time for assembly of reinforcing cages and placement of cages in the forms was reduced at least by half. In addition, quality of the fabricated (bent) steel ties as received from the suppliers was tremendously better for the welded wire fabric.

2) The use of high strength steel longitudinal reinforcement reduced congestion in the joint region since more steel is required when normal strength reinforcement is used.

3) Placement of high strength concrete was easier than normal strength concrete. High plasticity and a smaller maximum aggregate size contributed to better placement of the high strength concrete. While the slump (after addition of a high range

water reducer) measured when casting the high strength concrete specimens was usually in excess of 10 inches, slump for the normal strength concrete was usually less than 6 inches. In addition, less vibration of the high strength concrete was required, reducing the amount of site labor. The use of high strength concrete created no placement difficulties due to steel congestion in small cross sections.

CHAPTER 6 - SUMMARY AND CONCLUSIONS

6.1 SUMMARY OF TEST PROGRAM

An experimental program was developed to evaluate the behavior of beam-column-joint connections constructed using high strength materials. A series of four full-scale specimens constructed using normal and high strength materials were tested under cyclic bidirectional loading at the Ferguson Structural Engineering Laboratory of the University of Texas at Austin. High strength concrete, high strength steel reinforcement, and welded wire fabric reinforcing cages were used in three of the specimens. A fourth specimen was constructed using normal strength materials. The specimens were designed to demonstrate the influence of material variations on beam-column joint performance.

The specimens reported here were designed using recommendations of the ACI 318-83 Building Code. Beam reinforcement was chosen to produce high joint shear forces. Column reinforcement was designed so the column bidirectional moment capacity was higher than the beam moment capacity. Slab top reinforcement was #3 bars at 12 in. spacing and #3 bottom bars were placed every 24 in.

All specimens had the same dimensions. Two specimens were constructed with normal strength concrete, and two with high strength concrete. High strength steel (Grade 75) and welded wire fabric reinforcing cages (f_y =80 ksi) were used in two specimens. The control specimen had normal strength concrete (f'_c =4,000 psi) and Grade 60 steel. Joint transverse reinforcement consisted of at least three sets of stirrups located in the joint between beam bars. The use of welded wire fabric as transverse reinforcement for beams and columns significantly improved quality control and productivity during construction of reinforcing cages.

The cyclic loading was applied through a program of interstory drift angles. Unidirectional and bidirectional cycles up tp 4% drift levels were applied.

6.2 CONCLUSIONS

The main objective of this work was to evaluate the influence of high strength materials on the performance of slab-beam-column- joint connections. The following are the most important conclusions obtained from the analysis of the test results.

6.2.1. Summary of Behavior.

Joint Shear Strength. All specimens failed in joint shear after formation of plastic beam hinges next to the column faces at 4% drift levels. Measured maximum unidirectional

joint shear stresses varied from $23\sqrt{f_c'}$ to $26.6\sqrt{f_c'}$ and maximum bidirectional joint shear stresses varied from $25.4\sqrt{f_c'}$ to $34.4\sqrt{f_c'}$ at 2% drift. The tests indicate that current ACI 352 recommendations of 20 $\sqrt{f_c'}$ for joint shear strength can be used for a safe estimate for unidirectional joint shear strength of interior joints constructed with high strength materials.

Joint Transverse Reinforcement. The test results indicated that high strength (f_y =80 ksi) welded wire fabric joint hoops calculated according to current ACI 318 guidelines are effective in confining joint concrete. The use of welded wire fabric cages for transverse reinforcement did not result in any differences in performance of any of the joints.

Stiffness. No significant difference in stiffness was observed between specimens constructed of different steel grades. Stiffness reduced linearly with increase in drift angle for the high strength concrete specimens. Stiffness decreased along a parabolic curve for normal strength concrete specimens with greater losses in the initial cycles of loading. Cracking and spalling of the concrete appeared to affect stiffness more than did bond deterioration along longitudinal bars.

Energy Dissipation. The test results show that energy dissipation characteristics of the specimens were not influenced by the use of high strength (Grade 75) steel reinforcement. All specimens exhibited low equivalent viscous damping ratios (usually below 0.20) indicating poor energy dissipating capabilities. The high strength concrete specimens exhibited thin hysteretic loops in story shear-drift angle curves because the response was largely elastic up to 2% drift cycles.

Bond Behavior of Longitudinal Reinforcement. In general, beam top bars showed less bond deterioration than other longitudinal reinforcement. Presence of the slab was important in reducing bond loss along beam top bars. Several factors contributed to more bond deterioration in beam bottom bars: larger amount of top reinforcement, position of the neutral axis, more spalling and crushing of beam bottom concrete, large inelastic bottom bar strains. Bond deterioration along column bars probably started early in the test and increased considerably after yielding during 2% bidirectional drift cycles.

Slab Participation. The effect of the slab was evaluated using two methods for calculation of effective slab width. In the first method, effective slab width was calculated using slab bar stresses. At 2% drift, the test results showed that effective slab width is about 60% of the transverse span. In addition, effective slab width was evaluated by comparing calculated and measured beam moment capacities. Measured beam moments at 2% drift best compared with calculated values when 30% of the slab was used as effective slab width. Variations in material strengths did not affect slab participation.

6.2.2. Summary of Design Recommendations.

1) ACI 352 Committee recommendations can be extended to include the use of high strength concrete (f'_c up to 12,000 psi) and Grade 75 steel in interior beam-column joints. Such application includes the use of welded wire fabric (f_y up to 80 ksi) as joint transverse reinforcement.

2) Resistance to joint shear forces during bidirectional loading can be assumed to be reached if the unidirectional joint shear stress does not exceed the unidirectional shear strength in both directions independently.

3) When calculating beam negative moment capacities, a total slab overhang equal to half the transverse span can be used.

4) The use of the equation below developed by Kitayama et al [15] for column depth to beam bar diameter is suggested for bars passing through joints constructed using normal strength concrete.

$$(\frac{h_c}{d_b}) > \frac{f_y}{(38.2\sqrt{f'_c})}.$$

6.2.3. Summary of Implications in Construction. A significant improvement in labor productivity and construction quality was obtained by use of welded wire fabric reinforcing cages. Higher slump, more plasticity, and a smaller maximum aggregate size contributed to easier placement of the high strength concrete.

6.3 ADDITIONAL RESEARCH

The experimental study reported here satisfactorily met the intended objectives within the scope of this research. However, further investigation can be recommended in some areas.

1) Quantification and qualification of hysteretic behavior of beam-column joints is needed in order to unify different design philosophies. Defining the importance of quality of hysteresis loops on building response is necessary.

2) Optimum ratios of positive and negative moment capacities to improve energy dissipation characteristics need to be defined. Influence of the slab and its reinforcement should be included.

3) Although measured unidirectional joint shear stresses were in excess of $20\sqrt{f'_c}$, the use of higher unidirectional joint shear strength in design is not recommended. It was felt that the amount of longitudinal reinforcement necessary to produce such high shear stresses could result in bond problems leading to poor energy dissipation

capacities. A study correlating level of joint shear with bond deterioration and energy dissipation characteristics would be valuable, especially for joints constructed with high strength concrete.

4) The effect of high strength concrete on spectral response of structures subjected to different earthquakes should be studied. Cracking and degradation of high strength concrete is different than normal strength concrete. This could have an effect on the member internal forces during seismic excitation.

5) Amount of joint transverse reinforcement was not a variable in these tests. The tests on the high strength concrete specimens suggested that joint shear strength depends more on strength of the concrete than on the transverse joint reinforcement. A study aimed at determining the optimum transverse reinforcement to be used for confining effects in interior joints constructed using high strength concrete would be useful.

APPENDIX A - THE U.S.-NEW ZEALAND-JAPAN-CHINA COOPERATIVE RESEARCH PROJECT

Although considerable amount of experimental evidence has accumulated from tests conducted on beam-column joints, considerable differences still exist between design codes of different countries. Significant differences in U.S., Japan and New Zealand design recommendations have arisen because of different interpretation of tests results, different design criteria and performance levels. Therefore, a quadri-lateral cooperative program aimed at explaining these differences was developed by researchers in the U.S., New Zealand, Japan and China (P.R.C.) [17,18]. Experimental research was conducted in the Ferguson Structural Engineering Laboratory at the University of Texas at Austin in the United States, at the University of Canterbury in New Zealand, and at the University of Tokyo in Japan, and at the Chinese Academy of Building Research and Tongji University in China.

Three full-scale slab-beam-column connections were tested at the University of Texas at Austin as part of this program. The specimens were designed using ACI 318 and 352 Committee recommendations. The first two specimens (J1 and J2) were interior joints and the third specimen (J3) was an exterior joint. Specimens J2 and J3 were tested in bidirectional loading. Specimen J1 was tested unidirectionally. Normal strength steel (Grade 60) and normal strength concrete (f'_c =4,000 psi) was used in all three specimens. Specimen geometry included a 20in square column, 16in x 20in beams and a 5in thick floor slab. The loading history included bidirectional cycles up to 4% story drift.

The specimens, procedures and results of the tests on specimens J1, J2, and J3 are described in detail in Reference 5.

APPENDIX B - DESIGN RECOMMENDATIONS FOR JOINT SHEAR STRENGTH

Important guidelines for designing beam-column joints are given in the American Concrete Institute 352 Committee Report [2], the New Zealand Standard [4], and Architectural Institute of Japan design recommendations [3]. A summary of the shear strength provisions for interior joints is outlined below.

B.1 ACI 352 COMMITTEE RECOMMENDATIONS

ACI 352 Committee design recommendations for joint shear strength are based on the concrete strut mechanism. The shear strength of an interior joint is considered to be satisfied if the horizontal shear stress v_{jh} is less than $20\sqrt{f'_c}$:

$$v_{jh} \leq 20\sqrt{f'_c}$$

The shear stress v_{jh} is obtained by dividing the shear force V_{jh} given in section 1.2 by the joint area A_{jh} given as

$$A_{jh} = b_j * h_c$$

Where:

f'_c =concrete compressive strength, psi

b_j =average of beam and column widths, in.

h_c =column depth, in.

B.2 NEW ZEALAND RECOMMENDATIONS

The New Zealand Standard design recommendations for joint shear strength are based on the panel truss mechanism. When checking resistance to horizontal joint shear, both the steel reinforcement and the concrete contribute to joint shear strength. However, concrete contribution is to be neglected if beam plastic hinging occurs at the column face. The area of horizontal shear reinforcement is required to be at least

$$A_{jh} = \frac{V_{sh}}{f_{yh}}$$

and

$$V_{sh} = V_{jh} - V_{ch}$$

Where:

A_{jh} =area of horizontal shear reinforcement

V_{sh} =horizontal joint shear force resisted by the steel V_{jh} =horizontal joint shear force

V_{ch} =horizontal shear force due to contribution by the concrete (equal to zero for specimens J2, J4, J5 and J6)

B.3 JAPANESE DESIGN RECOMMENDATIONS

Architectural Institute of Japan guidelines for joint shear strength assign part of the joint resistance to the concrete and part to the joint transverse reinforcement. The shear strength of the interior joint is considered to be satisfied if the following requirement for horizontal shear stress v_{jh} is met.

$$v_{jh} \leq (2\phi f_s + p_{sh} f_{yh})$$

The shear stress v_{jh} is obtained by dividing the shear force V_{jh} by the joint area A_{jh} given as

$$A_{jh} = b_j * j_c$$

Where:

b_j =average of beam and column widths, in.

$j_c = 0.875 d_c$; d_c =column effective depth, in.

$\phi = 3$, for interior joints

$p_{sh} = \frac{A_{sh}}{b_c * s_h}$

A_{sh} =area of hoop reinforcement, in^2.

b_c =column width, in.

s_h =spacing of hoops, in.

f_s =minimum of $\{1.5 * (\text{f'}_c/100 + 71.4)$; $f'_c/20\ \}, psi$

LIST OF REFERENCES

1. ACI Committee 318: "Building Code Requirements for Reinforced Concrete", American Concrete Institute, Detroit, MI, 1983.

2. ACI-ASCE Committee 352: "Recommendations for Design for Beam-Column-Joints in Monolithic Reinforced Concrete Structures", Journal, American Concrete Institute, No. 3, Proc. vol. 82, Detroit, MI, May-June, 1985.

3. "AIJ Standard for Structural Calculation of Steel Reinforced Concrete Structures", Architectural Institute of Japan, 1975.

4. "New Zealand Standard Code of Practice for the Design of Concrete Structures", NZS 3101, Standards Association of New Zealand, Wellington, 1982.

5. KUROSE, Y., G.N. Guimaraes, M.E. Kreger and J.O. Jirsa: "Evaluation of Slab-Beam-Column Joint Response Under Bidirectional Loading", Ninth World Conference on Earthquake Engineering, Tokyo, Japan, August, 1988.

6. ZHANG, L. and J.O. Jirsa: "A Study of Shear Behavior of Reinforced Concrete Beam-Column Joints", Report No. 82-1, Phil M. Ferguson Structural Engineering Laboratory, The University of Texas at Austin, February, 1982.

7. MEINHEIT, D. and J. O. Jirsa: "Shear Strength of R/C Beam Column Connections", Journal of the Structural Division, ASCE, ST11, November, 1982.

8. LEON, R.: "The Inflence of Floor Members on the Behavior of Reinforced Concrete Beam-Column Joints Subjected to Severe Cyclic Loading", Ph.D. Dissertation, The University of Texas at Austin, December, 1983.

9. LEON, R. and J.O. Jirsa: "Bidirectional Loading of R.C. Beam-Column Joints", Earthquake Spectra, Vol. 2, No. 3, Earthquake Engineering Research Institute, 1986.

10. PARK, R. and T. Paulay: "Reinforced Concrete Structures", J. Wiley & Sons, New York, 1975.

11. CLOUGH, R. and J. Penzien: "Dynamics of Structures", McGraw-Hill Inc., New York, 1975.

12. ZHU, S. and J.O. Jirsa: "A Study of Bond Deterioration in Reinforced Concrete Beam-Column Joints", Report No. 83-1, Phil M. Ferguson Structural Engineering Laboratory, The University of Texas at Austin, July, 1983.

13. FILIPPOU, F.C., E.P. Popov and V.V. Bertero: "Effects of Bond Deterioration on Hysteretic Behavior of Reinforced Concrete Joints", Report No. UCB/EERC-83/19, Earthquake Engineering Research Center, University of California, Berkeley, CA, August, 1983.

14. DURRANI, A.J. and J.K. Wight: "Experimental and Analytical Study of Internal Beam to Column Connections Subjected to Reversed Cyclic Loading", Department of Civil Engineering, Report No. UMEE 82R3, The University of Michigan, Ann Arbor, MI, July, 1982.

15. KITAYAMA, K., S. Otani and H. Aoyama: "Earthquake Resistant Design Criteria for Reinforced Concrete Interior Beam-Column Joints", Pacific Conference on Earthquake Engineering, New Zealand, August, 1987.

16. PAULAY, T. and R. Park: "Joints in Reinforced Concrete Frames Designed for Earthquake Resistance", Report No. 84-9, Department of Civil Engineering, University of Canterbury, New Zealand, June, 1984.

17. Summary of Meeting, The U.S.-New Zealand-Japan Seminar on the Design of Reinforced Concrete Beam-Column Joints, Tokyo, Japan, July, 1984.

18. Summary of Meeting, The U.S.-New Zealand-Japan Seminar on the Design of Reinforced Concrete Beam-Column Joints, Tokyo, Japan, May, 1985.